GSK3α/β IN ATHEROSCLEROSIS

THE ROLE OF GLYCOGEN SYNTHASE-3α/β IN THE PROGRESSION AND REGRESSION OF ATHEROSCLEROSIS

By ARIC HUANG, B.Sc. (Hons.)

A Thesis Submitted to the School of Graduate Studies in Partial Fulfilment of the Requirements for the Degree Master of Science

MASTER OF SCIENCE (2017)	McMaster University
(Chemistry and Chemical Biology)	Hamilton, Ontario
TITLE:	The role of glycogen synthase kinase-3α/β in the progression and regression of atherosclerosis
AUTHOR:	Aric Huang, B.Sc. (Honours) (McMaster University)
SUPERVISOR:	Geoff H. Werstuck, B.Sc., Ph.D.
NUMBER OF PAGES:	xvii, 149

LAY ABSTRACT

Atherosclerosis is a disease involving the build-up of fatty plaques in the arteries, making them hard and narrow. This is the main cause of cardiovascular diseases such as heart attacks and strokes. We believe that the proteins, GSK3α and/or GSK3β, are involved in promoting atherosclerosis. The goal of this study is to determine if we can treat atherosclerosis by blocking the actions of GSK3α/β. The results of this study show that inhibiting GSK3α and GSK3β together stops atherosclerosis from getting worse and may help reduce the risk of getting cardiovascular diseases. Inhibiting GSK3α alone helps decrease inflammation, a major driver of atherosclerosis. However, we still need to do more research to find out how or if GSK3β contributes to atherosclerosis. This information may be used to help develop drugs to treat atherosclerosis and reduce the chances of people dying from heart attacks or strokes.

ABSTRACT

Atherosclerosis is a major underlying cause of cardiovascular disease; however, the molecular mechanisms by which cardiovascular risk factors promote the development of atherosclerosis are poorly understood. Recent evidence from our laboratory suggests that endoplasmic reticulum (ER) stress signaling through glycogen synthase kinase (GSK)-3α/β is involved in the activation of pro-atherosclerotic processes. The objective of this study was to examine the role of ER stress-GSK3α/β signaling on the progression and regression of atherosclerosis in a mouse model system.

We first investigated the effects of attenuating ER stress or inhibiting GSK3α/β in a low density lipoprotein receptor deficient (*Ldlr*$^{-/-}$) mouse model of atherosclerosis. Mice treated with the ER stress alleviator 4-phenylbutyric acid (4PBA) or the GSK3α/β inhibitor valproate (VPA) have significantly reduced lesion areas and volumes, indicating that these treatments attenuated the development of atherosclerosis.

Next, we examined the effects of 4PBA or VPA treatment in *Ldlr*$^{-/-}$ mice with established lesions. These treatments inhibited the progression of atherosclerosis in established plaques, but we did not see any evidence of plaque regression. However, the plaques appear to be more stable and less prone to rupture.

Lastly, to help determine the mechanism by which GSK3α/β is involved in atherosclerosis, cell culture experiments were performed to characterize GSK3α or GSK3β deficient macrophages. Bone marrow derived macrophages were obtained from *Ldlr*$^{-/-}$ mice with myeloid specific GSK3α or GSK3β deficiency, and were cultured in the

presence of the ER stress inducing agents thapsigargin (Tg) or tunicamycin (Tm). The absence of GSK3α attenuated M1 polarization, but did not significantly alter cell viability or the expression of genes involved in lipid biosynthesis and uptake. The deletion of GSK3β minimally affected apoptosis induced by Tg or Tm treatment. In contrast, the deletion of GSK3α and GSK3β significantly improved cell viability.

These data support the importance of ER stress-GSK3α/β signaling in atherogenesis. The pharmacological attenuation of ER stress or inhibition of GSK3α/β impedes the development of atherosclerosis in *Ldlr*$^{-/-}$ mice and appears to promote the stabilization of existing lesions. This may be due in part to a reduction in the pro-inflammatory M1 phenotype associated with the inhibition of the GSK3α homolog.

ACKNOWLEDGEMENT

My current success in graduate studies would not be possible without the help and guidance from my supervisor, colleagues, friends, and family. I am indebted to my supervisor, Dr. Geoff Werstuck. He enabled me to work independently, pushed me to learn by self-discovery, and assisted me along the way when needed. He was always available for guidance when I have issues with experiments and scientific writing.

I would also like to thank the previous and current members of the Werstuck lab who have helped me through my journey and made this experience enjoyable. In particular, my work would not be possible without the assistance of Tayler Young, the support from Vi Dang and Dr. Monica De Paoli, animal help from Dr. Peter Shi, and guidance from Dr. Cameron McAlpine. I would also like to express my gratitude towards Kevin Chathely and Alex Qian from the laboratory or Dr. Bernardo Trigatti, as well as Dhruva Dwivedi and Peter Grin for their technical assistance.

I thank my family and friends for their continuous support throughout my years of study and decisions. This accomplishment would not have been possible without them. Thank you.

TABLE OF CONTENTS

LIST OF FIGURES

LIST OF TABLES

LIST OF ABBREVIATIONS

4PBA	4-phenylbutyrate
ABCA1	ATP binding cassette subfamily A member 1
ABCG1	ATP-binding cassette subfamily G member 1
AcLDL	Acetylated low density lipoprotein
Ad	Adenovirus
ANOVA	Analysis of variance
APC	Allophycocyanin
Apoe$^{-/-}$	Apolipoprotein E deficient
Arg1	Arginase 1
ATF	Activating transcription factor
ATP	Adenosine triphosphate
BSA	Bovine serum albumin
CBP	CREB-binding protein
CD	Cluster of differentiation
cDCs	Classical dendritic cells
CHOP	C/EBP homologous protein
CLPCs	Common lymphoid progenitor cells
CMPCs	Common myeloid progenitor cells
CREB	Cyclic AMP response element binding protein
Csf1r	Colony stimulating factor 1 receptor
CV	Cardiovascular
CVD	Cardiovascular disbcease
CVDs	Cardiovascular diseases
DAPI	4′,6-diamidino-2-phenylindole dihydrochloride
DMEM	Dulbecco's modified eagle medium

DMSO	Dimethyl sulfoxide
DPBS	Dulbecco's phosphate buffered saline
dUTP	Deoxyuridine triphosphate
ER	Endoplasmic reticulum
ERAD	ER-associated protein degradation
FAS	Fatty acid synthase
FBS	Fetal bovine serum
FDA	Food and Drug Administration
Fl	Floxed
GADD	Growth arrest and DNA damage-inducible protein
GPT	N-acetylglucosamine-1-phosphate transferase
GRP	Glucose-related protein
GSK	Glycogen synthase kinase
HDAC	Histone deacetylase
HDACs	Histone deacetylases
HDL	High density lipoprotein
HFD	High fat diet
HMG-CoA	3-hydroxy-3-methylglutaryl-coenzyme A
HSCs	Hematopoietic stem cells
IDL	Intermediate density lipoprotein
IFN	Interferon
IL	Interleukin
iNOS	Inducible nitric oxide synthase

IRE1	Inositol-requiring enzyme-1
KO	Knockout
LCMS	Liquid chromatography mass spectrometry
LDL	Low density lipoprotein
Ldlr	low-density lipoprotein receptor
Ldlr$^{-/-}$	Low density lipoprotein receptor deficient
LPS	Lipopolysaccharide
Mer	Murine estrogen receptor
MMP	Matrix metalloproteinase
NF	Nuclear factor
NOX	Nicotinamide adenine dinucleotide phosphate oxidase
OCT	Optical cutting temperature
P	Phosphorylation/phosphorylated
PCSK9	Proprotein convertase subtilisin/kexin type 9
pDCs	Plasmacytoid dendritic cells
PE	Phycoerythrin
PERK	Protein kinase RNA-like ER kinase
PPARγ	Peroxisome proliferator activated receptor γ
ROS	Reactive oxygen species
RT-PCR	Real-time reverse transcription polymerase chain reaction
S1P	Site 1 protease
S2P	Site 2 protease
SD	Standard deviation
SEM	Standard error of the mean
SRA	Scavenger receptor A
SRB1	Scavenger receptor class B member 1
SRBP	Sterol regulatory element-binding protein

SREBPs	Sterol regulatory element-binding proteins
TdT	Terminal deoxynucleotidyl transferase
Tg	Thapsigargin
TGF	Tumor growth factor
Th1	T helper type 1
Th2	T helper type 2
Tm	Tunicamycin
TNF	Tumor necrosis factor
TUNEL	Terminal deoxynucleotidyl transferase dUTP nick end labeling
UPR	Unfolded protein response
UT	Untreated
VCAM	Vascular cell adhesion molecule
VPA	Valproate
VSMC	Vascular smooth muscle cell
VSMCs	Vascular smooth muscle cells
WT	Wildtype
XBP1	X-box binding protein-1

DECLARATION OF ACADEMIC ACHIEVEMENT

The experiments in this thesis were conducted by Aric Huang with the help with colleagues. Tayler Lee Young assisted with staining and analysis for the progression model in chapter 3, and mouse colony management, bone marrow progenitor cell isolation, and RT-PCR preparation and analysis in chapter 4. Dr. Peter Shi monitored and handled the *Ldlr*$^{-/-}$ mice utilized chapter 3. Vi Thuy Dang assisted with LC-MS and quantification. Dr. Cameron Stuart McAlpine and Dr. Geoff Hamilton Werstuck helped design the studies.

CHAPTER 1: GENERAL INTRODUCTION

1.1 Burdens of cardiovascular disease

Cardiovascular diseases (CVDs) are a group of conditions involving the heart and blood vessels. They are the leading cause of mortality worldwide accounting for approximately 30% of all deaths (17.3 million deaths in 2008)[1]. This number is expected to increase to over 23.6 million deaths per year by 2030[1]. In Canada, CVDs account for 25.2% of deaths in 2013[2], 16.9% of all hospitalizations in 2005/06[3], and 87.6 million prescriptions were dispensed for CVD treatment in 2014[4]. In 2000, CVDs contributed to an annual cost of $22.2 billion, with $7.6 billion in direct costs, to the Canadian economy[3].

There are many different risk factors that can be associated with CVDs. Some of these risk factors can be altered and/or treated, while other risk factors cannot be controlled. Modifiable risk factors include hypertension (high blood pressure, resting blood pressure >140/90 mmHg), dyslipidemia (total cholesterol >240 mg/dL, low-density lipoprotein (LDL) >160 mg/dL, and high density lipoprotein (HDL) < 40 mg/dL), physical inactivity, obesity (body mass index >30 kg/m^2), diabetes mellitus (high blood glucose, fasting glucose level >140 mg/dL), and tobacco use[5]. Non-modifiable risk factors include advancing age, ethnic characteristics (African Americans, Hispanic, and non-Hispanic white are at higher risk), and family history. However, the underlying mechanism by which these cardiovascular risk factors promotes CVDs is poorly understood.

1.2 Atherosclerosis

The major underlying cause of CVDs is atherosclerosis. Atherosclerosis is an inflammatory disease characterized by the accumulation of fatty plaques in the arterial wall. Atherosclerotic plaques, also known as lesions, initially accumulate in regions with turbulent, non-laminar blood flow, such as areas with bifurcations, branches, or inner curvatures[6]. At these sites, there is increased expression of endothelial cell surface proteins, including vascular cell adhesion molecule (VCAM)-1 and P-selectin, which mediate the migration of monocytes and T lymphocytes across the endothelium into the sub-endothelial intima layer **(Figure 1.1)**[7,8]. Once in the sub-endothelial space, monocytes differentiate into macrophages that endocytose LDL and modified-LDL particles. The lipid engorged macrophages, known as foam cells, make up the fatty streak which is the earliest type of lesion. Fatty streaks are benign but can mature into more advanced lesions. Macrophage foam cells and lymphocytes amplify the inflammatory response by secreting cytokines and growth factors, such as interferon (IFN)-γ, interleukin-1 (IL-1), and tumour necrosis factor (TNF)-α[9,10]. In addition, cytokines induce the migration of vascular smooth muscle cells (VSMCs) from the tunica media into the intima[11]. Advanced lesions are characterized by a lesion-stabilizing fibrous cap, containing VSMCs and VSMC-synthesized collagen, which covers the lipid core. As the lesion grows, foam cells continue to uptake lipids in the form of low density lipoprotein particles (LDL) and modified-LDLs. The accumulation of free cholesterol in the foam cells can ultimately initiate apoptosis. Apoptotic cells are typically cleared by macrophages through efferocytosis, preventing cellular necrosis and resolves

inflammation. However, efferocytosis is defective in advanced lesions, resulting in the formation of an acellular region within the lesion known as the necrotic core. Necrosis is a key feature of unstable plaques that are prone to rupture. Foam cells also release collagenases, such as matrix metalloproteinase (MMP)-1, -2, and -9, which disrupt the biomechanical stability of the fibrous cap[12–14]. The thinning of the fibrous cap destabilizes the lesion, making it susceptible to rupture. When the lesion ruptures, coagulation factors in the blood comes into contact with pro-coagulant factors, including tissue factor, in the necrotic core. This promotes platelet aggregation and atherothrombosis[15]. The thrombus formed may occlude the artery, resulting in cardiovascular complications such as myocardial ischemia or infarction.

Atherosclerosis appears to progress in an identical manner, regardless of the cardiovascular risk factor that is associated with disease development. This observation suggests that there may be a unifying pathway which links these factors to the development of the disease. Reactive oxygen species (ROS), such as superoxide and hydrogen peroxide, have been implicated in all stages of atherosclerosis – from the start of fatty streaks to the progression of plaque instability and rupture[16]. Furthermore, the major risk factors of atherosclerosis, such as aging, diabetes, hypercholesterolemia, hypertension, and smoking, increase the production of ROS. A major source of ROS is the nicotinamide adenine dinucleotide phosphate oxidase (NOX)[17]. NOX regulates cell proliferation and migration, apoptosis, lipid oxidation, and angiogenesis[18]. A study conducted by Judkin et al. demonstrated that NOX2 deficiency resulted in significantly reduced atherosclerosis in the descending aorta in apolipoprotein E deficient (*Apoe*$^{-/-}$)

mice[19]. Although NOX may be an attractive target for therapy, further research is needed to develop NOX inhibitors that are specific and appropriate for clinical trials[20]. Since there appears to be a major role of ROS in the progression of the disease, oxidative stress may be a potential molecular mechanism which drives atherogenesis. Despite the evidence of a role of oxidative stress in the development and progression of atherosclerosis, large clinical studies using anti-oxidant therapies have failed to prevent atherosclerosis or improve cardiovascular outcome[16,21]. Therefore, there may be additional molecular pathways or mechanisms that work in parallel, or in combination with oxidative stress. A better understanding of atherogenic pathways and processes, together with the development of treatments and strategies to reverse atherosclerosis, is of importance to help alleviate the burdens of CVDs.

Figure 1.1. The progression of atherosclerosis.

Atherosclerosis is triggered by endothelial injury, increasing cell permeability to LDL particles which are modified and retained in the intima. Endothelial dysfunction increases the expression of adhesion molecules to recruit monocytes to the vessel wall and transmigrate into the intimal layer. Monocytes differentiate into macrophages that take up the modified LDL particles and become foam cells. Activated macrophages express various pro-inflammatory cytokines and chemokines. Cytokines released from macrophages and foam cells stimulate the proliferation and migration of collagen secreting vascular smooth muscle cells (VSMCs) into the intimal layer above the lesion, forming a fibrous cap to help stabilize the plaque. The ineffective clearance of apoptotic foam cells and VSMCs (efferocytosis) leads to the formation of a necrotic core and accumulation of extracellular lipids, forming the necrotic core. Collagenases, including matrix metalloproteinases from foam cells, contribute to the thinning and destabilization of plaques. Lesion instability may result in rupture and thrombus formation, culminating in a possible cardiovascular event.

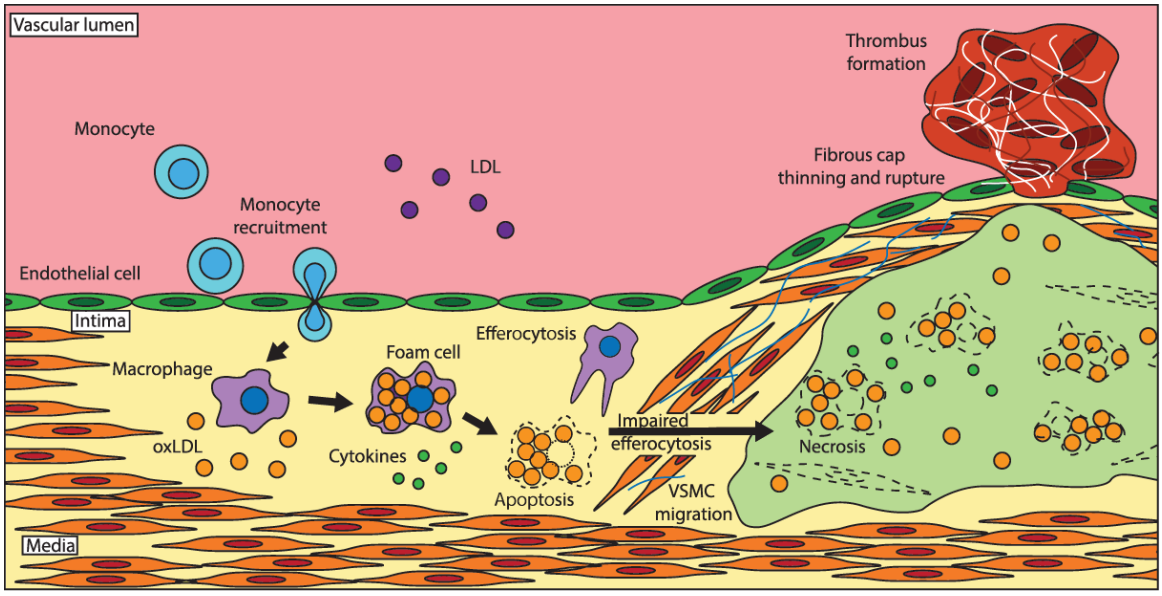
Vascular lumen
Thrombus formation
Monocyte
LDL
Fibrous cap thinning and rupture
Monocyte recruitment
Endothelial cell
Intima
Efferocytosis
Foam cell
Macrophage
oxLDL
Cytokines
Apoptosis
Impaired efferocytosis
Necrosis
VSMC migration
Media

1.3 Endoplasmic reticulum stress and the unfolded protein response

The endoplasmic reticulum (ER) is a eukaryotic organelle responsible for protein modification, protein folding, and protein trafficking. A disturbance in ER function can disrupt the homeostatic balance between folded and misfolded protein resulting in an accumulation of misfolded and unfolded proteins, a condition known as ER stress **(Figure 1.2)**. In response to ER stress, the cell activates the unfolded protein response (UPR) to help alleviate ER stress and restore ER homeostasis[22,23]. The UPR can be divided into three signalling pathways, each initiated and regulated by an ER transmembrane signalling protein: protein kinase RNA-like ER kinase (PERK), inositol-requiring enzyme-1 (IRE1), and activating transcription factor (ATF)-6.

In unstressed conditions, the ER-resident protein chaperone, glucose-related protein (GRP)78, is bound to and inhibits the ER transmembrane proteins PERK, IRE1, and ATF6[22,23]. During ER stress, GRP78 is recruited away from the transmembrane proteins, activating the three signaling cascades. In the PERK signalling pathway, the released PERK homodimerizes and undergoes *trans*-autophosphorylation. The phosphorylated PERK then phosphorylates and inactivates the translation factor, eukaryotic initiation factor 2α (eIF2α), resulting in translational inhibition of most proteins. Under these conditions, only specific mRNAs are translated, such as the transcription factor ATF4. ATF4 translocates to the nucleus and upregulates the expression of the pro-apoptotic factor C/EBP homologous protein (CHOP), as well as the phosphatase, growth arrest and DNA damage-inducible protein (GADD)-34. GADD34 negatively feedback to dephosphorylate and activate eIF2α function[24]. In the IRE1

signalling pathway, the released IRE1 homodimerizes and undergoes *trans*-autophosphorylation[22,23]. The phosphorylated IRE1 is an endoribonuclease which is involved in the alternative splicing of the X-box binding protein-1 (XBP1) mRNA. XBP1 is a transcription factor which induces the expression of ER chaperones such as GRP78 and GRP94, and the expression of genes involved in unfolded protein degradation, known as ER-associated protein degradation (ERAD). Lastly, for the ATF6 signalling pathway, the released ATF6 translocates to the Golgi, where it is cleaved by site 1 protease (S1P) and site 2 protease (S2P). The released N-terminal fragment is an active transcription factor which enhances ER chaperone expression such as GRP78.

Together, these signalling pathways contribute to the adaptive response of the UPR, where the cell inhibits general protein synthesis, increases ER folding capacity by enhancing ER chaperone expression, and promotes the degradation of irreversibly misfolded proteins. If the ER stress persists, the UPR upregulates pro-apoptotic factors such as CHOP to mediate apoptosis to eliminate the cell[25]. Although these signalling pathways are presented as separate signalling pathways, there is potential crosstalk between the three UPR pathways, where signal transduction pathways are not independent of each other[26].

Figure 1.2. The unfolded protein response.

Upon endoplasmic reticulum (ER) stress, unfolded and misfolded proteins bind and sequester the ER chaperone 78 kDa glucose-regulated protein (GRP78), thereby activating the unfolded protein response (UPR). Signaling through the protein kinase R-like endoplasmic reticulum kinase (PERK), inositol requiring enzyme (IRE)-1, and activating transcription factor (ATF)-6 pathways results in the inhibition of protein synthesis (translation), activation of components involved in the ER-associated protein degradation (ERAD) pathway, and increase protein folding capacity by upregulating the production of ER chaperones. The activated PERK phosphorylates and inactivates the translation factor, eukaryotic initiation factor 2α (eIF2α), resulting in reduced mRNA translation. Only certain mRNAs get translated, such as activating transcription factor 4 (ATF4). ATF4 is a transcription factor which upregulates the expression of the phosphatase GADD34, which dephosphorylates and inhibits eIF2α creating a negative feedback loop. The activated IRE1 alternatively splices the transcript of X-box binding protein-1 (XBP1), producing an active transcription factor which induces the expression of ER chaperones and ERAD proteins. Activated ATF6 translocates to the Golgi, where it is cleaved by proteases site 1 protease (S1P) and site 2 protease (S2P). The resulting N-terminal fragment is an active transcription factor which enhances various ER chaperone expression. If ER stress persists, cells undergo apoptosis through the activation of the pro-apoptotic factor, C/EBP homologous protein (CHOP) in PERK signalling.

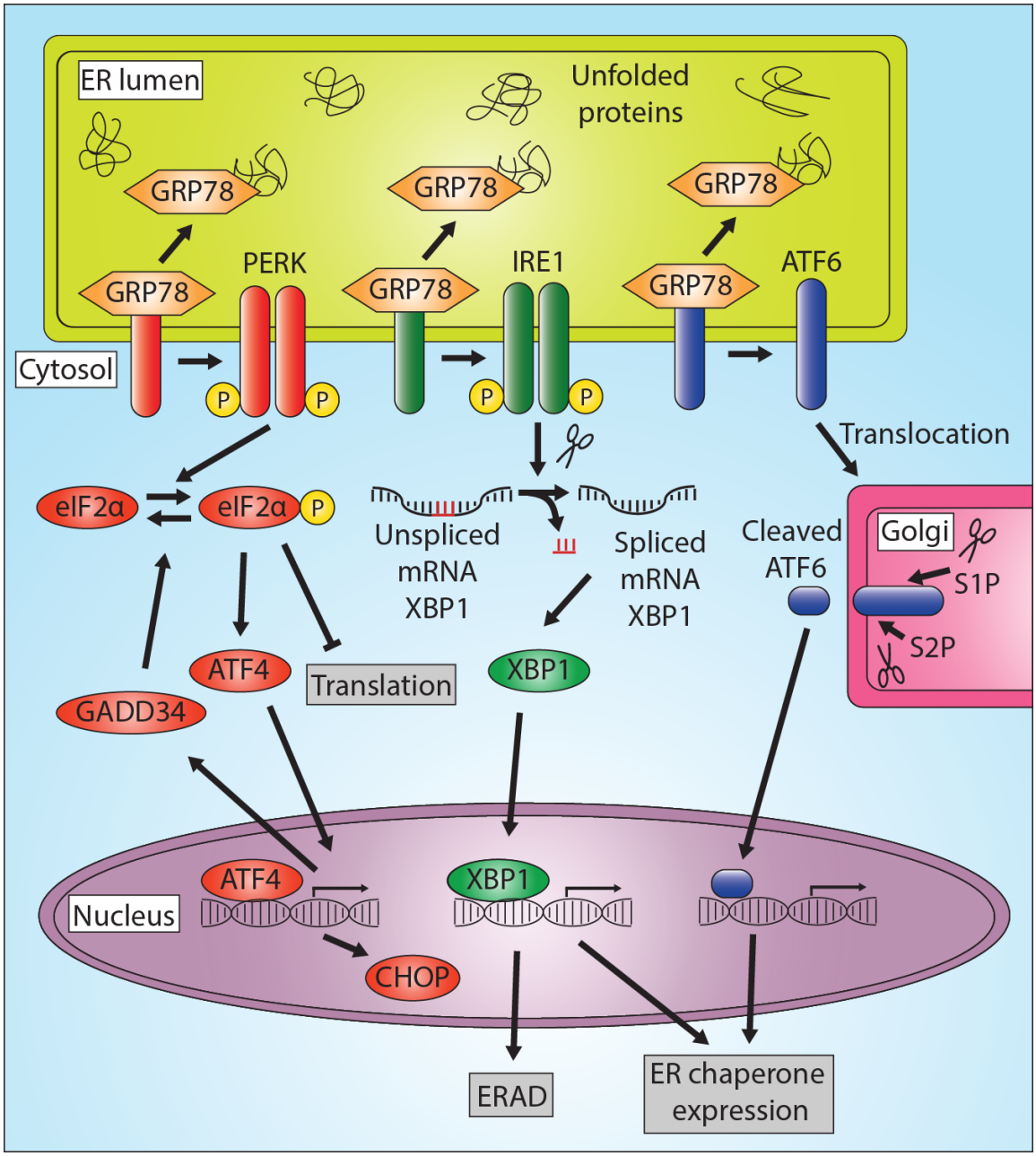
ER lumen
Unfolded proteins
GRP78
GRP78
GRP78
GRP78
GRP78
GRP78
PERK
IRE1
ATF6
Cytosol
P
P
P
P
Translocation
eIF2α
eIF2α
P
Unspliced mRNA XBP1
Spliced mRNA XBP1
Cleaved ATF6
Golgi
S1P
S2P
ATF4
Translation
XBP1
GADD34
Nucleus
ATF4
XBP1
CHOP
ERAD
ER chaperone expression

1.4 The role of endoplasmic reticulum stress in atherosclerosis

There is evidence suggesting a causative role for ER stress in the pathology of several chronic diseases including atherogenesis[27–30]. ER stress has been shown to promote lipid accumulation by activating transcription factors which regulate cholesterol and triglyceride biosynthesis and uptake, known as sterol regulatory element-binding proteins (SREBPs).[24-26] ER stress also activates nuclear factor (NF)-κB, a transcription factor responsible for the upregulation of inflammatory cytokines such as tumor necrosis factor (TNF)-α and IL-6.[27-29] Further, ER stress has been shown to promote caspase activity, which induces apoptosis.[30, 31] The dysregulation of lipid metabolism and lipid accumulation, increased inflammation, and apoptosis are hallmark features of atherosclerosis. However, the underlying molecular mechanisms by which ER stress activates these pro-atherogenic pathways are not well understood.

1.5 Glycogen synthase kinase-3

Glycogen synthase kinase (GSK3), a serine/threonine kinase, is involved in various cellular pathways and has also been linked to a number of other diseases including bipolar mood disorder[31], diabetes[32], and Alzheimer's disease[33]. There are two forms of GSK3 in mammals: GSK3α (51 kDa) and GSK3β (47 kDa); as well as the splice variant of GSK3β, GSK3β2, which contains a 13 residue insert in the kinase domain and is primarily localized to neuronal cell bodies[34]. The two main isoforms are 98% homologous in the kinase domain and are expressed ubiquitously[35]. Nevertheless, the two isoforms appear to have both redundant and distinct functionality. For example, both isoforms appear to display similar roles in the phosphorylation of the transcriptional

regulator β-catenin[36]. On the other hand, GSK3β is significantly more efficient at phosphorylating phosphatase inhibitor 2, a regulatory subunit of the ATP-Mg-dependent protein phosphatase, compared to GSK3α[37]. Many potential common and specific substrates of GSK3α/β have been identified, and the list is still growing. The physiological significance of most of these substrates is unclear.

1.6 Endoplasmic reticulum stress and glycogen synthase kinase-3

Our lab and others have demonstrated that ER stress activates GSK3α/β [38–40]. We have previously shown that GSK3α/β regulates the distal components of the PERK signalling pathway, rather than the adaptive components of the UPR[40]. The activation of GSK3α/β upregulate the transcription factors ATF4 and CHOP. Furthermore, GSK3α/β have been shown to regulate lipid uptake and biosynthesis, and the expression of inflammatory cytokines in macrophages. The inhibition of GSK3α/β attenuated the uptake of free and modified cholesterol, as well as the expression of genes involved in regulating lipid and cholesterol metabolism, such as fatty acid synthase (FAS), sterol regulatory element binding protein (SREBP)-1c, SREBP-2, 3-hydroxy-3-methylglutaryl-coenzyme A (HMGCoA) reductase, and low-density lipoprotein receptor (Ldlr)[40]. GSK3α/β is involved in the production of several pro-inflammatory cytokines including IL-6, IL-1β, and tumor necrosis factor TNF-α through activating the transcriptional activity of nuclear factor NF-κB[41]. Moreover, inhibiting GSK3α/β reduced the expression of pro-inflammatory cytokines and augments anti-inflammatory cytokine production such as IL-10. These findings indicate a role of GSK3α/β in cell survival, and the formation of

foam cells, and the production of inflammatory cytokines. Moreover, GSK3α/β may represent a link between ER stress and the pro-atherosclerotic processes.

1.7 Blocking the progression of atherosclerosis

In vivo data have shown that the modulation of the ER stress-GSK3α/β pathway can impede atherogenic development. For example, Erbay and colleagues have shown that the mitigation of ER stress, using a chemical chaperone known as 4-phenylbutyrate (4PBA), is protective against atherosclerosis in *Apoe*$^{-/-}$ mice[42]. Our group has shown that atherosclerosis is attenuated in *Apoe*$^{-/-}$ treated with valproate (VPA), an anti-epileptic drug and a known GSK3α/β inhibitor[43]. Whole body[39] or myeloid GSK3α deficiency[44] protects against atherosclerosis in low density lipoprotein receptor deficient (*Ldlr*$^{-/-}$) mice. Mice with myeloid GSK3β deficiency were not protected against atherosclerosis, which may suggest a greater role of GSK3α in macrophages in the development of atherosclerosis compared to the beta isoform[44]. Consistent with these findings, a pharmacoepidemiological study revealed that patients with epilepsy who were treated with VPA had a significantly lower risk of myocardial infarctions, a potential complication of atherosclerosis[45]. Together, these studies suggest that the ER stress-GSK3α/β pathway is involved in atherosclerotic processes; intimating that ER stress and GSK3α/β may be potential therapeutic targets for anti-atherosclerotic therapies **(Figure 1.3)**. Nothing is known with regard to the potential role of this pathway in the regression of atherosclerosis.

Figure 1.3. Working model: The endoplasmic reticulum (ER) stress-glycogen synthase kinase (GSK)-3α/β signaling pathway in promoting atherosclerosis.

Multiple cardiovascular risk factors, such as dyslipidemia, hypertension, and smoking, induce ER stress. In response to ER stress, the cell activates the adaptive components of the unfolded protein response (UPR) to attenuate translation, promote ER-associated protein degradation (ERAD), and upregulate the expression of ER chaperones. Downstream of these adaptive mechanisms, protein kinase R-like endoplasmic reticulum kinase (PERK) signaling activates GSK3α/β through the phosphorylation (P) and activation of eukaryotic initiation factor 2α (eIF2α). Subsequently, GSK3α and/or GSK3β mediate the distal components of the UPR including cell C/EBP homologous protein (CHOP) expression, foam cell formation, and inflammation, which contribute towards the acceleration of atherosclerosis.

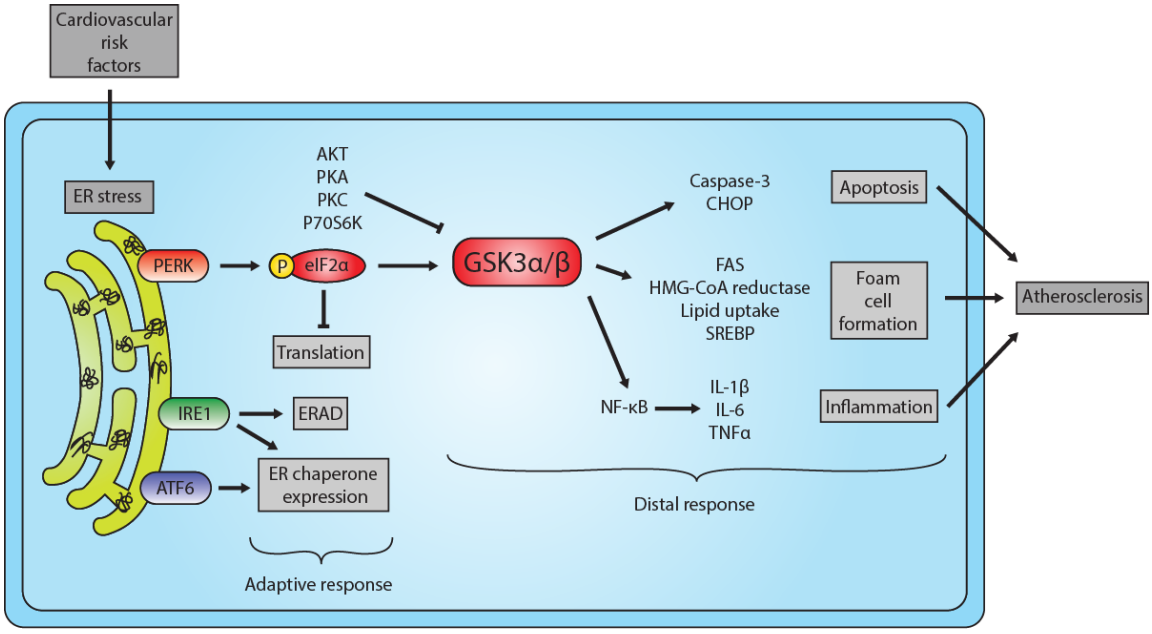
Cardiovascular risk factors
ER stress
PERK
IRE1
ATF6
AKT
PKA
PKC
P70S6K
P
eIF2α
Translation
ERAD
ER chaperone expression
Adaptive response
GSK3α/β
Caspase-3
CHOP
FAS
HMG-CoA reductase
Lipid uptake
SREBP
NF-κB
IL-1β
IL-6
TNFα
Distal response
Apoptosis
Foam cell formation
Inflammation
Atherosclerosis

1.8 Statin therapy

Although there is currently no cure for atherosclerosis, treatment can impede the advancement of the disease and prevent further complications of atherosclerosis. Lowering LDL cholesterol is a primary goal of preventing atherosclerotic CV events[72]. Healthy lifestyle changes, which include limiting cholesterol intake to <200mg/day, increasing physical activity, and ceasing to smoke, are the first line of therapy to reduce LDL cholesterol and prevent CV consequences. However, lifestyle changes alone may not be sufficient in achieving target goals, and patients may need additional medicine to help lower LDL cholesterol levels. Lipid lowering therapy include the use of bile acid sequestrants (such as colesevelam), the cholesterol absorption inhibitor ezetimibe, fibrates (such as gemfibrozil), niacin, and statins[75]. Other medications may be prescribed to help prevent inflammation, to lower blood pressure, or to lower blood glucose levels.[72–74].

Statins, also known as HMG-CoA reductase inhibitors, are considered to be the lipid-lowering agent of choice because they are currently the most effective and most safe in reducing LDL cholesterol levels[72,75]. The cardiovascular protective effects may also be a result of the pleiotropic effects of statins, which include its anti-inflammatory and anti-oxidant properties, as well as the improvement of endothelial dysfunction[76]. There are many different statins available on the market (e.g. atorvastatin, fluvastatin, lovastatin, pravastatin, rosuvastatin, and simvastatin). They can decrease LDL cholesterol and triglyceride levels up to 55% and 30% respectively, and increase HDL cholesterol of up to 15% depending on the dose and statin used[72]. The use of statins in clinical trials have

been shown to significantly reduce the risk of coronary heart disease, CV events, and mortality[72,75].

1.9 Atherosclerosis regression

Evidence suggests that atherosclerotic plaques can be stabilized and/or resolved. Atherosclerotic regression is possible through the removal of lipids and necrotic bodies, improvement of endothelial function, and restoration of denuded areas[46]. The earliest interventional study to show effective regression was performed in the 1950s[47]. The rabbits displayed elevated levels of total plasma cholesterol (~26 mmol/L) and large lesions in the aorta after fed a high fat diet for three months. However, 10 days of intravenous injections containing phosphatidylcholine resulted in a significant reduction in arterial cholesterol stores and a reduction in plaque size. Since then, others have demonstrated that atherosclerosis can be reversed in various animal models such as rabbits, primates, mice, and pigs. These studies typically employed strategies to aggressively lower plasma LDL cholesterol levels through dietary changes, transplantation of vessels with lesions to normal hosts, transgene therapy, or methods to promote lipid efflux or enhance HDL cholesterol levels[48,49]. In these studies, large reductions in plasma LDL cholesterol levels were required to achieve regression. However, lipid lowering strategies (statin therapy) in humans is usually insufficient to reach or maintain the low LDL cholesterol levels that is possible in non-human primates. Therefore, the use of stronger lipid lowering strategies, such as proprotein convertase subtilisin/kexin type 9 (PCSK9) inhibitors, or the use of alternative therapies targeting

other aspects of atherogenesis, in parallel to lipid lowering strategies, may be required to achieve regression in human patients.

1.10 Myeloid cell biology

Hematopoietic stem cells (HSCs) generate all blood cells through the process called haematopoiesis[50]. HSCs differentiate into lymphoid or myeloid cell lines. The production of lymphocytes begins with the differentiation of HSCs into common lymphoid progenitor cells (CLPCs). CLPCs can differentiate to give rise to T cells, B cells, and natural killer cells. Conversely, myeloid cell production starts with the differentiation of HSCs into common myeloid progenitor cells (CMPCs). CMPCs differentiate into megakaryocytes, erythrocytes, mast cells, or myoblasts. Myoblasts produce basophils, neutrophils, eosinophils and monocytes.

Monocytes are released from the bone marrow and circulate in the blood[51]. Monocytes further differentiate into dendritic cells or macrophages during inflammation. There are two subtypes of dendritic cells: Classical dendritic cells (cDCs) which are specialized in antigen-processing and presenting, and plasmacytoid dendritic cells (pDCs) which are specialized to respond to viral infections by producing type I interferons. Conversely, macrophages are believed to maintain tissue homeostasis via clearing apoptotic cells and producing growth factors.

Macrophages can be polarized into distinctly different sub-types by exposure to diverse cytokines. Exposure to T helper type 1 (Th1) cell products, such as IFNγ or microbial products such as lipopolysaccharide (LPS), give rise to classical M1 macrophages[52]. T helper type 2 (Th2) cell products, such as IL-4 or tumor growth factor

(TGF)-β, produces the alternative M2 macrophages. The M1 macrophages phenotype can be characterized by the high production levels of pro-inflammatory cytokines, which M2 macrophages are characterized by their tissue remodelling properties and secretion of anti-inflammatory cytokines[53,54]. Other subtypes of macrophages have been identified (M_{ox}, $M_{hem,}$ M4 etc), but the M1 and M2 macrophages are considered to be the polar extremes of the broad range of macrophage phenotypic subtypes[55] **(Figure 1.4)**. Macrophages of the M1 phenotype are considered to be pro-atherogenic and are involved plaque progression[57]. Conversely, there appears to be a protective role of M2 macrophages in atherosclerosis and may be important in regression atherosclerotic plaques. M1 and M2 macrophages localize in different regions of the atherosclerotic lesions[58]. M1 macrophages are predominantly found in rupture prone shoulder regions while M2 macrophages localize to more stable cell-rich areas of plaque away from the necrotic core[59]. There were no differences in the distribution of the subsets at the fibrous caps[58]. Furthermore, macrophages have been shown to be plastic and can actively change their physiology/subtype depending on environmental stimuli[60]. It should also be noted that the M1-M2 paradigm may require further scrutiny due to the discovery of more polarized states which cannot be categorized along the M1-M2 spectrum[61–63].

Figure 1.4. Macrophage polarization.

Precursor M0 macrophages are polarized to M1 macrophages through the classical pathway, where type 1 T-helper (Th1) inflammatory cytokines and/or bacterial components promote the expression of pro-inflammatory cytokines such as TNFα, IL-1β, and IL-6. Conversely, polarization to M2 macrophages through the alternatively activated pathway are induced by type 2 T-helper (Th2) cytokines such as IL-4 and IL-13. M2 macrophages are involved in tissue remodeling and wound repair though the production of cytokines such as IL-10. Although macrophages can be broadly categorized as being pro-inflammatory (M1) or alternatively activated (M2), plasticity results in a spectrum of macrophage subtypes with fully polarized M1 and M2 macrophages at the polar extremes.

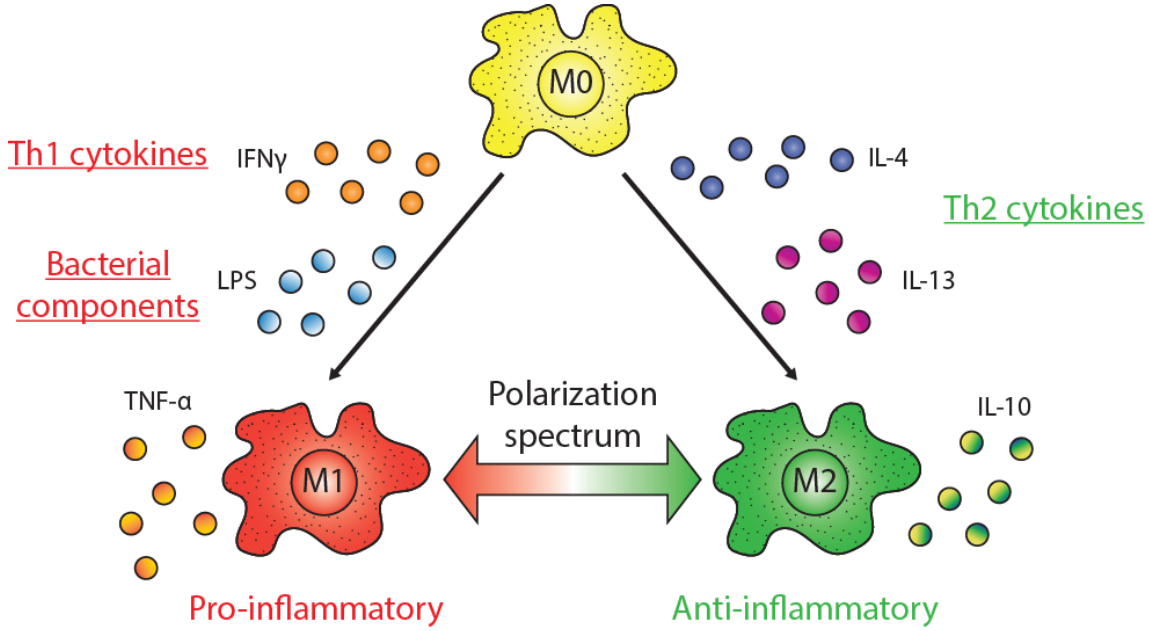
M0
Th1 cytokines
IFNγ
Bacterial components
LPS
IL-4
Th2 cytokines
IL-13
TNF-α
Polarization spectrum
IL-10
M1
M2
Pro-inflammatory
Anti-inflammatory

1.11 Monocyte and macrophage dynamics in atherosclerosis

Monocytes/macrophages are the main cellular components within atherosclerotic lesions[64]. Until recently, it was believed the accumulation of macrophages resulted solely from the recruitment of blood monocytes. However, recent evidence suggests that local macrophage proliferation greatly contributes to macrophage accumulation, and the turnover of macrophages are replenished predominately by local proliferation rather than monocyte influx[65]. Furthermore, it has recently been shown that resident macrophages found in the adventitia originate from the yolk sac embryonically, and are maintained via local proliferation[64,66]. These residential macrophages may also contribute to the progression of the disease, however, their contributions towards atherogenesis are not yet clear.

The lack of effective efferoctyosis, where apoptotic bodies are engulfed and cleared by phagocytic cells such as macrophages, contributes towards the growing necrotic core. The impairment of clearance is associated with an upregulation of anti-phagocytic 'don't eat me' signals, such as cluster of differentiation (CD)-47[67]. This impairment, along with the reduced capacity of accumulated macrophages to migrate out of the lesion,[68] compounds inflammation and further contributes to the progression of more advanced lesions. The resolution of impaired efferocytosis and egress can revert the accumulation of macrophages within plaques, alleviate necrotic bodies, and help facilitate regression.

Traditionally, VSMCs and macrophages have been thought to originate from mutually exclusive cell lineages. However, recent cell lineage tracing experiments have

revealed that cells of VSMCs origin can become foam cell-like, and myeloid foam cells can behave like VSMCs[69]. This leads to the possibility of transdifferentation, where some macrophages may have be derived from VSMCs and *vice versa*[70].

These studies demonstrate our current lack of understanding of atherosclerosis. However, the model of the disease is constantly revised as new evidence emerges. Novel findings will allow us to better understand the progression of atherosclerosis and help identify new targets or innovative strategies to combat the disease.

CHAPTER 2: HYPOTHESIS AND OBJECTIVES

2.1 Hypothesis

We hypothesize that ER stress induced activation of GSK3α and/or β promotes pro-atherosclerotic processes.

We believe that attenuating ER stress or inhibiting GSK3α/β will impede the progression of atherosclerosis and promote regression in existing lesions. These effects may be a result of reduced inflammation, increased cell viability, and/or reduced lipid accumulation.

2.2 Objectives

The objectives of these studies are to:

1. Determine the effect of attenuating ER stress or inhibiting GSK3α/β in a *Ldlr*$^{-/-}$ pro-atherogenic mouse model.

2. Assess whether attenuating ER stress or inhibiting GSK3α/β can reverse atherosclerosis.

3. Investigate the potential pro-atherogenic effects of ER stress – GSK3α/β signaling in cultured bone marrow derived macrophages.

CHAPTER 3: 4-PHENYLBUTYRATE AND VALPROATE TREATMENT ATTENUATE THE PROGRESSION OF ATHEROSCLEROSIS AND STABILIZE EXISTING PLAQUES

Aric Huang[a,b], Tayler L. Young[a], Vi T. Dang[a,b], Yuanyuan Shi[a], Cameron S. McAlpine[a,c], and Geoff H. Werstuck[a,b,c]

[a]Thrombosis and Atherosclerosis Research Institute, [b] Department of Chemistry and Chemical Biology, [c]Department of Medicine, McMaster University, Hamilton Ontario

3.1 Foreword

This study investigates the possibility to prevent and treat atherosclerosis by using small molecule inhibitors which modulates the ER stress-GSK3α/β pathway. We showed here that treatment with 4-phenylbutyrate or valproate attenuates atherosclerotic progression. Moreover, these treatment do not regress atherosclerosis, but appear to stabilize existing lesions.

This work was submitted in the journal Atherosclerosis on March 8, 2017. The experiments in this study was carried out by Aric Huang with assistance from the co-authors. The manuscript was written by Aric Huang in collaboration with Dr. Geoff Werstuck. The content of Chapter 3 is a direct representation of the submitted manuscript.

3.2 ABSTRACT

Objective

Recent evidence suggests that endoplasmic reticulum (ER) stress signaling through glycogen synthase kinase (GSK)-3α/β is involved in the activation of pro-atherosclerotic processes. In this study, we examined the effects of small molecules that interfere with ER stress-GSK3α/β signaling on the progression and regression of atherosclerosis in a mouse model.

Approach and results

To examine atherosclerotic progression, low density lipoprotein receptor deficient (*Ldlr*$^{-/-}$) mice were placed on a high fat diet (HFD) and treated with the chemical chaperone, 4-phenylbutyrate (4PBA, 3.8g/L drinking water), or the GSK3α/β inhibitor, valproate (VPA, 625mg VPA/kg diet), for 10 weeks. The 4PBA- and VPA-treated mice had significantly reduced lesion and necrotic core size. Treatments had no effect on metabolic parameters, including plasma and hepatic lipid levels, or plaque composition. To examine potential effects on atherosclerotic regression, 4 week old *Ldlr*$^{-/-}$ mice were placed on a HFD for 16 weeks. Subsets of mice were harvested at this time or switched to a chow (low fat) diet, or a chow diet with 4PBA or VPA treatment for 4 weeks. Mice with 4PBA or VPA treatment showed no alterations in lesion size, but the lesions had significantly smaller necrotic cores, increased vascular smooth muscle cell content, and increased collagen content. These features are consistent with more stable plaques.

Conclusions

The pharmacological attenuation of ER stress or inhibition of GSK3α/β impedes the development of atherosclerosis in *Ldlr*$^{-/-}$ mice and appears to promote the stabilization of existing lesions.

3.3 INTRODUCTION

Atherosclerosis is an inflammatory disease characterized by the accumulation of fatty plaques within the arterial wall. It is the major underlying cause of cardiovascular disease, which is the leading cause of mortality worldwide, accounting for approximately 30% of all deaths[1,2]. Risk factors that contribute to the progression of atherosclerosis include diabetes mellitus, dyslipidemia, hypertension, obesity, and smoking[3]. The major complications of atherosclerosis can be attributed to thrombus formation following plaque rupture, which may occlude the artery and result in myocardial ischemia or infarction[4,5]. Despite many advances, our understanding of the molecular mechanisms that link cardiovascular risk factors to the development of atherosclerosis is incomplete. Furthermore, the potential to reverse the atherogenic process, through the resolution or stabilization of existing plaques, has only just begun to be investigated.

Recently, our group and others have established a causative role for endoplasmic reticulum (ER) stress in the development and progression of atherosclerosis[6–8]. The ER is a eukaryotic organelle responsible for protein modification, protein folding, and protein trafficking. When the processing capacity of the ER is exceeded, there is an accumulation of misfolded and unfolded proteins in the ER, a condition known as ER stress. The

proximal intracellular response to ER stress is the activation of the unfolded protein response, which acts to reduce the protein load and increase ER folding capacity[9]. Chronic, unresolved ER stress can lead to activation of intracellular pathways that, depending on the magnitude and cell type, can include increased expression of inflammatory cytokines[10], increased biosynthesis and accumulation of cholesterol and triglycerides[11], and activation of pro-apoptotic processes[12]. There is a growing body of evidence that implicates ER stress in the development of several metabolic diseases and disorders including cancer, neurodegeneration, type 2 diabetes, liver disease, and atherosclerosis[13].

The mitigation of ER stress using a chemical chaperone, 4-phenylbutyrate (4PBA), has been shown to be protective against atherosclerosis in apolipoprotein E deficient (*ApoE*$^{-/-}$) mice[14]. However, the underlying molecular mechanisms by which ER stress affects downstream pro-atherogenic pathways are not well understood. Results from our lab and others have suggested that ER stress may signal through the activation of glycogen synthase kinase (GSK)-3α/β to promote the development of atherosclerosis[15–17]. GSK3α/β is a serine/threonine kinase that is involved in the regulation of several different metabolic pathways and implicated in the development of a number of diseases[18]. We have shown that atherosclerosis is attenuated in *ApoE*$^{-/-}$ mice treated with valproate (VPA), an anti-epileptic drug and a known GSK3α/β inhibitor, as well as in low density lipoprotein receptor deficient (*Ldlr*$^{-/-}$) mice with either whole body or myeloid GSK3α deficiency[17,19,20]. Together, these studies suggest that the ER stress-GSK3α/β pathway is involved in the activation of pro-atherosclerotic processes, and therefore may

be a target for anti-atherosclerotic therapies. The effect of pharmacological mitigation of ER stress and the inhibition of GSK3α/β on established atherosclerotic lesions have not been investigated. Therefore, in this study we examined the impact of the chemical chaperone 4PBA, and the GSK3α/β inhibitor VPA, on the development, progression and regression of atherosclerosis in *Ldlr*$^{-/-}$ mice.

3.4 METHODS

Mouse models

All animal experiments were pre-approved by the McMaster University Animal Research Ethics Board. Female *Ldlr*$^{-/-}$ mice (B6.129S7-*Ldlr*^{tm1Her}/J) were purchased from Jackson Labs. Mice were fed a high fat diet (HFD) containing 21% fat and 0.2% cholesterol, with 42% calories from fat (Harlan Teklad, TD97363) or a standard chow diet containing 18% protein and 5% fat, with 18% calories from fat (Envigo, 2918). Treatment of the chemical chaperone, sodium 4-phenylbutyate (4PBA), consisted of 3.8g/L drinking water. This concentration was determined by monitoring water intake by the mice, which corresponds to approximately 1g 4PBA/kg body weight/day. Treatment of the GSK3α/β inhibitor, sodium valproate (VPA) consisted of 625 mg VPA/kg diet. All mice had unrestricted access to food and water, and were maintained on a 12-hour light/dark cycle. Mice were fasted for 6 hours prior to sacrifice. Fasting blood glucose was measured using an UltraMini blood glucose meter (OneTouch). Mice were anesthetized with 3% isoflurane, blood was collected via cardiac puncture and livers and perigonadal fat pads were weighed and flash frozen. Perigonadal fat pads were collected as they are large, easily identified, and readily accessible. The vasculature was flushed

with 1X PBS buffer and perfusion fixed with 10% neutral buffer formalin. Hearts and aortas were collected and formalin fixed.

Plasma PBA and VPA quantification

Sample preparation, liquid chromatographic system and mass spectrometer parameters were as previously described[21]. L-phenylalanine-d8 and L-tryptophan-d5 were used as recovery and internal standards, respectively. Gradient elution was modified to allow for a faster method for targeted quantification. Mobile phase A was 100% acetonitrile (LCMS grade, Sigma Aldrich) and mobile phase B was 100% water (LCMS grade, Sigma Aldrich). Gradient elution started with 95% A for 0.5 min and then linearly decreased to 30% A at 10 min, held at 30% A for 1 min followed by a ramping up to 95% A for 1 min. The columns were then re-equilibrated for 12 min at 95% A prior to subsequent sample analysis.

The acquired mass spectra were calibrated internally using endogenous sodium formate clusters (Bruker Daltonics DataAnalysis 4.0). Peak areas integrated were normalized with both recovery and internal standards.

Determination of lipid content

Plasma was fractioned using fast performance liquid chromatography with the FRAC-950 FPLC (Amersham Pharmacia Biotech) as previously described[22], and the cholesterol concentration was measured using the Infinity cholesterol reagent (Thermo Scientific). Frozen livers were homogenized and lipids were extracted with chloroform, followed by resuspension in isopropanol. Total plasma and tissue cholesterol and

triglyceride levels were determined using the Infinity Reagent (Thermo Scientific).

Characterization of aortic lesions

Hearts and aortas were embedded in paraffin and 5 μm sections of the aortic root were collected onto slides as previously described[23]. Sections were deparaffinized and stained with Harris hematoxylin and eosin (Sigma) or Masson's Trichrome (Sigma) for atherosclerotic lesion, necrotic core, and lesional collagen quantification. After removing surrounding fat and connective tissue, aortic arch and descending aorta were opened longitudinally and stained with Sudan IV solution.

For immunofluorescent and immunohistochemical staining, sections were deparaffinized and antigen retrieval performed, where necessary. After blocking with 10% normal serum, sections were immunostained with primary antibodies against the macrophage marker CD107b (Mac3, BD Transductions), vascular smooth muscle cell (VSMC) marker α-actin (Santa Cruz), and cell proliferation marker Ki67 [SP2] (Abcam). Secondary antibodies (BD transductions) conjugated to a fluorophore were used for detection. Separate sections were stained with pre-immune IgG instead of primary antibodies to control for non-specific staining **(Supplemental Figure 3.1)**. The DeadEnd™ Fluorometric TUNEL System kit (Promega) was used according to manufacturer's instructions to measure apoptotic cell death. 4′,6-diamidino-2-phenylindole dihydrochloride (DAPI, Invitrogen) was used for immunofluorescent counterstaining. On a separate subset of mice, hearts were imbedded in optical cutting temperature (OCT) compound (Tissue-Tek) and frozen. OCT imbedded frozen tissue was serial sectioned at 10 μm and stained with Oil Red O (Sigma). Images of the stained

sections were collected using Leitz LABORLUX S microscope connected to a DP71 Olympus camera. Lesion area and immunofluorescent staining was quantified using Image J 1.48v software.

Statistical analysis

GraphPad Prism 7 was used to perform all statistical analysis. Data were analyzed by one or two-way ANOVA, followed by the Bonferroni multiple comparison test between all groups. Error bars on all graphs represent the standard error of the mean. Data on tables are expressed as arithmetic means ± standard deviation. For all experiments, a p value lower than 0.05 was considered statistically significant. * $p<0.05$, ** $p<0.01$, *** $p<0.001$, **** $p<0.0001$.

3.5 RESULTS

4PBA and VPA attenuate the development of atherosclerosis

Ldlr$^{-/-}$ mice do not develop atherosclerosis lesions spontaneously, but do develop lesions when fed a high fat diet (HFD)[24]. Four week old female *Ldlr*$^{-/-}$ mice were placed on a HFD containing 21% milk fat and 0.2% cholesterol, for 10 weeks. To determine the impact of 4PBA and VPA treatment on the early stages of atherosclerotic development, separate groups of mice were fed the HFD and treated with 3.8g 4PBA/L drinking, or 625mg VPA/kg diet. All mice were sacrificed at 14 weeks of age and tissues were processed as previously described **(Figure 3.1A)**[20,25].

Relative to the control, no significant differences in total body weight, fasting blood glucose, liver weight, or fat pad weight were observed after 10 weeks of treatment with either 4PBA or VPA **(Supplemental Table 3.1)**. 4PBA or VPA were only detected in the plasma of the mice treated with 4PBA or VPA, respectively. There were also no significant differences in plasma or hepatic cholesterol and triglyceride levels, or plasma lipid profiles **(Supplemental Figure 3.2)**.

To investigate the effects of 4PBA and VPA on atherosclerosis, cross-sections of the aortic root were stained with hematoxylin and eosin and the atherosclerotic lesion areas and volumes were quantified. Results show that both treatments significantly reduced atherosclerotic lesion area (~50% at 240 μm from the start of the aortic sinus), lesion volume (~46%), and necrosis (necrotic core volume normalized to lesion volume, 50.2% for 4PBA and 77.8% for VPA treatment) **(Figure 3.1B-E)**. Within the

atherosclerotic lesions, phospho-GSK3β-Ser9 staining co-localized with $Mac3^+$ cells, while intense phospho-GSK3β-Tyr216 staining was observed in the acellular necrotic region of the plaque. The treatments did not significantly affect phosphorylation staining patterns **(Supplemental Figure 3.3A-C, E)**.

To further characterize the plaque and to determine the vascular smooth muscle cell (VSMC) and macrophage content of the lesion, aortic cross sections were stained with antibodies against α-actin or Mac3, respectively. No change in VSMC content or macrophage content was observed for either treatment, relative to the control **(Supplemental Figure 3.4)**. Furthermore, analysis of lesions revealed no significant changes in caspase-3 activation **(Supplemental Figure 3.5),** collagen content **(Supplemental Figure 3.6)**, the expression of the M1 macrophage marker CD36, or the expression of the M2 macrophage marker Arg1 **(Supplemental Figure 3.7)**. These results indicate that the treatment with 4PBA or VPA for 10 weeks can impede the development of atherosclerosis without significantly altering plaque composition in *Ldlr*$^{-/-}$ mice.

Figure 3.1. 4PBA and VPA inhibit progression of atherosclerosis in *Ldlr*$^{-/-}$ mice.

A. Experimental design of the atherosclerotic progression model. *Ldlr*$^{-/-}$ female mice at 4 weeks of age were fed a high fat diet (HFD, 21% milk fat and 0.2% cholesterol) for 10 weeks. Subsets of mice were treated with 4PBA (1g/kg body weight/day in drinking water) or VPA (625 mg/kg diet). **B.** Representative hematoxylin and eosin stained sections of aortic root from mice fed HFD (control), or HFD along with 4PBA or VPA treatment for 10 weeks. Atherosclerotic lesions are outlined in yellow. Quantification of the **C.** lesion area at the aortic sinus and ascending aorta, **D.** lesion volume, and **E.** necrosis normalized to lesion volume. Data are the mean ± SEM; n = 10 mice/group, except in **E.** where numbers were lower due to outliers (n = 8-10); *$p < 0.05$, **$p < 0.01$ compared with the HFD control.

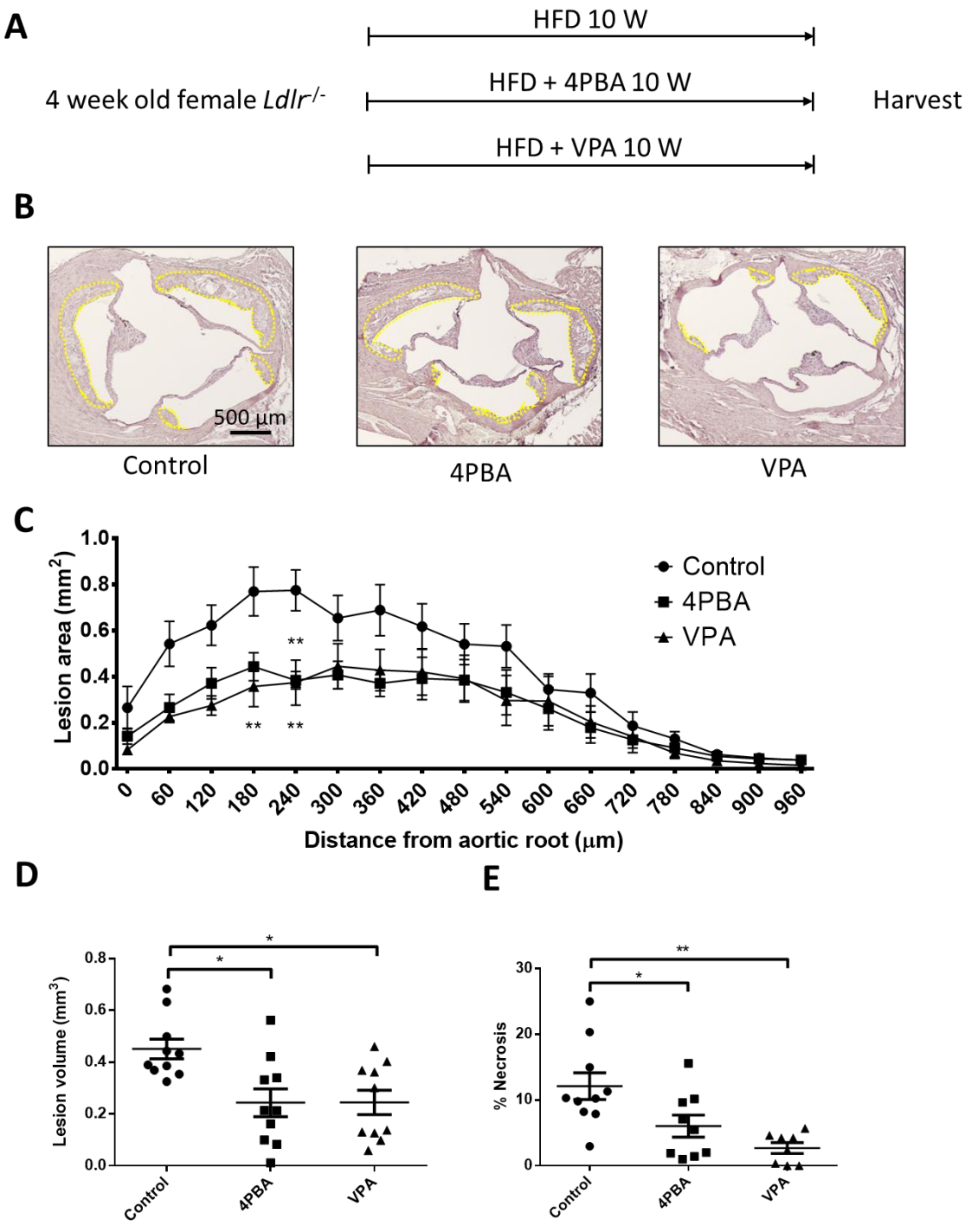
A
HFD 10 W
HFD + 4PBA 10 W
HFD + VPA 10 W
4 week old female Ldlr-/-
Harvest
B
500 µm
Control
4PBA
VPA
C
Lesion area (mm2)
Control
4PBA
VPA
Distance from aortic root (µm)
D
Lesion volume (mm3)
E
% Necrosis

4PBA and VPA attenuate further progression of established atherosclerotic lesions

To investigate the effect of 4PBA or VPA on established plaques, *Ldlr*$^{-/-}$ mice were placed on a HFD for 10 weeks prior to the treatment with 4PBA or VPA. After 10 weeks, subsets of mice were; sacrificed (baseline), switched to a low fat chow diet for 4 weeks (control), or switched to a low fat chow diet along with 4PBA or VPA treatment for four weeks. All mice were sacrificed by 18 weeks of age **(Figure 3.2A)**.

There were no significant differences in body weight, fasting blood glucose, liver weight, or fat pad weight between the treatment groups **(Supplemental Table 3.2)**. However, the control and both 4PBA- and VPA-treated mice had significantly lower total plasma cholesterol (~50%) and triglyceride (~75%) levels compared to the baseline **(Supplemental Figure 3.8A, B)**. There was also a significant decrease in cholesterol (~90%) and triglyceride (~55%) levels in the liver compared to the baseline **(Supplemental Figure 3.8C, D)**. These differences in lipid concentration are likely attributed to the diet of the mice. The baseline group, which were fed a HFD and not switched to standard chow, had elevated levels of very low density lipoprotein (VLDL), intermediate density lipoprotein (IDL), and low density lipoprotein (LDL). The diet switch to the standard chow lowered the VLDL, IDL, and LDL level in all other groups **(Supplemental Figure 3.8E)**.

The control group had significantly larger lesion area (77.0% at 240 μm from the start of the aortic sinus) and volume (56.2%) compared to the 10 week HFD baseline group indicating that the lesions continued to grow after the switch to a chow diet **(Figure 3.2B-D)**. This was unexpected since published regression studies indicated no significant

changes in lesion size in *Ldlr*$^{-/-}$ mice after a switch to chow diet[26,27]. Treatment with 4PBA significantly reduced lesion area (34.5% at 240 µm from the start of the aortic sinus), and VPA treatment significantly reduced lesion area (43.6% at 240 µm from the start of the aortic sinus) and volume (35.5%) compared to the control **(Figure 3.2B-D)**. The relative volume of the lesion that was necrotic was not significantly different between the groups **(Figure 3.2E)**. Together, these results indicate that treatment with 4PBA or VPA can prevent the atherosclerotic progression in *Ldlr*$^{-/-}$ mice with established plaques.

Figure 3.2. 4PBA and VPA inhibit the progression of atherosclerosis in *Ldlr*$^{-/-}$ mice with established atherosclerotic plaques.

A. Experimental design of the late stage atherosclerotic progression model. *Ldlr*$^{-/-}$ female mice at 4 weeks of age were fed a HFD for 10 weeks (baseline); followed by a diet change to chow (control), or a chow diet switch along with 4PBA or VPA treatment for 4 weeks. **B.** Representative hematoxylin and eosin stained sections of aortic root from each experimental group. The atherosclerotic lesions are outlined in yellow. **C.** Quantification of the lesion area at the aortic sinus and ascending aorta. Quantification of the **D.** lesion volume and **E.** necrosis volume normalized to lesion volume. n = 9-10 mice/group; *$p < 0.05$, **$p < 0.01$, ***$p < 0.001$, ****$p < 0.0001$, compared with the baseline; †$p < 0.05$, †† $p < 0.01$, compared with the control.

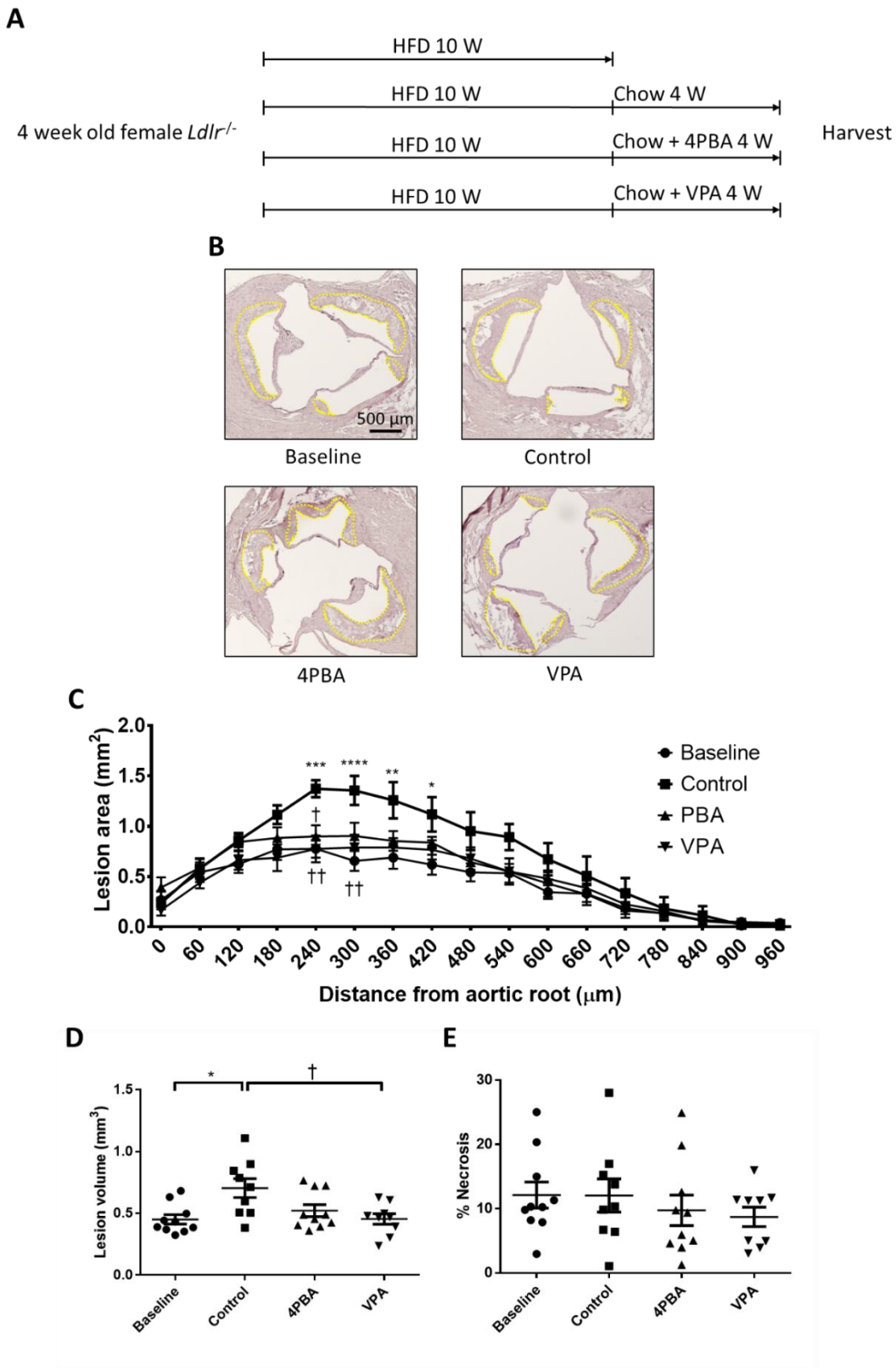
A
HFD 10 W
HFD 10 W
Chow 4 W
4 week old female Ldlr-/-
HFD 10 W
Chow + 4PBA 4 W
Harvest
HFD 10 W
Chow + VPA 4 W
B
500 µm
Baseline
Control
4PBA
VPA
C
Lesion area (mm2)
Baseline
Control
PBA
VPA
Distance from aortic root (µm)
D
Lesion volume (mm3)
Baseline
Control
4PBA
VPA
E
% Necrosis
Baseline
Control
4PBA
VPA

Treatment with 4PBA or VPA does not promote regression of established lesions

To determine if 4PBA or VPA treatment can induce the regression of atherosclerotic lesions, 4 week old female *Ldlr*$^{-/-}$ mice were placed on a HFD for 16 weeks. At this time, a subset of mice were sacrificed (baseline) whereas other subsets of mice were switched to chow (control), or chow plus 4PBA or VPA treatment for 4 weeks. All mice were sacrificed by 24 weeks of age **(Figure 3.3A)**.

There were no significant changes in body weight between experimental groups. However, there was a significant increase in fasting blood glucose in the control group (19.0%) relative to the baseline. There was a significant reduction in liver weight (~25%) between all groups relative to the baseline. Further, there was a significant reduction in fat pad weight for the control (44.2%) and 4PBA treatment group (55.8%) compared to the baseline **(Supplemental Table 3.3)**. The control and both 4PBA and VPA treated groups had a significant decrease in hepatic cholesterol (~80%) and a non- significant reduction in triglyceride, compared to the baseline **(Supplemental Figure 3.9A-B)**. The control and both 4PBA- and VPA- treated mice had significantly lower total plasma cholesterol (~60% decrease) and triglyceride (~65% decrease) levels compared to the baseline **(Supplemental Figure 3.9C-D)**. The plasma lipoprotein profiles for these mice are very similar to the late-progression mouse model, where the chow diet switch greatly reduced VLDL, IDL, and LDL levels compared to the baseline **(Supplemental Figure 3.8E, 3.9E)**. Together, the changes in metabolic parameters appear to be influenced by diet rather than the treatment with 4PBA or VPA.

To determine if 4PBA- or VPA-treatment affected lesion size, histochemical analysis was performed. Quantification of atherosclerotic plaque within the whole aorta as well as the cross-sectional aortic sinus was determined by Sudan IV and hematoxylin and eosin staining, respectively. In this model, a switch to chow diet after 16 weeks of HFD arrested lesion growth. Furthermore, no significant changes in lesion area or volume were detected between any of the experimental groups **(Figure 3.3B-E)**. However, both 4PBA and VPA treatment resulted in a significant reduction (34.7% and 42.7%, respectively) in necrosis compared to the control **(Figure 3.3F)**. The treatments did not significantly alter the phosphorylation of GSK3β at Ser9 or Tyr216 **(Supplemental Figure 3.3D, F)**, caspase-3 activation, or TUNEL staining **(Supplemental Figure 3.10)**.

Figure 3.3. 4PBA or VPA treatment does not regress atherosclerosis, but does reduce lesional necrosis.

A. Experimental design of the atherosclerotic regression model. *Ldlr*$^{-/-}$ female mice at 4 weeks of age were fed a HFD for 16 weeks (baseline); followed by a diet change to chow (control), or a chow diet switch along with 4PBA or VPA treatment for 4 weeks. **B.** Representative *en face* images of the aortic arch and thoracic aorta from experimental groups stained with Sudan IV. **C.** Quantification of the Sudan IV staining to the total area; n = 4-5 mice/group. **D.** Representative hematoxylin and eosin stained sections of aortic root from baseline, control, or 4PBA- or VPA-treated mice. Atherosclerotic lesions are outlined in yellow. Quantification of the **E.** lesion area at the aortic sinus and ascending aorta, **F.** lesion volume, and **G.** necrosis volume normalized to lesion volume. Data are the mean ± SEM; n = 9-14 mice/group, more mice were placed in the control group to ensure that lesion size have stabilized; *$p < 0.05$, **$p < 0.01$.

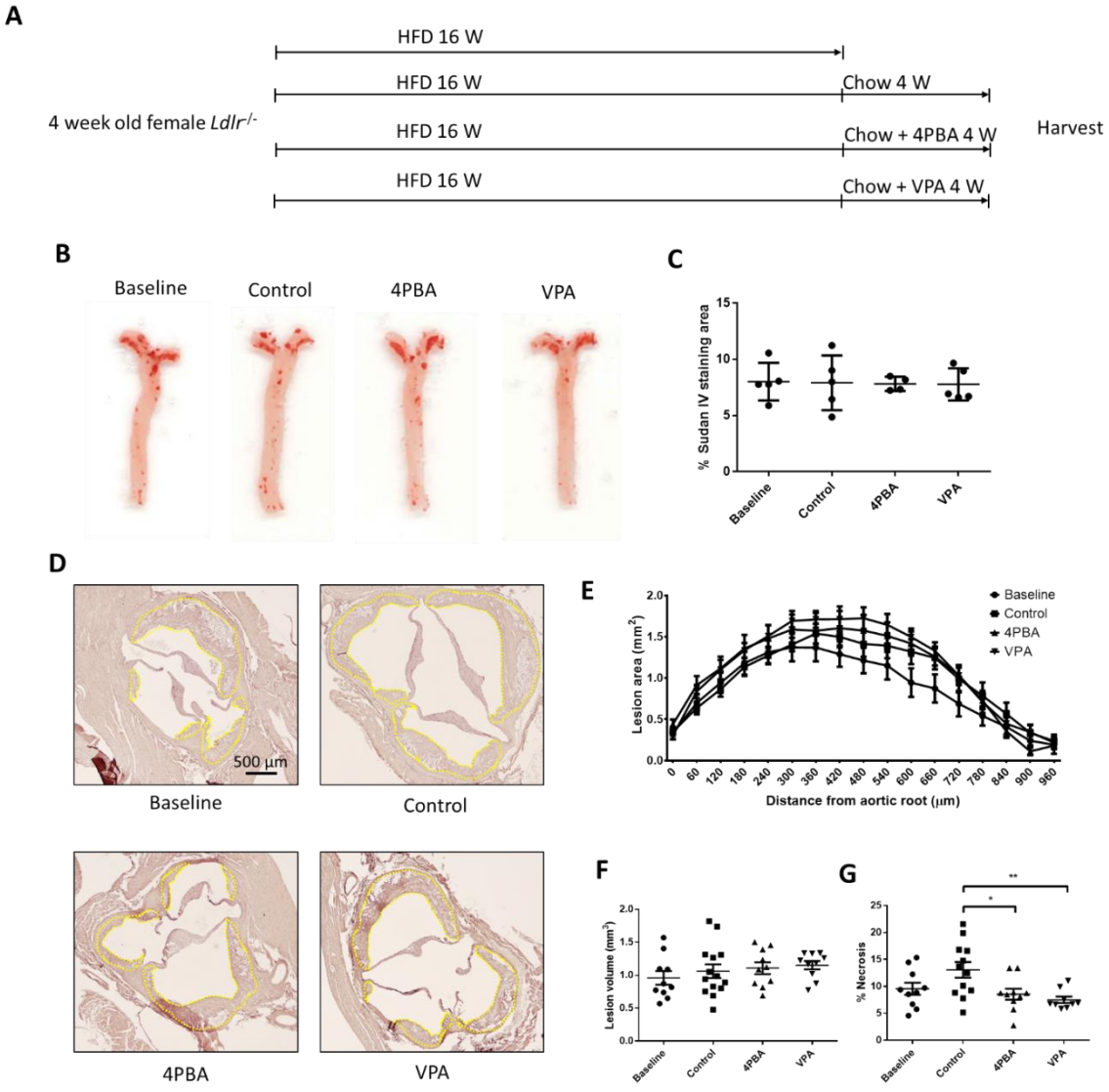
A
HFD 16 W
HFD 16 W
Chow 4 W
4 week old female Ldlr-/-
HFD 16 W
Chow + 4PBA 4 W
Harvest
HFD 16 W
Chow + VPA 4 W
B
Baseline
Control
4PBA
VPA
C
% Sudan IV staining area
Baseline
Control
4PBA
VPA
D
500 µm
Baseline
Control
4PBA
VPA
E
Lesion area (mm2)
Distance from aortic root (µm)
Baseline
Control
4PBA
VPA
F
Lesion volume (mm3)
G
% Necrosis

4PBA or VPA treatment increases lesional VSMC and collagen content

Immunofluorescence staining was used to characterize the lesion composition in each of the experimental groups. Both 4PBA and VPA treatment significantly increased lesional VSMC content by approximately 60%, relative to the control **(Figure 3.4A, C)**. 4PBA reduced lesional macrophage content by 51% compared to the baseline. Since the chow diet switch resulted in a slightly lower macrophage content (although not significant), this reduction may have resulted in part due to the alleviation of lipid burden **(Figure 3.4B, D)**. No indications of differences in macrophage or VSMC proliferation were detected in serial sections stained with the proliferation marker Ki67 (**Supplemental Figure 3.11**). Consistent with the increase in VSMC content, trichrome staining revealed that mice treated with 4PBA or VPA had a significant increase in collagen content within the plaque compared with the baseline and control, respectively **(Figure 3.5A, B)**. The quantification Oil red O staining showed no variance in neutral lipid staining between the experimental groups **(Figure 3.5C, D)**. Neither treatment appeared to alter the expression of the M1 macrophage marker CD36 **(Supplemental Figure 3.12A, C)**, or the expression of the M2 macrophage marker Arg1 **(Supplemental Figure 3.12B, D)**.

Figure 3.4. 4PBA or VPA treatment alters atherosclerotic plaque composition during atherosclerotic regression in *Ldlr*$^{-/-}$ mice.

Representative sections of aortic root stained with **A.** α-actin (red) or **B.** Mac3 (green) merged with DAPI nuclei stain (blue). Atherosclerotic lesions are outlined (yellow). Quantification of **C.** α-actin and **D.** Mac3 staining area normalized to the lesion area. Data are the mean ± SEM; n = 9-10 mice/group; *$p < 0.05$.

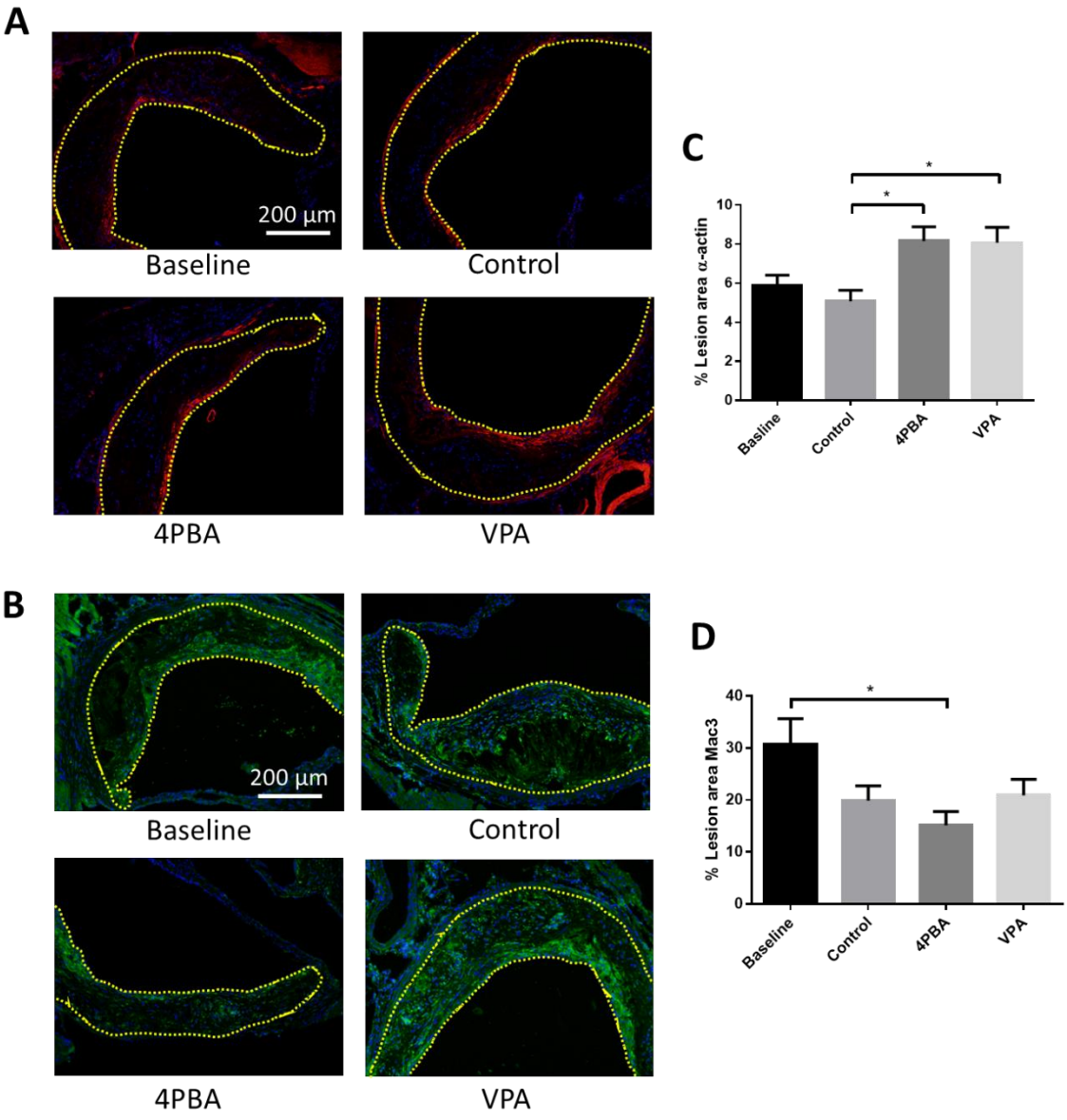
A
200 µm
Baseline
Control
4PBA
VPA
B
200 µm
Baseline
Control
4PBA
VPA
C
% Lesion area α-actin
0
2
4
6
8
10
Basline
Control
4PBA
VPA
*
*
D
% Lesion area Mac3
0
10
20
30
40
Baseline
Control
4PBA
VPA
*

Figure 3.5. 4PBA or VPA treatment increases lesional collagen content during atherosclerotic regression in *Ldlr*$^{-/-}$ mice.

Representative sections of aortic root stained with **A.** Masson's trichrome (collagen stains blue), or **B.** Oil Red O. Atherosclerotic lesions are outlined (yellow). Quantification of **C.** collagen staining area normalized to the lesion area; n = 10, and **D.** Oil Red O staining area normalized to lesion area. Data are the mean ± SEM; n = 5 mice/group; *$p < 0.05$, **$p < 0.01$.

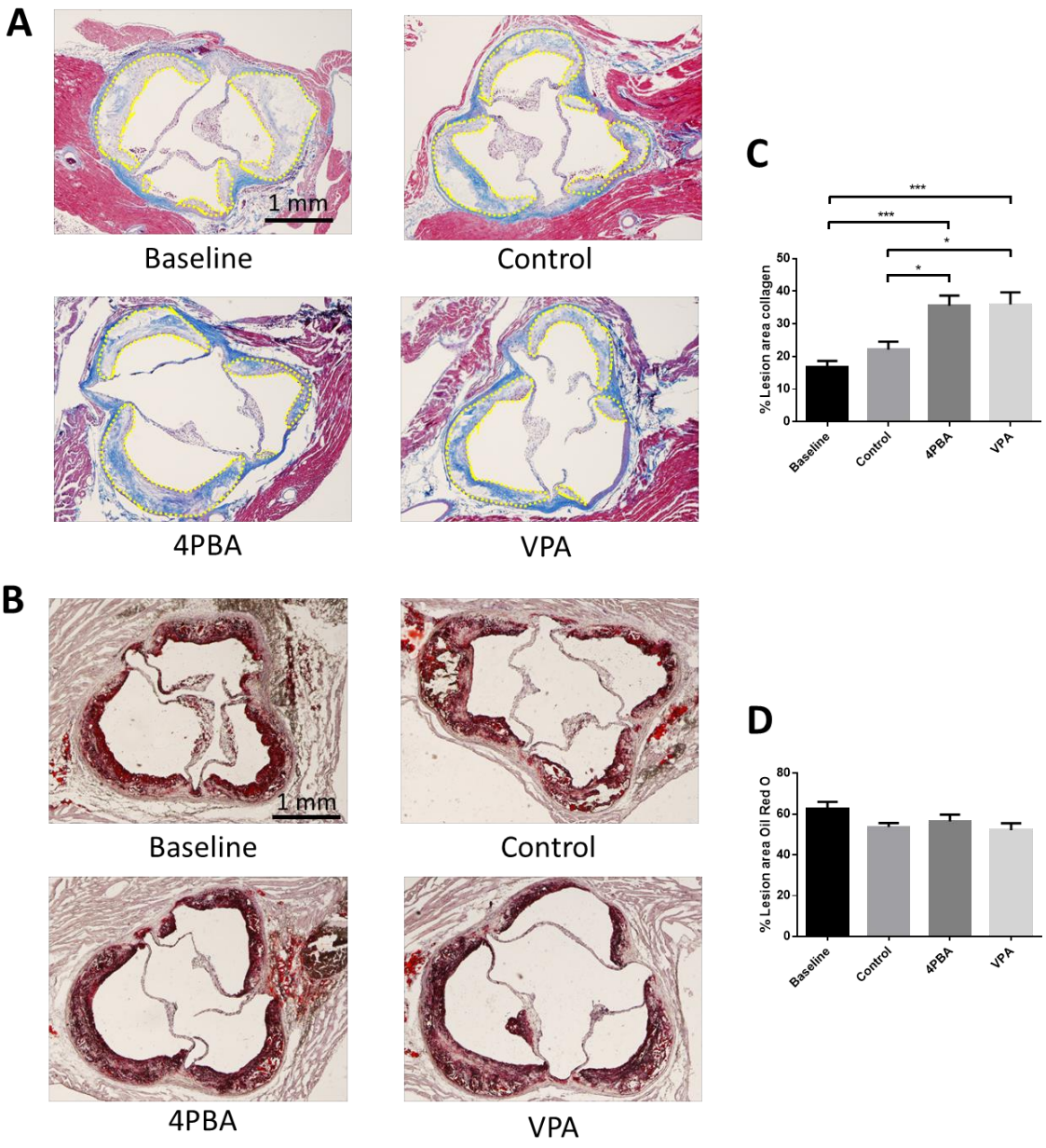
A
1 mm
Baseline
Control
4PBA
VPA
B
1 mm
Baseline
Control
4PBA
VPA
C
% Lesion area collagen
0
10
20
30
40
50
***
***
*
*
Baseline
Control
4PBA
VPA
D
% Lesion area Oil Red O
0
20
40
60
80
Baseline
Control
4PBA
VPA

3.6 DISCUSSION

We have previously identified a role for ER stress signalling through GSK3α/β in the development of accelerated atherosclerosis[28]. Here we utilize small molecule interventions to explore how this pathway may regulate atherosclerotic progression and regression in mouse models. Past studies have identified 4PBA as a chemical chaperone that can alleviate ER stress by preventing protein aggregation in the ER, both *in vitro* and in animal models[29]. We and others have shown that 4PBA can attenuate the development of atherosclerosis in *ApoE*$^{-/-}$ mice[14,30]. VPA is a short branch chain fatty acid that has been shown to inhibit GSK3α/β both directly and indirectly[31–33]. We have shown that VPA treatment can attenuate accelerated atherosclerosis in *Ldlr*$^{-/-}$ and *ApoE*$^{-/-}$ mice[17,20]. In this study, we investigated the effects of small molecule interventions, 4PBA and VPA, on the initiation, progression and regression of atherosclerosis in *Ldlr*$^{-/-}$ mice.

We have previously shown that VPA can be used *in vivo* to attenuate GSK3α/β activity using an *Apoe*$^{-/-}$ mouse model of atherosclerosis[28]. Our laboratory and others have previously shown that VPA can both directly and indirectly inhibit GSK3α/β[31,32]. The activity of GSK3α/β can be regulated by multiple mechanisms including phosphorylation (inhibitory Ser21/S9 or activating Tyr279/216), association with different protein partners, or cellular localization[34,35]. Our results indicated that neither 4PBA or VPA significantly affected the phosphorylation of GSK3β in *Ldlr*$^{-/-}$ mice.

We show that HFD fed *Ldlr*$^{-/-}$ mice presented with significantly smaller atherosclerotic lesions with smaller necrotic cores when treatment with either 4PBA or VPA was introduced prior to the initiation of atherogenesis. We also show that treatment

with either 4PBA or VPA can prevent the further progression of established lesions in *Ldlr*$^{-/-}$ mice. These results further support a role for ER stress-GSK3α/β signalling in atherosclerotic lesion development and progression. Finally, we show that treatment with 4PBA or VPA for four weeks does not reduce the size of established lesions in this model. However, the lesions of these 4PBA- or VPA-treated mice did have increased VSMC and collagen content; attributes that are indicative of more stable atherosclerotic lesions. These results are consistent with a previous study which showed that inducing ER stress in *ApoE*$^{-/-}$ mice caused a reduction in lesional VSMCs and collagen content, and an increase in necrotic core destabilization[36,37]. Furthermore, the increase in lesional VSMC and collagen found in VPA-treated mice are consistent with previous studies which have suggested a role of GSK3α/β in regulating VSMC migration and survival, and plaque stability[38,39]. Although our data suggest that ER stress/GSK3α/β regulate apoptotic pathways, we did not identify downstream pathways which mediates cell survival. However, previous studies have identified a role of GSK3α/β in regulating the anti-apoptotic protein Mcl1[40,41]. These studies implicate the possibility of the inhibition of GSK3α/β which allowed for the stabilization of Mcl1 and promote cell survival of VSMCs.

Despite recent advances in diagnostic technologies to detect atherosclerosis, the presence of this disease is often not revealed until the later stage when atherosclerotic plaques are already established[42]. Rather than looking for preventative medication, patients seeking therapeutic intervention typically already have established atherosclerosis and are looking to reverse the disease. As such, it is critical to identify the

therapeutic drug targets for regressing or reversing atherosclerosis. Toward this goal, atherosclerosis regression models have been established in rodents, swine and primates. Most of these systems have involved the drastic reduction of plasma lipid levels accomplished through dietary changes, transplant of diseased vessels into normolipidemic hosts, or induction of reverse cholesterol transport by a variety of means[43].

To investigate atherosclerotic regression, atherosclerosis was first established in an *Ldlr*$^{-/-}$ mouse by HFD feeding, after which lesion progression is stabilized by switching the mouse diet to a standard chow. Rayner *et al* (2011) have previously used this model to show that inhibition of the microRNA, miR-33, can reduce the area of established lesions by inducing the expression of the cholesterol transporter ABC transporter A1[27]. To determine if blocking the ER stress-GSK3α/β pathway can also induce regression, we treated the mice with established plaques with 4PBA or VPA, after switching to the chow diet. Similar to what we observed in the atherosclerosis progression models, neither 4PBA nor VPA treatment significantly affected body weight or plasma lipid levels. Although we did not see a reduction in lesion area or volume, we did observe changes in the morphology of the lesion that are consistent with plaque stabilization. These observations are similar to the findings of Hewing *et al* (2013), where they saw beneficial alterations in plaque composition, but no reduction in plaque size, when inhibiting microsomal triglyceride transfer protein in a similar regression model[26]. Together, our results may indicate that ER stress-GSK3α/β signalling is a driving force in the activation of proatherogenic pathways involved in lesion growth and progression. This is consistent with our previous finding that HFD fed GSK3α-deficient *Ldlr*$^{-/-}$ mice

are protected from accelerated atherosclerosis[17]. However, based on the neutral lipid and macrophage staining, the interference in ER stress-GSK3α/β signalling in established atherosclerotic lesions do not appear to promote reverse cholesterol transport and/or macrophage egress from the artery wall that would be required to significantly shrink the size of the lesions.

The results of this study support a role for ER stress signalling through GSK3α/β in the development of atherosclerosis in *Ldlr*$^{-/-}$ mice. Treatment with 4PBA or VPA also prevented the progression of established lesions. Moreover, although these treatments do appear to help stabilize the plaques in existing lesions, they do not reverse atherosclerosis. Nevertheless, increasing plaque stability is believed to be more important than decreasing absolute plaque size because unstable plaques are prone to rupture and increases the risk of cardiovascular events[44,45]. These findings are particularly interesting given that epileptic patients who were treated with VPA had a significantly lower risk of myocardial infarctions, a potential complication of atherosclerosis[46]. Indeed, 4PBA (buphenyl) is currently used in human patients to manage urea cycle disorder, and VPA is used to treat both epilepsy and bipolar disorder. The efficacy of these drugs in humans suggests that they may represent a feasible treatment option for cardiovascular disease. However, it is more likely that they represent leads in the development of compounds that more specifically targets GSK3α/β in order to minimize associated off-target side effects. Together, these results suggest that targeting the ER stress-GSK3α/β pathway with small molecule inhibitors may be a viable strategy to prevent further complications of atherosclerosis.

3.7 REFERENCES

1. Mozaffarian, D. *et al.* Executive summary: heart disease and stroke statistics—2015 update. *Circulation* **131,** 434–441 (2015).
2. Yusuf, S., Reddy, S., Ounpuu, S. & Anand, S. Global burden of cardiovascular diseases: part I: general considerations, the epidemiologic transition, risk factors, and impact of urbanization. *Circulation* **104,** 2746–53 (2001).
3. Yusuf, S. *et al.* Effect of potentially modifiable risk factors associated with myocardial infarction in 52 countries (the INTERHEART study): case-control study. *Lancet* **364,** 937–952 (2004).
4. Moore, K. J. & Tabas, I. Macrophages in the pathogenesis of atherosclerosis. *Cell* **145,** 341–355 (2011).
5. Libby, P., Ridker, P. M. & Hansson, G. K. Progress and challenges in translating the biology of atherosclerosis. *Nature* **473,** 317–325 (2011).
6. Scull, C. M. & Tabas, I. Mechanisms of ER stress-induced apoptosis in atherosclerosis. *Arterioscler. Thromb. Vasc. Biol.* **31,** 2792–2797 (2011).
7. Minamino, T. & Kitakaze, M. ER stress in cardiovascular disease. *J. Mol. Cell. Cardiol.* **48,** 1105–1110 (2010).
8. Khan, M. I., Pichna, B. A., Shi, Y., Bowes, A. J. & Werstuck, G. H. Evidence supporting a role for endoplasmic reticulum stress in the development of atherosclerosis in a hyperglycaemic mouse model. *Antioxid. Redox Signal.* **11,** 2289–2298 (2009).
9. Ron, D. & Walter, P. Signal integration in the endoplasmic reticulum unfolded

protein response. *Nat. Rev. Mol. Cell Biol.* **8,** 519–529 (2007).

10. Sage, A. T. *et al.* Hexosamine biosynthesis pathway flux promotes endoplasmic reticulum stress, lipid accumulation, and inflammatory gene expression in hepatic cells. *Am. J. Physiol. Endocrinol. Metab.* **298,** (2010).
11. Lee, J. N. & Ye, J. Proteolytic activation of sterol regulatory element-binding protein induced by cellular stress through depletion of Insig-1. *J. Biol. Chem.* **279,** 45257–65 (2004).
12. Tabas, I. & Ron, D. Integrating the mechanisms of apoptosis induced by endoplasmic reticulum stress. *Nat. Cell Biol.* **13,** 184–190 (2011).
13. Ozcan, L. & Tabas, I. Role of endoplasmic reticulum stress in metabolic disease and other disorders. *Annu. Rev. Med.* **63,** 317–28 (2012).
14. Erbay, E. *et al.* Reducing endoplasmic reticulum stress through a macrophage lipid chaperone alleviates atherosclerosis. *Nat. Med.* **15,** 1383–1391 (2009).
15. McAlpine, C. S. & Werstuck, G. H. Protein kinase R-like endoplasmic reticulum kinase and glycogen synthase kinase-3α/β regulate foam cell formation. *J. Lipid Res.* **55,** 2320–2333 (2014).
16. Song, L., Sarno, P. De & Jope, R. S. Central role of glycogen synthase kinase-3beta in endoplasmic reticulum stress-induced caspase-3 activation. *J. Biol. Chem.* **277,** 44701–44708 (2002).
17. Banko, N. S. *et al.* Glycogen synthase kinase 3α deficiency attenuates atherosclerosis and hepatic steatosis in high fat diet–fed low density lipoprotein receptor–deficient mice. *Am. J. Pathol.* **184,** 3394–3404 (2014).

18. Cohen, P. & Goedert, M. GSK3 inhibitors: development and therapeutic potential. *Nat. Rev. Drug Discov.* **3,** 479–487 (2004).

19. McAlpine, C. S. *et al.* Deletion of myeloid GSK3α attenuates atherosclerosis and promotes an M2 macrophage phenotype. *Arterioscler. Thromb. Vasc. Biol.* **35,** 1113–1122 (2015).

20. Bowes, A. J., Khan, M. I., Shi, Y., Robertson, L. & Werstuck, G. H. Valproate attenuates accelerated atherosclerosis in hyperglycemic ApoE-deficient mice: evidence in support of a role for endoplasmic reticulum stress and glycogen synthase kinase-3 in lesion development and hepatic steatosis. *Am. J. Pathol.* **174,** 330–342 (2009).

21. Dang, V. T., Huang, A., Zhong, L. H., Shi, Y. & Werstuck, G. H. Comprehensive Plasma Metabolomic Analyses of Atherosclerotic Progression Reveal Alterations in Glycerophospholipid and Sphingolipid Metabolism in Apolipoprotein E-deficient Mice. *Sci. Rep.* **6,** 35037 (2016).

22. Rigotti, A. *et al.* A targeted mutation in the murine gene encoding the high density lipoprotein (HDL) receptor scavenger receptor class B type I reveals its key role in HDL metabolism. *Proc. Natl. Acad. Sci. U. S. A.* **94,** 12610–5 (1997).

23. Venegas-Pino, D. E., Banko, N., Khan, M. I., Shi, Y. & Werstuck, G. H. Quantitative analysis and characterization of atherosclerotic lesions in the murine aortic sinus. *J. Vis. Exp.* 50933 (2013). doi:10.3791/50933

24. Towler, D. A., Bidder, M., Latifi, T., Coleman, T. & Semenkovich, C. F. Diet-induced diabetes activates an osteogenic gene regulatory program in the aortas of

low density lipoprotein receptor-deficient mice. *J. Biol. Chem.* **273,** 30427–30434 (1998).

25. Özcan, U. *et al.* Chemical chaperones reduce ER stress and restore glucose homeostasis in a mouse model of type 2 diabetes. *Science (80-.).* **313,** 1137–1140 (2006).
26. Hewing, B. *et al.* Rapid regression of atherosclerosis with MTP inhibitor treatment. *Atherosclerosis* **227,** 125–129 (2013).
27. Rayner, K. J. *et al.* Antagonism of miR-33 in mice promotes reverse cholesterol transport and regression of atherosclerosis. *J. Clin. Invest.* **121,** 2921–2931 (2011).
28. McAlpine, C. S., Bowes, A. J., Khan, M. I., Shi, Y. & Werstuck, G. H. Endoplasmic Reticulum Stress and Glycogen Synthase Kinase-3β Activation in Apolipoprotein E-Deficient Mouse Models of Accelerated Atherosclerosis. *Arterioscler. Thromb. Vasc. Biol.* **32,** 82–91 (2012).
29. Cao, S. S. & Kaufman, R. J. Unfolded protein response. *Curr. Biol.* **22,** R622–R626 (2012).
30. Dang, V. T., Beriault, D. R., Deng, A., Shi, Y. & Werstuck, G. H. Glucosamine-induced ER stress accelerates atherogenesis: a potential link between diabetes and cardiovascular disease. *J. Mol. Genet. Med.* **9,** 1–7 (2015).
31. Werstuck, G. H. *et al.* Examining the correlations between GSK-3 inhibitory properties and anti-convulsant efficacy of valproate and valproate-related compounds. *Bioorg. Med. Chem. Lett.* **14,** 5465–5467 (2004).
32. Chen, G., Huang, L.-D., Jiang, Y.-M. & Manji, H. K. The mood-stabilizing agent

valproate inhibits the activity of glycogen synthase kinase-3. *J. Neurochem.* **72,** 1327–1330 (2008).

33. De Sarno, P., Li, X. & Jope, R. S. Regulation of Akt and glycogen synthase kinase-3β phosphorylation by sodium valproate and lithium. *Neuropharmacology* **43,** 1158–1164 (2002).
34. Sutherland, C., Leighton, I. A. & Cohen, P. Inactivation of glycogen synthase kinase-3β by phosphorylation: new kinase connections in insulin and growth-factor signalling. *Biochem. J.* **296,** (1993).
35. Hughes, K., Nikolakaki, E., Plyte, S. E., Totty, N. F. & Woodgett, J. R. Modulation of the glycogen synthase kinase-3 family by tyrosine phosphorylation. *EMBO J.* **12,** 803–8 (1993).
36. Herck, J. L. *et al.* Proteasome inhibitor bortezomib promotes a rupture-prone plaque phenotype in ApoE-deficient mice. *Basic Res. Cardiol.* **105,** 39–50 (2010).
37. Tabas, I. The role of endoplasmic reticulum stress in the progression of atherosclerosis. *Circ. Res.* **107,** 839–50 (2010).
38. Allard, D., Figg, N., Bennett, M. R. & Littlewood, T. D. Akt regulates the survival of vascular smooth muscle cells via inhibition of FoxO3a and GSK3. *J. Biol. Chem.* **283,** 19739–47 (2008).
39. Fernández-Hernando, C., József, L., Jenkins, D., Di Lorenzo, A. & Sessa, W. C. Absence of Akt1 reduces vascular smooth muscle cell migration and survival and induces features of plaque vulnerability and cardiac dysfunction during atherosclerosis. *Arterioscler. Thromb. Vasc. Biol.* **29,** 2033–2040 (2009).

40. Morel, C., Carlson, S. M., White, F. M. & Davis, R. J. Mcl-1 integrates the opposing actions of signaling pathways that mediate survival and apoptosis. *Mol. Cell. Biol.* **29,** 3845–52 (2009).

41. Maurer, U., Charvet, C., Wagman, A. S., Dejardin, E. & Green, D. R. Glycogen Synthase Kinase-3 Regulates Mitochondrial Outer Membrane Permeabilization and Apoptosis by Destabilization of MCL-1. *Mol. Cell* **21,** 749–760 (2006).

42. Sanz, J. & Fayad, Z. A. Imaging of atherosclerotic cardiovascular disease. *Nature* **451,** 953–957 (2008).

43. Williams, K. J., Feig, J. E. & Fisher, E. A. Rapid regression of atherosclerosis: insights from the clinical and experimental literature. *Nat. Clin. Pract. Cardiovasc. Med.* **5,** 91–102 (2008).

44. Whayne, T. F. & Jr. Atherosclerosis: current status of prevention and treatment. *Int. J. Angiol.* **20,** 213–22 (2011).

45. Weber, C. & Noels, H. Atherosclerosis: current pathogenesis and therapeutic options. *Nat. Med.* **17,** 1410–1422 (2011).

46. Olesen, J. B. *et al.* Valproate attenuates the risk of myocardial infarction in patients with epilepsy: a nationwide cohort study. *Pharmacoepidemiol. Drug Saf.* **20,** 146–153 (2011).

3.8 SUPPLEMENTAL TABLES AND FIGURES

Supplemental Table 3.1. *Metabolic parameters of 14 weeks old Ldlr$^{-/-}$ mice with 4PBA or VPA treatment*

	Control	4PBA	VPA
Body weight at sacrifice (g)	23.1 ± 1.8	23.0 ± 2.3	22.1 ± 1.8
Fasting blood glucose (mM)	8.4 ± 1.4	8.0 ± 1.6	8.0 ± 1.0
Liver weight (g)	1.14 ± 0.12	1.19 ± 0.11	1.07 ± 0.22
Fat pad weight (g)	0.28 ± 0.11	0.24 ± 0.15	0.27 ± 0.09
Plasma 4PBA (mM)	0 ± 0.00	0.16 ± 0.09 **	0 ± 0.00
Plasma VPA (mM)	0 ± 0.00	0 ± 0.00	1.34 ± 0.48 ***

Data are the mean ± SD;
n = 12 mice for body weight, blood glucose, liver weight, and fat pad weight;
n = 4 mice for 4PBA and VPA levels;
**p < 0.01, ***p < 0.001, compared with control

Supplemental Table 3.2. *Metabolic parameters of 14(+4) weeks old Ldlr$^{-/-}$ mice with 4PBA or VPA treatment*

	Baseline	Control	4PBA	VPA
Body weight at sacrifice (g)	22.7 ± 1.6	24.4 ± 1.7	23.7 ± 1.9	23.4 ± 2.1
Fasting blood glucose (mM)	8.2 ± 1.4	8.7 ± 1.0	8.1 ± 0.8	7.9 ± 0.9
Liver weight (g)	1.10 ± 0.15	1.02 ± 0.18	1.05 ± 0.10	1.01 ± 0.13
Fat pad weight (g)	0.32 ± 0.24	0.28 ± 0.13	0.28 ± 0.12	0.20 ± 0.10

Data expressed as mean ± SD; n = 19 mice in each group

Supplemental Table 3.3. *Metabolic parameters of 20(+4) weeks old Ldlr$^{-/-}$ with 4PBA or VPA treatment*

	Baseline	Control	4PBA	VPA
Body weight at sacrifice (g)	25.0 ± 2.5	24.3 ± 1.3	23.3 ± 1.8	25.2 ± 2.4
Fasting blood glucose (mM)	7.9 ± 0.8	9.4 ± 1.6 *	9.2 ± 1.6	9.3 ± 1.6
Liver weight (g)	1.31 ± 0.28	1.00 ± 0.10 ****	1.01 ± 0.11 ****	0.97 ± 0.16 ****
Fat pad weight (g)	0.43 ± 0.15	0.24 ± 0.09 **	0.19 ± 0.07 ***	0.36 ± 0.22
Plasma 4PBA (mM)	0 ± 0.00	0 ± 0.00	0.29 ± 0.14 $^{***}_{\dagger\dagger\dagger}$	0 ± 0.00
Plasma VPA (mM)	0 ± 0.00	0 ± 0.00	0 ± 0.00	1.18 ± 0.18 $^{****}_{\dagger\dagger\dagger\dagger}$

Data are the mean ± SD;
n = 15 mice for body weight, blood glucose, liver weight, and fat pad weight;
n = 4 mice for 4PBA and VPA levels;
*p < 0.05, **p < 0.01, ***p < 0.001, ****p < 0.0001, compared with baseline;
†††p < 0.001, ††††p < 0.0001, compared with control

Supplemental Figure 3.1. Negative immunofluorescent staining controls.

Representative images of control IgG immunofluorescent staining and specific antibody staining for **A.** p-GSK3β-Ser9, **B.** p-GSK3β-Tyr219, **C.** α-actin, **D.** Mac3, **E.** CD36, and **F.** Arg1.

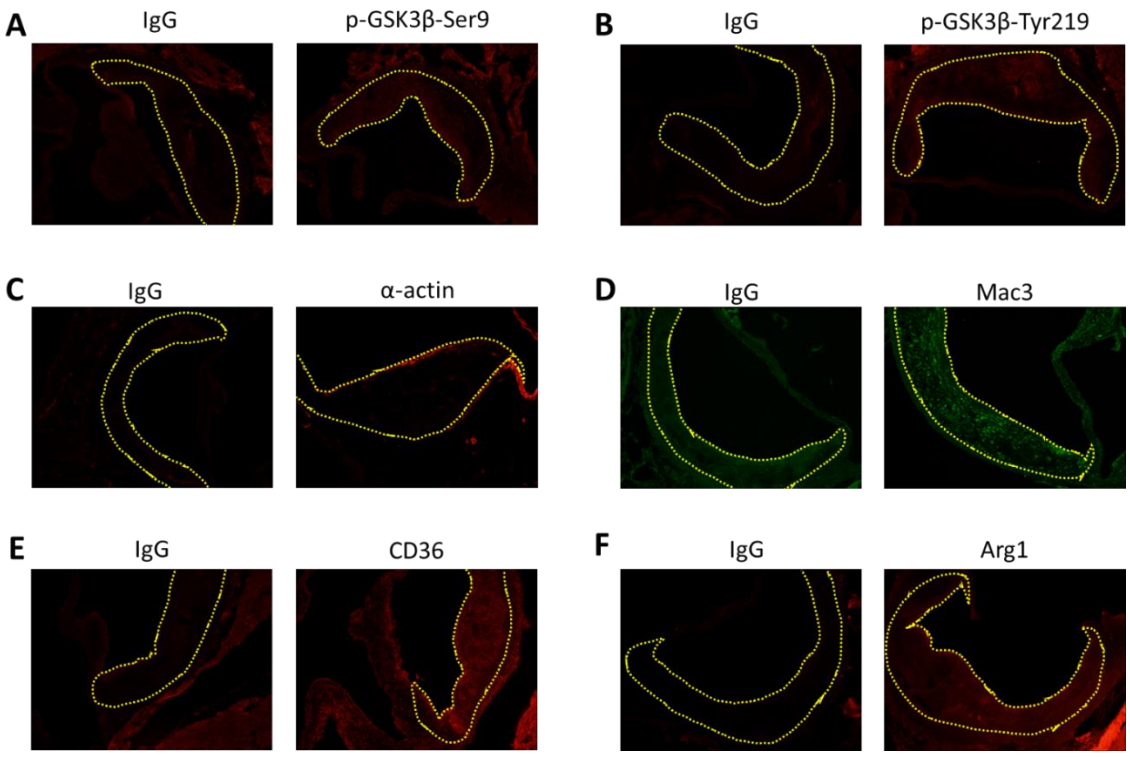
A
IgG
p-GSK3β-Ser9
B
IgG
p-GSK3β-Tyr219
C
IgG
α-actin
D
IgG
Mac3
E
IgG
CD36
F
IgG
Arg1

Supplemental Figure 3.2. Hepatic and plasma lipid and plasma lipoproteins in the *Ldlr*$^{-/-}$ atherosclerotic progression model.

Ldlr$^{-/-}$ mice were fed a HFD or a HFD with 4PBA or VPA treatment for 10 weeks. No significant differences were observed in **A.** total hepatic cholesterol, **B.** hepatic triglycerides, **C.** fasting plasma cholesterol, or **D.** plasma triglycerides. **E.** Plasma lipid profiles between the two treatment groups compared to the control. Plasma is pooled from four mice per group.

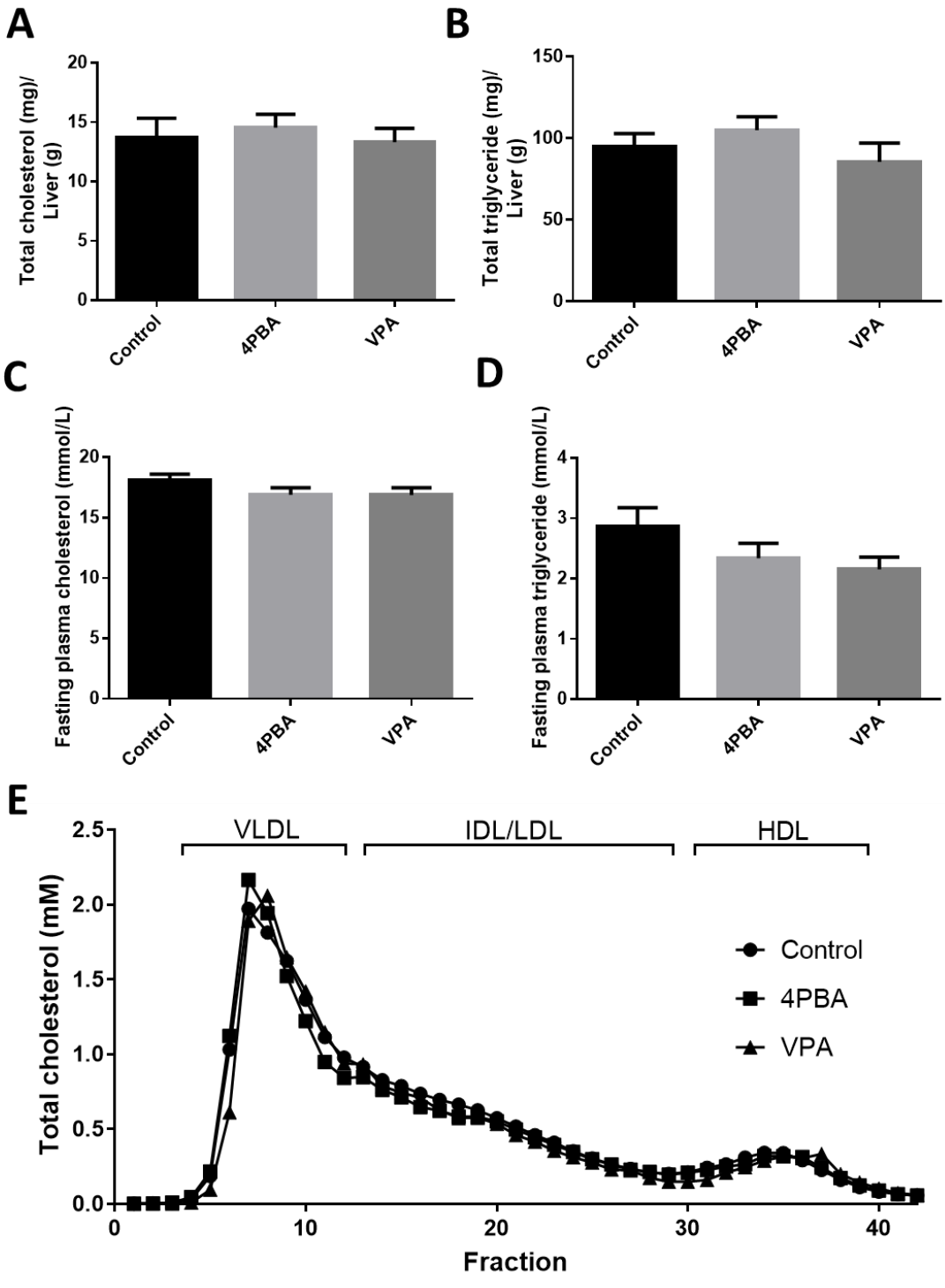
A
Total cholesterol (mg)/ Liver (g)
20
15
10
5
0
Control
4PBA
VPA
B
Total triglyceride (mg)/ Liver (g)
150
100
50
0
Control
4PBA
VPA
C
Fasting plasma cholesterol (mmol/L)
20
15
10
5
0
Control
4PBA
VPA
D
Fasting plasma triglyceride (mmol/L)
4
3
2
1
0
Control
4PBA
VPA
E
VLDL
IDL/LDL
HDL
Total cholesterol (mM)
2.5
2.0
1.5
1.0
0.5
0.0
0
10
20
30
40
Fraction
Control
4PBA
VPA

Supplemental Figure 3.3. 4PBA and VPA do not affect GSK3β phosphorylation status in atherosclerotic plaques in the progression or regression models.

Representative sections of aortic root stained with **A.** phospho-GSK3β-Ser9 (red), or **B.** phospho-GSK3β-Tyr216 from the regression baseline group. Sections were co-stained with the macrophage marker Mac3 (green), and the atherosclerotic lesions are outlined (yellow). Similar staining patterns were observed between all groups. Quantification of **C.** phospho-GSK3β-Ser9 and **E.** phospho-GSK3β-Tyr216 staining intensity in arbitrary units (A.U.) in the *Ldlr*$^{-/-}$ atherosclerotic progression model. Quantification of **D.** phospho-GSK3β-Ser9 and **F.** phospho-GSK3β-Tyr216 staining intensity in the *Ldlr*$^{-/-}$ atherosclerotic regression model. Data are the mean ± SEM; n = 5 mice/group.

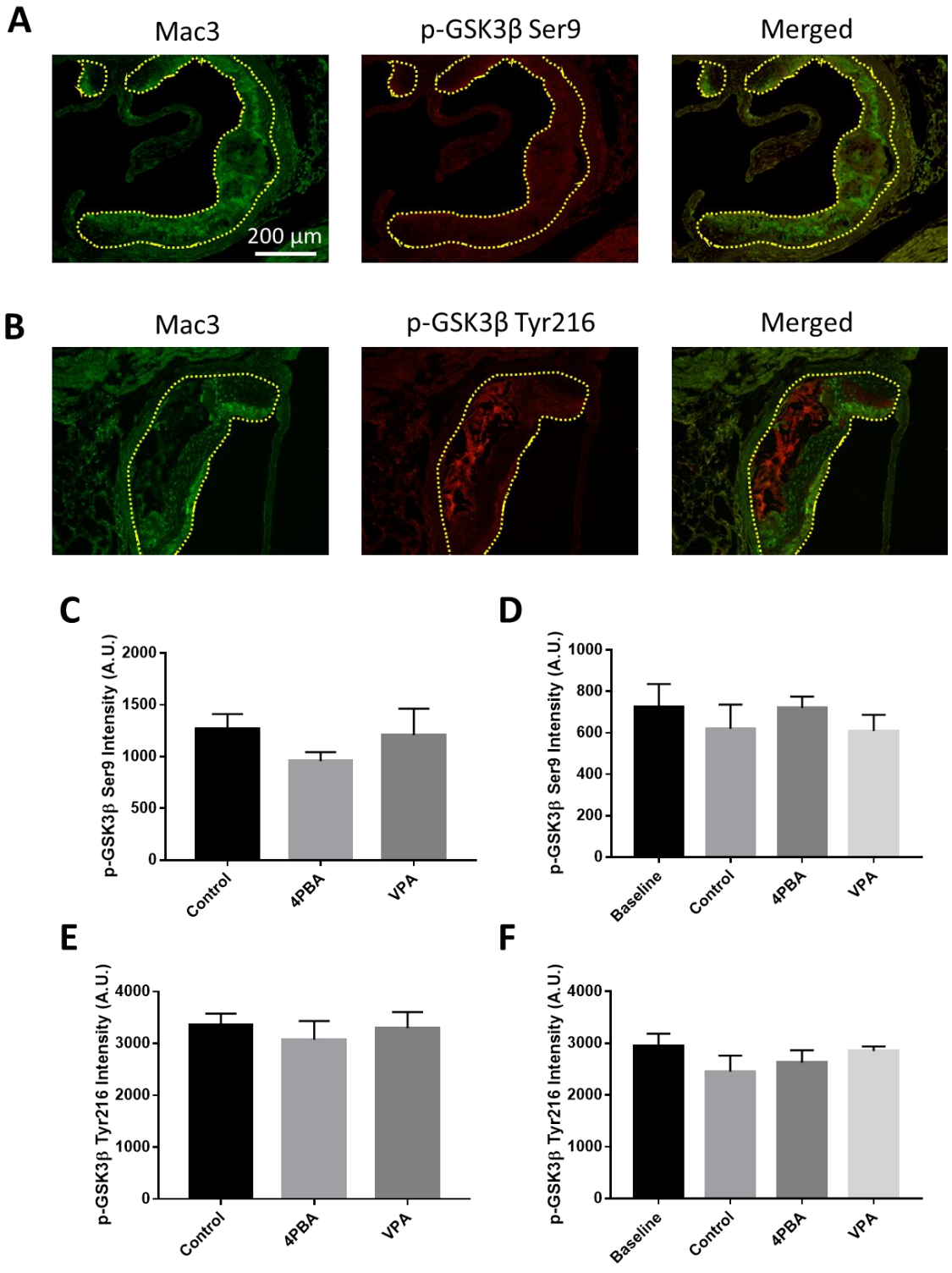
A
Mac3
p-GSK3β Ser9
Merged
200 µm
B
Mac3
p-GSK3β Tyr216
Merged
C
p-GSK3β Ser9 Intensity (A.U.)
2000
1500
1000
500
0
Control
4PBA
VPA
D
p-GSK3β Ser9 Intensity (A.U.)
1000
800
600
400
200
0
Baseline
Control
4PBA
VPA
E
p-GSK3β Tyr216 Intensity (A.U.)
4000
3000
2000
1000
0
Control
4PBA
VPA
F
p-GSK3β Tyr216 Intensity (A.U.)
4000
3000
2000
1000
0
Baseline
Control
4PBA
VPA

Supplemental Figure 3.4. 4PBA or VPA treatment does not change atherosclerotic plaque composition during atherosclerotic progression in *Ldlr*$^{-/-}$ mice.

Representative sections of aortic root were stained with **A.** α-actin (red) or **B.** Mac3 (green). Atherosclerotic lesions are outlined (yellow). Quantification of **C.** α-actin and **D.** Mac3 staining area normalized to the lesion area. Data are the mean ± SEM; n = 5 mice/group.

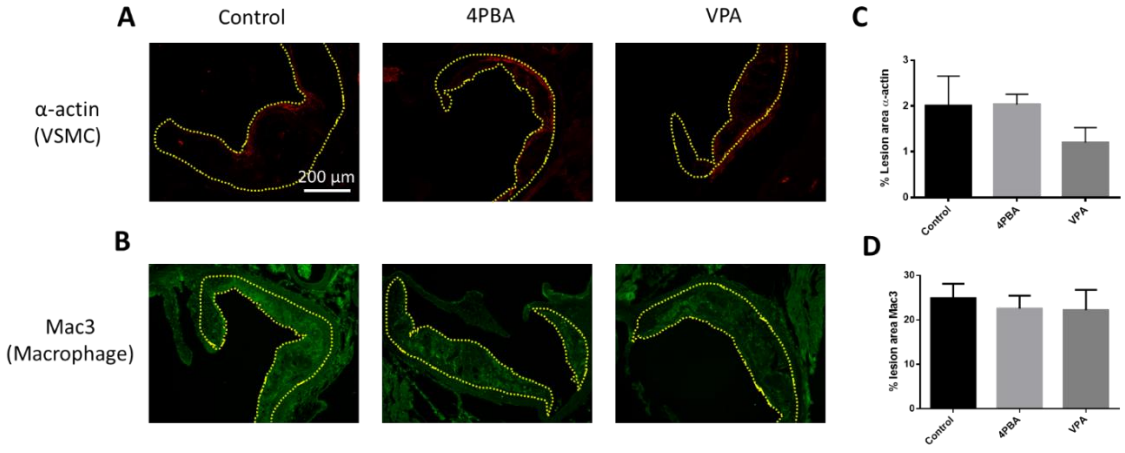
A
Control
4PBA
VPA
α-actin
(VSMC)
200 μm
B
Mac3
(Macrophage)
C
% Lesion area α-actin
Control
4PBA
VPA
D
% lesion area Mac3
Control
4PBA
VPA

Supplemental Figure 3.5. 4PBA or VPA treatment does not alter caspase-3 activation during atherosclerotic progression in *Ldlr*$^{-/-}$ mice.

Representative sections of aortic root stained with **A.** cleaved caspase-3 (brown). Atherosclerotic lesions are outlined (yellow). **B.** Quantification of cleaved caspase-3 staining area normalized to the lesion area. Data are the mean ± SEM; n = 5 mice/group.

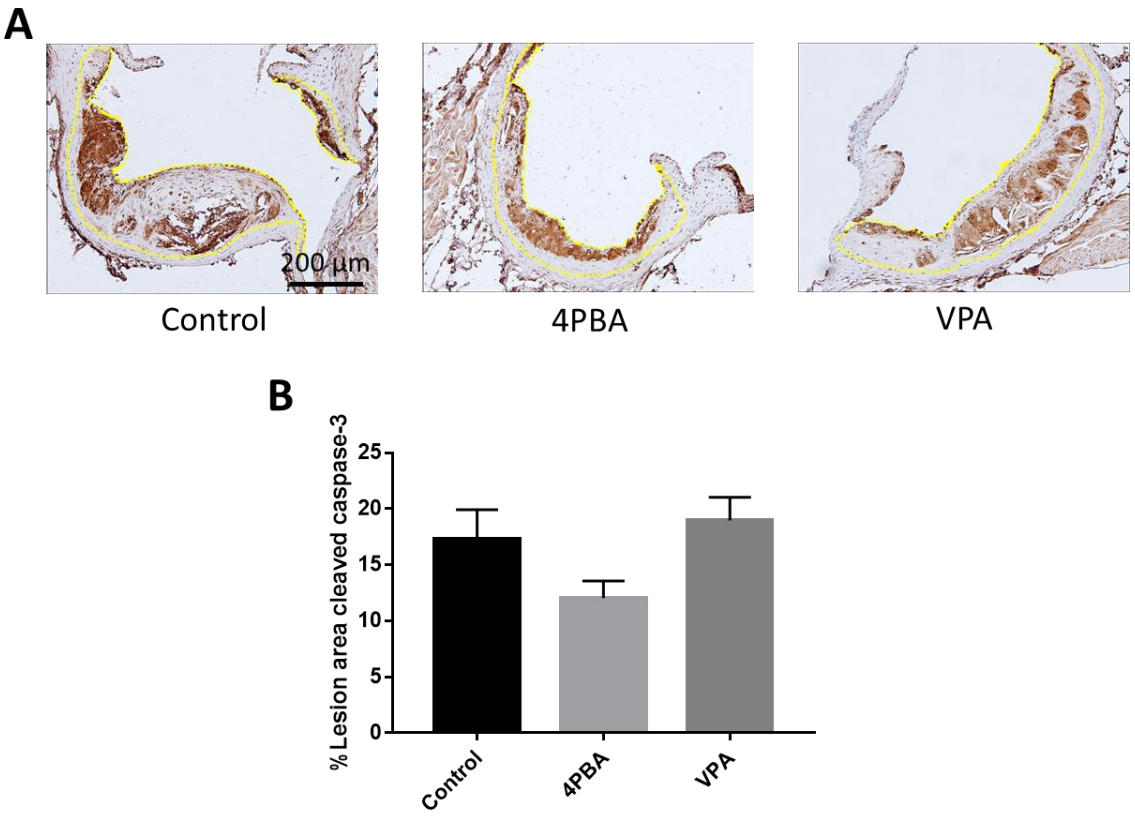
A
200 µm
Control
4PBA
VPA
B
% Lesion area cleaved caspase-3
25
20
15
10
5
0
Control
4PBA
VPA

Supplemental Figure 3.6. 4PBA or VPA treatment does not alter lesional collagen content during atherosclerotic progression in *Ldlr*$^{-/-}$ mice.

Representative sections of aortic root stained with **A.** Masson's trichrome (collagen stains blue). Atherosclerotic lesions are outlined (yellow). **B.** Quantification of collagen staining area normalized to the lesion area. Data are the mean ± SEM; n = 5 mice/group.

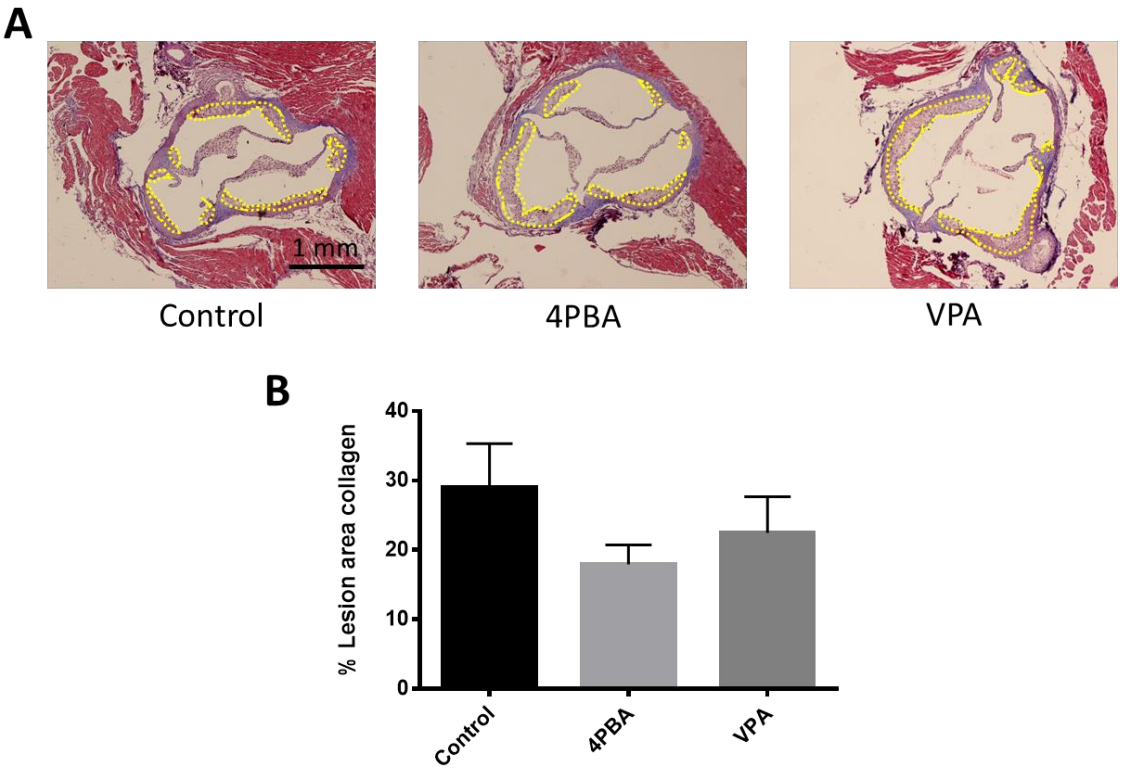
A
1 mm
Control
4PBA
VPA
B
% Lesion area collagen
40
30
20
10
0
Control
4PBA
VPA

Supplemental Figure 3.7. 4PBA or VPA treatment does not affect M1 or M2 polarization of macrophages during atherosclerotic progression in *Ldlr*$^{-/-}$ mice. Representative sections of aortic root stained for **A.** the M1 polarization marker CD36 (red) or **B.** the M2 polarization marker Arg1 (red). Atherosclerotic lesions are outlined (yellow). Quantification of **C.** CD36 and **D.** Arg1 staining area are normalized to the macrophage area obtained from Mac3 staining. Data are the mean ± SEM; n = 5 mice/group.

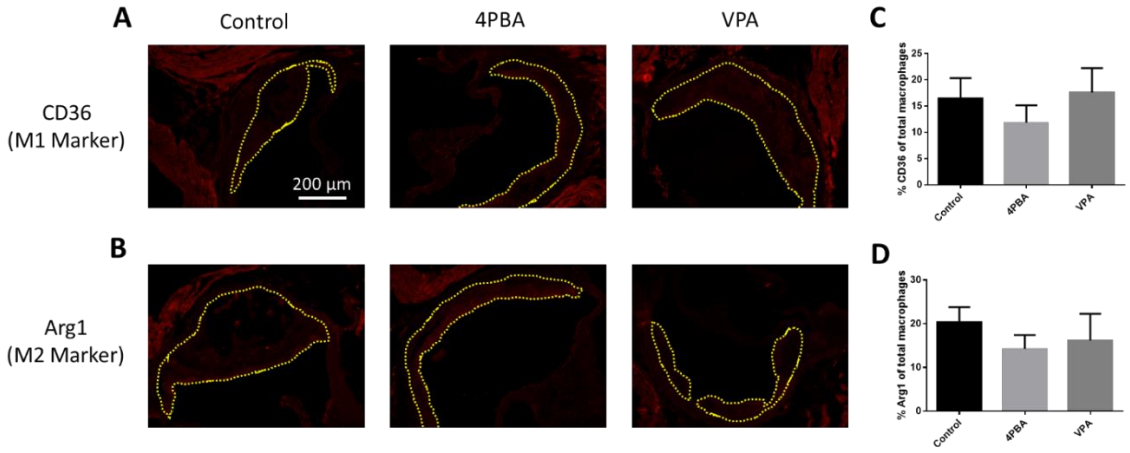
A
Control
4PBA
VPA
CD36
(M1 Marker)
200 µm
B
Arg1
(M2 Marker)
C
% CD36 of total macrophages
0
5
10
15
20
25
Control
4PBA
VPA
D
% Arg1 of total macrophages
0
10
20
30
Control
4PBA
VPA

Supplemental Figure 3.8. Hepatic and plasma lipid and plasma lipoproteins in the *Ldlr*$^{-/-}$ late stage progression model.

Ldlr$^{-/-}$ mice were fed a HFD for 10 weeks (baseline), and then switched to chow diet (control) or a chow diet along with 4PBA or VPA treatment for 4 weeks. Hepatic **A.** cholesterol and **B.** triglycerides, as well as fasting plasma **C.** total cholesterol and **D.** triglycerides were quantified. Data are the mean ± SEM; n = 5 mice/group; ***$p < 0.001$, ****$p < 0.0001$. **E.** Plasma lipoprotein profiles of baseline, control, and 4PBA and VPA treatment groups. Plasma is pooled from four mice per group.

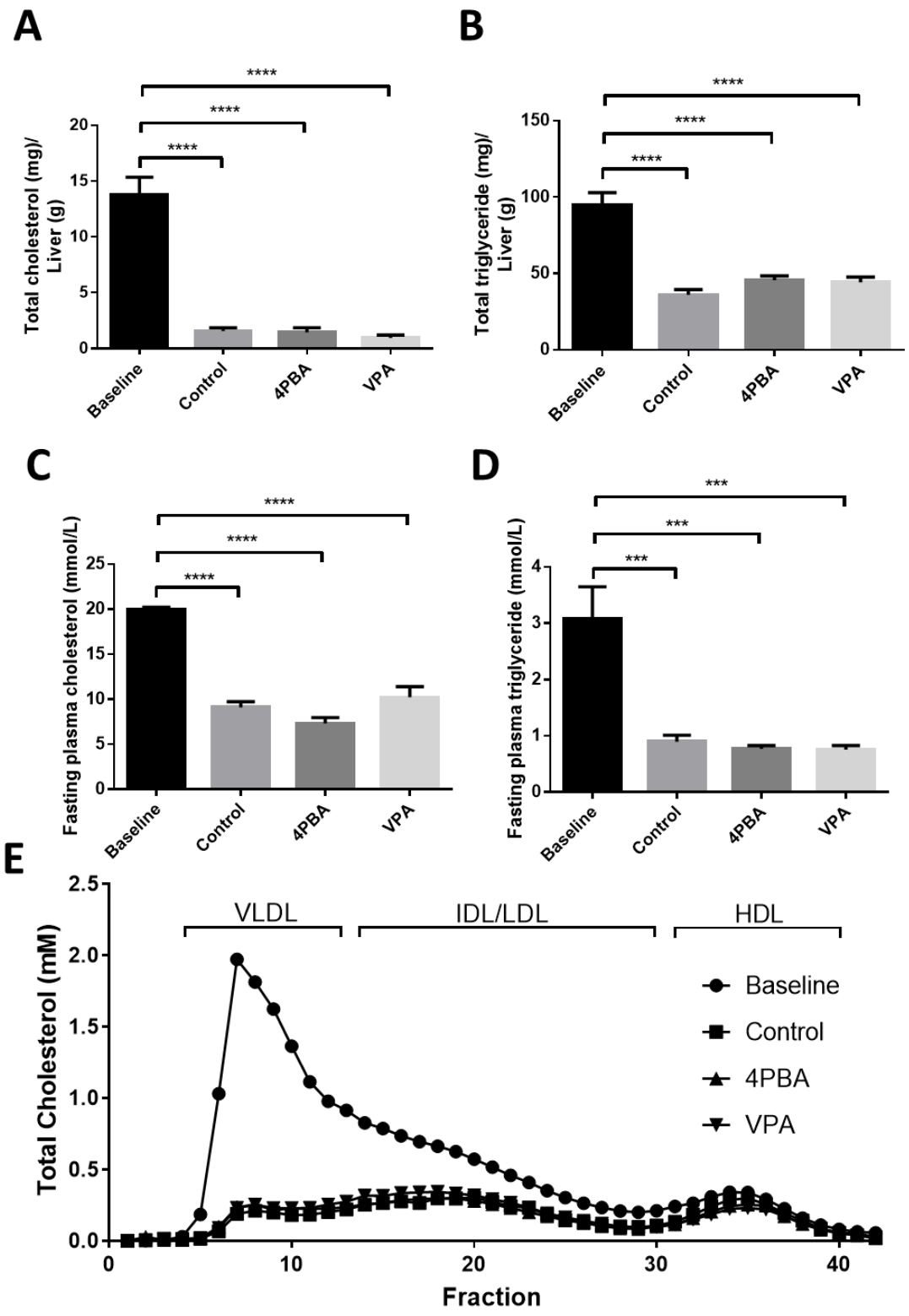
A
Total cholesterol (mg)/ Liver (g)
****
****
****
Baseline
Control
4PBA
VPA
B
Total triglyceride (mg)/ Liver (g)
****
****
****
C
Fasting plasma cholesterol (mmol/L)
****
****
****
D
Fasting plasma triglyceride (mmol/L)
***
***
***
E
Total Cholesterol (mM)
VLDL
IDL/LDL
HDL
Baseline
Control
4PBA
VPA
Fraction

Supplemental Figure 3.9. Hepatic and plasma lipid and plasma lipoproteins in the *Ldlr*$^{-/-}$ regression model.

Ldlr$^{-/-}$ mice were fed a HFD for 16 weeks (baseline), and then switched to chow diet (control) or a chow diet along with 4PBA or VPA treatment for 4 weeks. Hepatic **A.** cholesterol and **B.** triglycerides, as well as fasting plasma **C.** total cholesterol and **D.** triglyceride were quantified. Data are the mean ± SEM; n = 5 mice in each group; $^{**}p < 0.01$, $^{***}p < 0.001$, $^{****}p < 0.0001$. **E.** Plasma lipid profiles of baseline, control, and 4PBA and VPA treatment groups. Plasma is pooled from four mice per group.

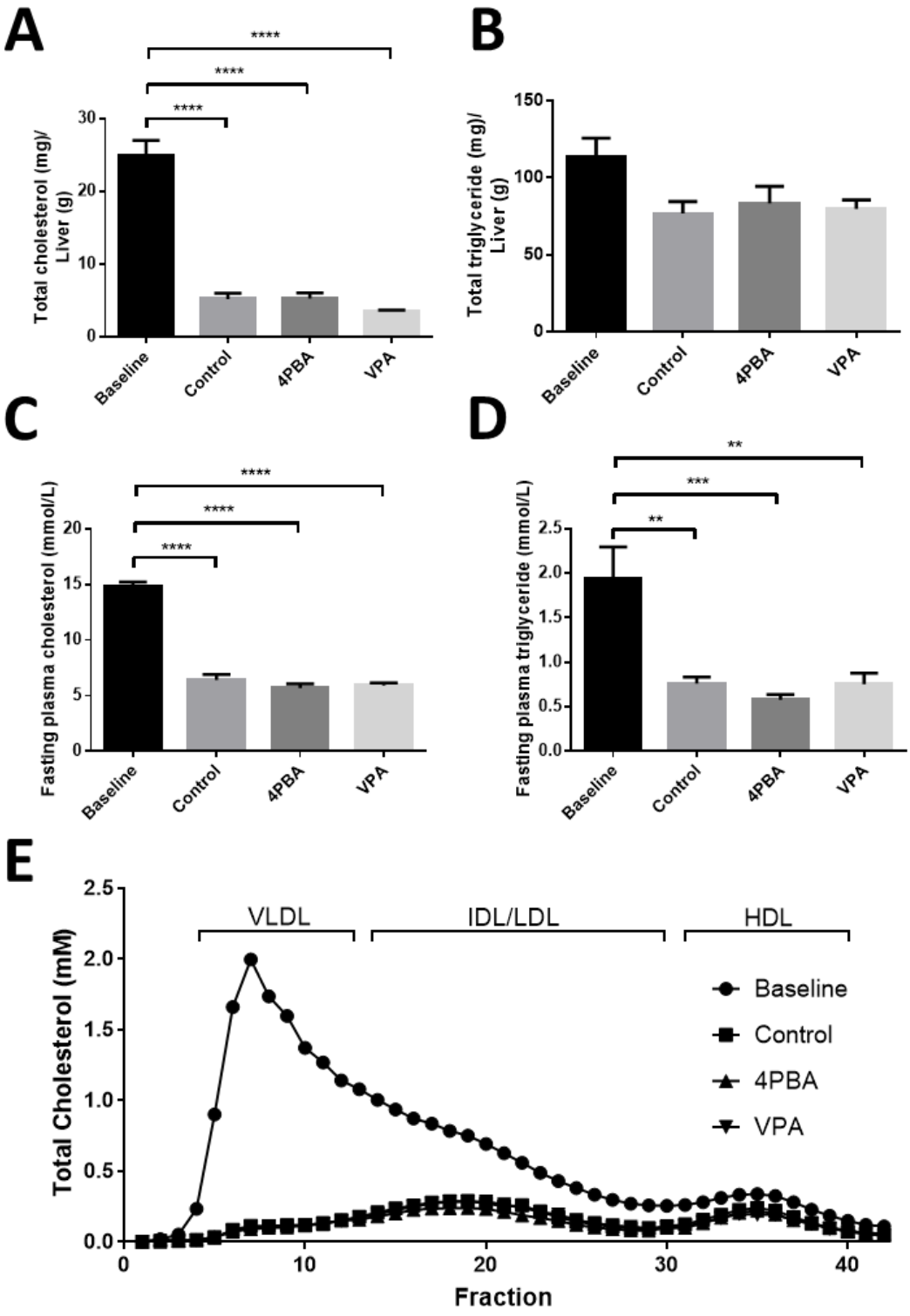
A
****
****
****
Total cholesterol (mg)/ Liver (g)
30
20
10
0
Baseline
Control
4PBA
VPA
B
Total triglyceride (mg)/ Liver (g)
150
100
50
0
Baseline
Control
4PBA
VPA
C
****
****
****
Fasting plasma cholesterol (mmol/L)
20
15
10
5
0
Baseline
Control
4PBA
VPA
D
**
***
**
Fasting plasma triglyceride (mmol/L)
2.5
2.0
1.5
1.0
0.5
0.0
Baseline
Control
4PBA
VPA
E
VLDL
IDL/LDL
HDL
Total Cholesterol (mM)
2.5
2.0
1.5
1.0
0.5
0.0
0
10
20
30
40
Fraction
Baseline
Control
4PBA
VPA

Supplemental Figure 3.10. 4PBA and VPA do not affect apoptosis in atherosclerotic plaques in regression model using *Ldlr*$^{-/-}$ mice.

Representative sections of aortic root stained with **A.** cleaved caspase-3 (brown), or **B.** Terminal deoxynucleotidyl transferase (TdT) dUTP Nick-End Labeling (TUNEL) (green) merged with DAPI (blue). Arrows indicate positively stained nuclei in the arterial wall. Atherosclerotic lesions are outlined (yellow). Quantification of **C.** cleaved caspase-3 staining area normalized to the lesion area, and **D.** positively TUNEL stained nuclei relative to total nuclei within the lesion area. Data are the mean ± SEM; n = 5 mice/group.

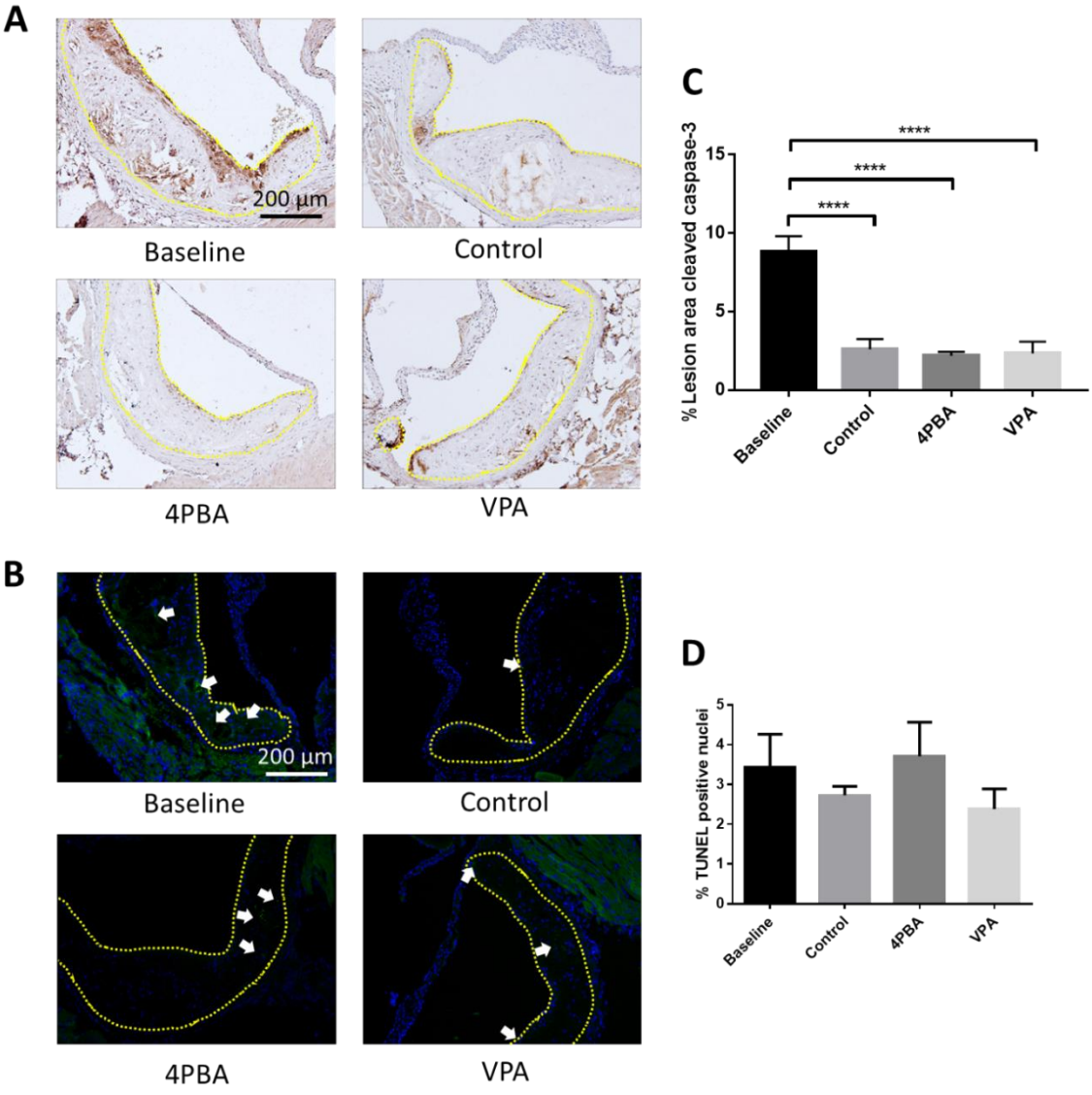
A
200 µm
Baseline
Control
4PBA
VPA
B
200 µm
Baseline
Control
4PBA
VPA
C
% Lesion area cleaved caspase-3
15
10
5
0
****
****
****
Baseline
Control
4PBA
VPA
D
% TUNEL positive nuclei
5
4
3
2
1
0
Baseline
Control
4PBA
VPA

Supplemental Figure 3.11. 4PBA and VPA do not affect cell proliferation in atherosclerotic plaques.

A. Representative sections of aortic root stained with an antibody against cell proliferation marker Ki67 (green) merged with DAPI (blue) and α-actin (red). Atherosclerotic lesions are outlined (yellow). Quantification of **B.** the percentage of positively stained Ki67 cell which are also positively stained with α-actin, and **C.** the percentage of positively stained Ki67 cell which are negatively stained with α-actin. Data are the mean ± SEM; n = 5 mice/group.

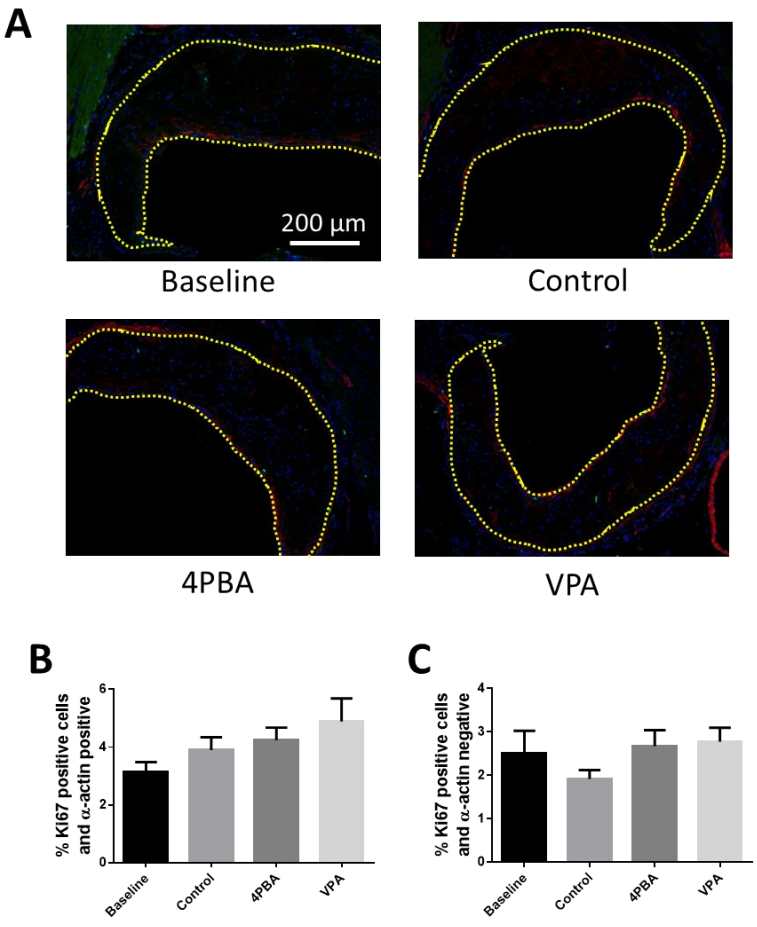
A
200 µm
Baseline
Control
4PBA
VPA
B
% Ki67 positive cells and α-actin positive
0
2
4
6
Baseline
Control
4PBA
VPA
C
% Ki67 positive cells and α-actin negative
0
1
2
3
4
Baseline
Control
4PBA
VPA

Supplemental Figure 3.12. 4PBA and VPA do not alter the expression of markers of M1 or M2 macrophage polarization.

Representative sections of aortic root stained with **A.** an antibody against the M1 macrophage polarization marker CD36 (red) or **B.** an antibody against the M2 macrophage polarization marker Arg1 (red). Atherosclerotic lesions are outlined (yellow). Quantification of **C.** CD36 and **D.** Arg1 staining area are normalized to the macrophage area obtained from Mac3 staining. Data are the mean ± SEM; n = 4-5 mice/group.

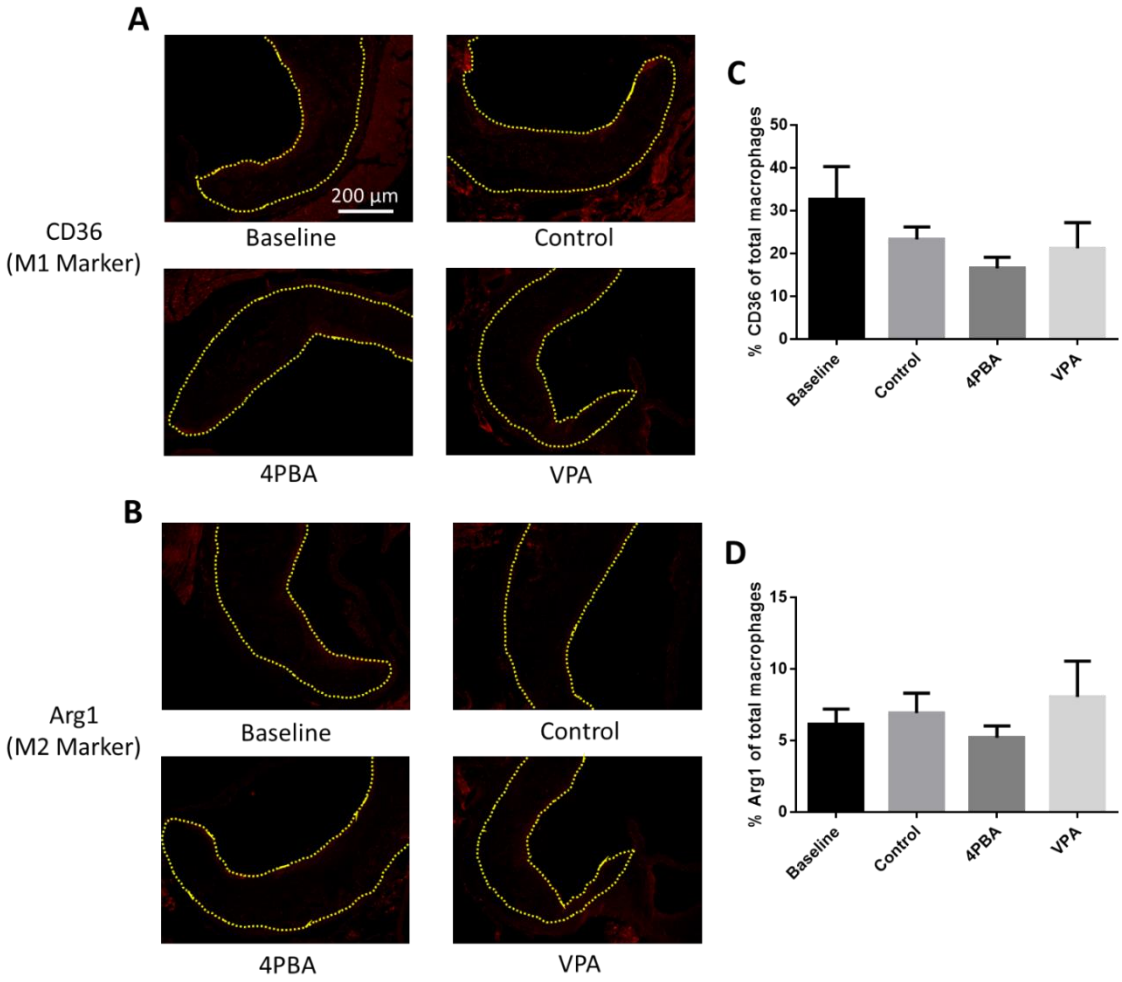
A
200 µm
CD36
(M1 Marker)
Baseline
Control
4PBA
VPA
B
Arg1
(M2 Marker)
Baseline
Control
4PBA
VPA
C
% CD36 of total macrophages
50
40
30
20
10
0
Baseline
Control
4PBA
VPA
D
% Arg1 of total macrophages
15
10
5
0
Baseline
Control
4PBA
VPA

CHAPTER 4: INVESTIGATING THE ROLE OF GLYCOGEN SYNTHASE KINASE-3α/β IN FOAM CELL FORMATION

4.1 FOREWORD

This study investigates the role of GSK3α and GSK3β in macrophages in the progression of atherosclerosis. Bone marrow derived macrophages were obtained from *Ldlr*$^{-/-}$ mice with myeloid GSK3α, GSK3β, or GSK3α/β deficiency. We demonstrate that the GSK3α and GSK3β isoforms are both involved in regulating cell viability, and the deletion of both isoforms are required to impede ER stress induced apoptosis. Further, GSK3α deficiency inhibited M1 polarization in macrophages. There were no alterations in the expression of genes involved in lipid biosynthesis and uptake in GSK3α deficient macrophages. These studies provide an initial look at the potential role of GSK3α and GSK3β in foam cell formation. Additional work will be required to more fully delineate the molecular mechanisms.

4.2 ABSTRACT

Objective

Evidence suggests a role for ER stressed induced glycogen synthase kinase (GSK)-3α/β signalling in the development of atherosclerosis. The specific functions of the GSK3α and GSK3β homologs in atherosclerosis are unknown. This study investigated the role of the GSK-3α/β isoforms in the formation of foam cells.

Approach and results

GSK3α, GSK3β, or GSK3α/β deficient bone marrow derived macrophages were isolated and differentiated into M1 or M2 macrophages. These macrophages were then treated in culture with the ER stress inducing agents, thapsigargin (Tg) or tunicamycin (Tm). The deletion of GSK3α attenuated M1 polarization but did not affect M2 polarization, resulting in a lower M1/M2 ratio. GSK3α deficiency did not significantly affect cell viability or the expression of the transcripts associated with lipid biosynthesis or uptake. The ablation of GSK3β did not have a large impact on cell viability or apoptosis. However, the deletion of GSK3α/β improved cell viability.

Conclusions

These findings suggest that GSK3α may play a role in atherosclerosis by promoting M1 macrophage polarization. Further, GSK3α and GSK3β may have redundant roles in regulating cell viability.

4.3 INTRODUCTION

Atherosclerosis is the underlying cause of heart attacks and strokes which is the leading cause of morbidity and mortality worldwide. Myeloid lineage cells account for the majority of the cellular components of atherosclerotic lesions and these cells play a critical role in the development and progression of atherosclerosis[1,2]. Macrophages within the atherosclerotic lesion endocytose modified lipid particles, becoming lipid engorged foam cells. Macrophages are often classified as pro-inflammatory (M1) or anti-inflammatory (M2) depending on whether a Th1 or Th2 immune response was induced. M1 macrophages produce pro-inflammatory cytokines and promote atherosclerotic lesion

development and complexity[3,4]. M2 macrophages produce anti-inflammatory and tissue remodeling cytokines, patrol tissue, promote tissue repair and healing, and display enhanced efferocytosis. Macrophages are highly plastic and can switch from one phenotype to the other depending on stimuli from the microenvironment. Plaque stability depends on the balance between these polarization states. Other macrophage phenotypes have been identified, including M4, Mhem, and Mox. All of these have been found within the complex and heterogeneous environment of an atherosclerotic plaque[5,6]. However, these macrophage subtypes are not as well studied. The modulation of macrophage phenotype may be a potential strategy to treat atherosclerosis. However, currently our understanding of the mechanisms which regulates macrophage polarization is limited.

Glycogen synthase kinase (GSK)-3 α and β are homologous serine/threonine kinases encoded by separate genes and are involved in various metabolic signaling networks[7]. Although GSK3α and GSK3β share some common substrates, they are not redundant and do have distinct functions[8,9]. The inhibition of GSK3α/β in macrophages attenuated the expression genes associated with apoptosis and exhibited reduced lipid biosynthesis and uptake[10]. Further, the pharmacological inhibition of GSK3α/β in mice attenuates the formation of atherosclerotic lesion and hepatic steatosis[11,12] (also evident in Chapter 3). Mice with whole body GSK3α deficiency are viable and have no overt phenotype[13,14]. Furthermore, we have shown that GSK3α deficiency attenuates atherosclerosis in low-density lipoprotein receptor deficient (*Ldlr*$^{-/-}$) mice. However, whole body GSK3β deletion is embryonically lethal. We have recently found that the deficiency in myeloid GSK3α exhibited reduced atherosclerosis and less advanced

plaques in *Ldlr*$^{-/-}$ mice[15]. Further, the deletion of GSK3α appeared to enhance macrophages to polarize towards the M2 phenotype and suppressed the inflammatory M1 phenotype *in vivo*. Myeloid GSK3β deficiency did not detectibly affect atherosclerosis. Despite the evidence of a role for GSK3α/β in atherosclerosis, the specific roles of the two isoforms in atherogenesis is not known. In this study, to further delineate the role of GSK3α and GSK3β in the context of atherosclerosis, we investigated the alterations in functionality in GSK3α and GSK3β deficient macrophages *in vitro*.

4.4 METHODS

Mouse models

All animal experiments were conducted with the approval from the McMaster University Animal Research Ethics Board. All mice were fed a standard chow diet (Harlan Teklad, TD92078) beginning at 3 weeks. Mice had unlimited access to food and water and were maintained on a 12-hour light/dark cycle. Myeloid GSK3α or GSK3β deficient mice, were obtained as previously described[15]. Briefly, low-density lipoprotein receptor deficient mice with loxP-flanked GSK3α gene (*Ldlr*$^{-/-}$*GSK3α*$^{fl/fl}$) were crossed with mice expressing a single copy of the Cre recombinase gene controlled by the myeloid specific lysozyme M promoter (*Ldlr*$^{-/-}$*LyzMCre*$^{+/-}$*GSK3α*$^{fl/fl}$). By using this breeding method, we were able to generate the *Ldlr*$^{-/-}$ myeloid-specific GSK3α knockout mice (*Ldlr*$^{-/-}$*LyzMCre*$^{+/-}$*GSK3α*$^{fl/fl}$) and the control *Ldlr*$^{-/-}$ GSK3α floxed mice (*Ldlr*$^{-/-}$*GSK3α*$^{fl/fl}$) at the expected Mendelian ratio of 1:1. The *Ldlr*$^{-/-}$ myeloid specific GSK3β deficient mice were bred similarly to obtain *Ldlr*$^{-/-}$ myeloid-specific GSK3β knockout mice (*Ldlr*$^{-/-}$*LyzMCre*$^{+/-}$*GSK3β*$^{fl/fl}$) and the control *Ldlr*$^{-/-}$ GSK3β floxed mice

(*Ldlr*$^{-/-}$*GSK3β*$^{fl/fl}$). Breeding strategies using the above mice were also used to generate *Ldlr*$^{-/-}$ myeloid-specific GSK3α/β deficient mice (*Ldlr*$^{-/-}$*LyzMCre*$^{+/-}$*GSK3α*$^{fl/fl}$*GSK3β*$^{fl/fl}$) and the control *Ldlr*$^{-/-}$ GSK3α/β floxed mice (*Ldlr*$^{-/-}$*GSK3α*$^{fl/fl}$*GSK3β*$^{fl/fl}$).

Bone marrow derived macrophage isolation and polarization

Bone marrow was collected from tibias and femurs of 10 week old mice, passed through a 70 µm nylon mesh to remove small pieces of bone and debris, and resuspended in Dulbecco's Modified Eagle Medium (DMEM) containing 15% (v/v) fetal bovine serum, 100 IU/mL penicillin and 100 µg/mL streptomycin, 1X MEM non-essential amino acids, and 20 ng/mL recombinant macrophage colony-stimulating factor (M-CSF). Viable cells were cultured in 100 mm bacterial plates containing 5 x 10^6 cells in 10 mL of medium. At day 3, 5 mL of fresh medium was added to the cultured cells. At day 6, macrophages were washed twice with warm Dulbecco's phosphate buffered saline (DPBS) without calcium or magnesium, detached with Accutase, counted with a hemocytometer, and plated for subsequent experiments. Macrophages were polarized into M1 macrophages by exposure to 10 ng/ml lipopolysaccharide (LPS, Sigma) or M2 macrophages by exposure to 10ng/ml IL-4 (PeproTech) for 24 hours, or left unstimulated as M0 macrophages using 1X DPBS. ER stress was then induced using 5 or 10 µM thapsigargin (Tg, Sigma), or 5 or 10 µg/mL tunicamycin (Tm, Cayman Chemical Company), or left untreated for 24 hours. Dimethyl sulfoxide (DMSO) vehicle was used as control. M0, M1, or M2 inducing agents were maintained during ER stress induction. Humidified 37°C incubators with 5% CO_2 were used for all cell incubations.

To confirm that we have successfully induced the bone marrow progenitor cells to differentiate into macrophages, cells were labelled with antibodies against the macrophage-specific surface markers, CD11b and F4/80. Briefly, cells were detached with Accutase and cells were incubated with the fluorescently labelled antibodies, anti-CD11b-APC (Life Technologies, 1:50) and anti-F4/80-PE (BD Pharmagen, 1:50), for 1 hour after 30 minutes of blocking with an Fc-receptor blocking antibody (anti-CD16/32, eBioscience, 1:100). Cells were then washed with FACS buffer (PBA, 0.1% BSA, 0.1% sodium azide). Flow cytometry was performed to determine the presence of $CD11b^+$ and $F4/80^+$ cells **(Figure 4.1)**. We demonstrated here we have a large population of the cells have differentiated into macrophages. Our gating method was able to capture over 95% of $CD11b^+$ and $F4/80^+$ cells.

Alamar Blue cell viability assay

Bone marrow derived macrophages were cultured in 96 well tissue culture plates at 1 x 10^5 cells/well/100 µL medium. After polarization, cells were then treated with the ER stress inducing agent, Tg or Tm, at the indicated concentrations for 24 hours as described above. Cell viability was determined using the Alamar Blue assay (Bio-rad). Reduction wavelength was measured at 570 nm and oxidation wavelength was measured at 600 nm.

Gene expression

Bone marrow derived macrophages were cultured in 12-well tissue culture plates at 4 x 10^5 cells/well/1 mL medium. Following polarization and ER stress induction, total

RNA was isolated with the TRIzol® Reagent (Invitrogen). Purified RNA was resuspended in DNase/RNase-free water and concentration was measured by absorbance at 260 nm. RNA purity was verified by calculating the ratio of the absorbance at 260 and 280 nm. 1 μg of total RNA was transcribed into cDNA using the High Capacity cDNA Reverse Transcription kit (Applied Biosystems).

Quantitative real-time reverse transcription polymerase chain reaction (RT-PCR) was performed on the StepOne Plus (Applied Biosystems) using 1 μL of resulting cDNA (corresponding to 0.1 μg of total RNA used to reverse transcription), 12.5 μl SensiFAST SYBR No-Rox Kit (Bioline), 1.25 μl of forward and reverse primers (500 nM, **Table 4.1**), and 8 μl of RNase-water for a total volume of 24 μl/well. cDNA was amplified under the following conditions: 10-minute hold at 95 °C, followed by 40 cycles consisting of a 15-second melt at 95 °C, followed by a 1-minute annealing at 60 °C. Relative quantitative analysis (2^{-ddCt}) was performed by normalizing data to the β-actin reference gene.

Lipid uptake

Bone marrow derived macrophages were cultured in 12-well suspension plates at 4 x 10^5 cells/well/400 μL medium. Cells were polarized and treated as indicated above. Cells where then treated with 2.5, 5, or 10 μg/mL of Alexa Fluor® 488 conjugated AcLDL (Molecular Probes) in serum free medium containing 0.3% fatty acid free bovine serum albumin (BSA, Sigma) for 2 hours. AcLDL uptake was detected using the BD

FACSCalibur flow cytometer. Staining intensity was quantified using FlowJo v10.2 to determine median fluorescent intensity.

Statistical analysis

Fold changes were calculated relative to the untreated M0 GSK3α floxed macrophages. Data are reported as the mean ± standard deviation. Data were analyzed using two- or three-way ANOVA with Tukey multiple comparison test. A value of $p < 0.05$ was considered statistically significant.

Figure 4.1. F4/80 and CD11b expression on cultured bone marrow–derived macrophages.

Bone marrow progenitor cells were isolated from *Ldlr*$^{-/-}$ mice with myeloid GSK3α or GSK3α deficiency. Cells were cultivated in medium containing 20 ng/mL M-CSF for 6 days, and processed for flow cytometry the following day. Cells were incubated with a PE-conjugated rat anti-mouse F4/80 mAb (1:50 dilution) and an APC-conjugated rat anti-mouse CD11b Ab (1:50 dilution). 30000 cells from each experimental group were examined on a BD FACScalibur flow cytometer. Bone marrow derived macrophages ($F4/80^{+}CD11b^{+}$) were gated at the indicated box. A small population of mostly $F4/80^{-}$ $CD11b^{-}$ cells were observed.

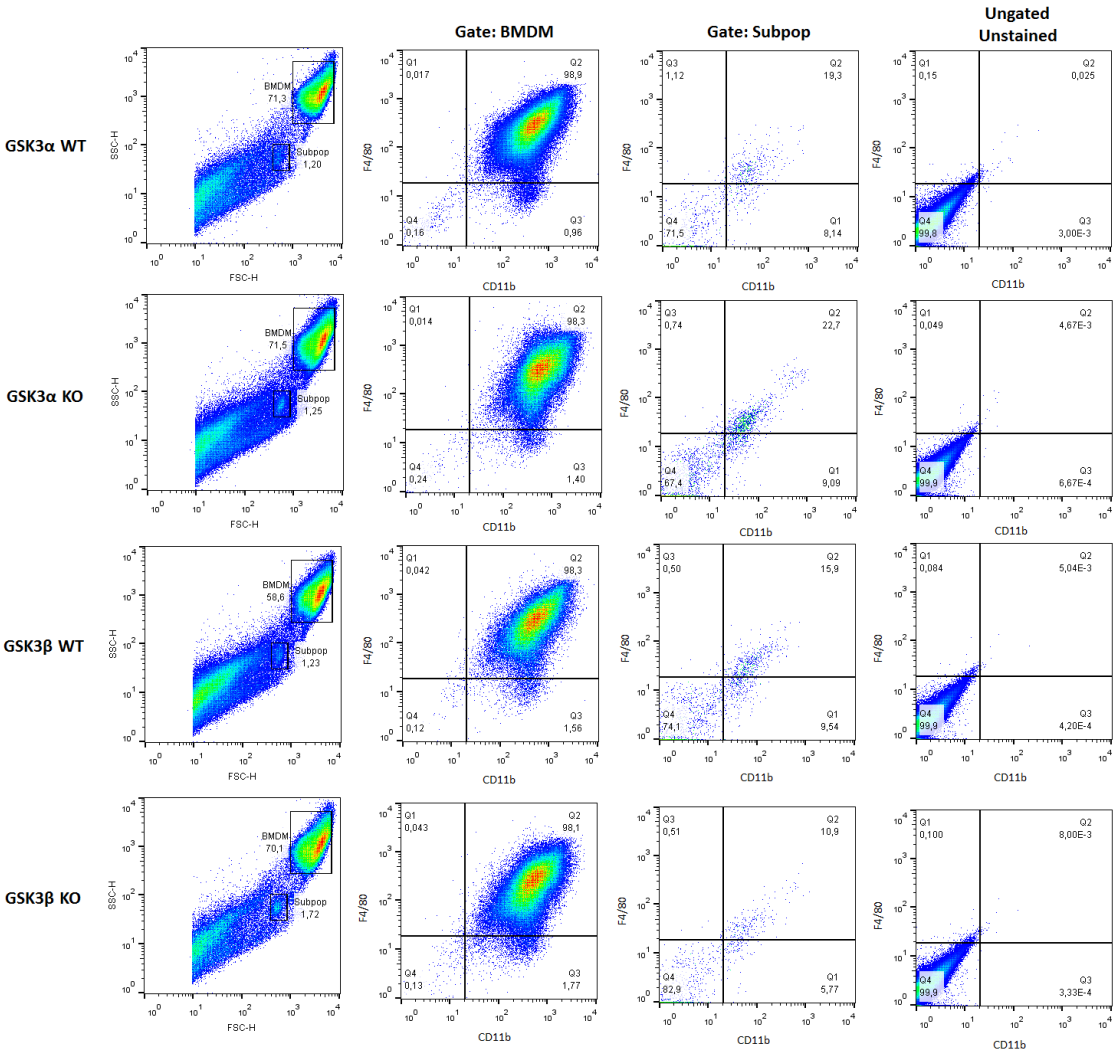
Gate: BMDM
Gate: Subpop
Ungated
Unstained
GSK3α WT
GSK3α KO
GSK3β WT
GSK3β KO
SSC-H
FSC-H
F4/80
CD11b
BMDM
71,3
Subpop
1,20
Q1 0,017
Q2 98,9
Q4 0,16
Q3 0,96
Q3 1,12
Q2 19,3
Q4 71,5
Q1 9,14
Q1 0,15
Q2 0,025
Q4 99,8
Q3 3,00E-3
BMDM
71,5
Subpop
1,25
Q1 0,014
Q2 98,3
Q4 0,24
Q3 1,40
Q3 0,74
Q2 22,7
Q4 67,4
Q1 9,09
Q1 0,049
Q2 4,67E-3
Q4 99,3
Q3 6,67E-4
BMDM
58,6
Subpop
1,23
Q1 0,042
Q2 98,3
Q4 0,12
Q3 1,56
Q3 0,50
Q2 15,9
Q4 74,1
Q1 9,54
Q1 0,084
Q2 5,04E-3
Q4 99,9
Q3 4,20E-4
BMDM
70,1
Subpop
1,72
Q1 0,043
Q2 98,1
Q4 0,13
Q3 1,77
Q3 0,51
Q2 10,9
Q4 82,9
Q1 5,77
Q1 0,100
Q2 8,00E-3
Q4 99,9
Q3 3,33E-4

Table 4.1. RT-PCR primer sequences.

Gene	Primer Sequence (5'-3')
iNOS	Fwd: CAG CTG GGC TGT ACA AAC CTT Rev: CAT TGG AAG TGA AGC GGT TCG
Arg1	Fwd: ACC TGG CCT TTG TTG ATG TCC CTA Rev: AGA GAT GCT TCC AAC TGC CAG ACT
GRP78	Fwd: ACC TGG GTG GGG AAC ACT TT Rev: TCT TCA AAT TTG GCC CGA GT
GRP94	Fwd: ACC GAA AAG GAC TTG CGA CT Rev: CTC TGA CGA ACC CGA AGG TC
CHOP	Fwd: GTC CCT AGC TTG GCT GAC AGA Rev: TGG AGA GCG AGG GCT TTG
βactin	Fwd: GGC ACC ACA CCT TCT ACA ATG Rev: GGG GTG TTG AAG GTC TCA AAC

4.5 RESULTS

M1 and M2 polarization of bone marrow derived macrophages

Bone marrow was isolated from the tibia and femurs of *Ldlr*$^{-/-}$*GSK3α*$^{fl/fl}$ mice. Because we want to determine the effects of GSK3α/β deficiency in different macrophage subtypes, the macrophages were left unpolarized (M0) or polarized into classical M1 or alternative M2 macrophages by 24 hour exposure to 10 ng/mL lipopolysaccharide (LPS) or IL-4, respectively. To assess our ability to polarize the bone marrow derived cells into M1 or M2 macrophages, total RNA was isolated from the cells and the expression level of iNOS and Arg1, indicative of M1 and M2 polarization respectively, were determined by RT-PCR. As expected, the exposure to LPS resulted in the elevated expression of the M1 marker iNOS, and exposure to IL-4 increased the expression of the M2 marker Arg1 **(Figure 4.2A, B)**. These results show that we can effectively polarize mouse macrophages towards the M1 or M2 phenotype. Interestingly, macrophages with deficiency in GSK3α were more polarized towards the M2 phenotype, rather than an M1 phenotype, when treated with LPS compared to the GSK3α floxed (wildtype, WT) control **(Figure 4.2C)**.

Figure 4.2. M1 and M2 polarization in cultured bone marrow derived macrophages. Bone marrow derived macrophages were isolated from Ldlr-deficient mice with floxed GSK3α or deficiency in GSK3α. Macrophages were left uninduced as M0, or exposed to 10 ng/ml LPS to induce M1 polarization or 10 ng/ml IL-4 for 24 hours to induced M2 polarization. The expression of the gene associated with M1 and M2 macrophage polarization were determined by RT-PCR. **A.** M1 polarization marker iNOS. **B.** M2 polarization marker Arg1. **C.** M1/M2 ratio of iNOS/Arg1 mRNA expression. Data are normalized to the βactin reference gene. Results are reported as the fold change relative to *GSK3α* floxed (WT) uninduced control (M0). n=3-4; mean ± SD; ****$p < 0.0001$ (Two-way ANOVA).

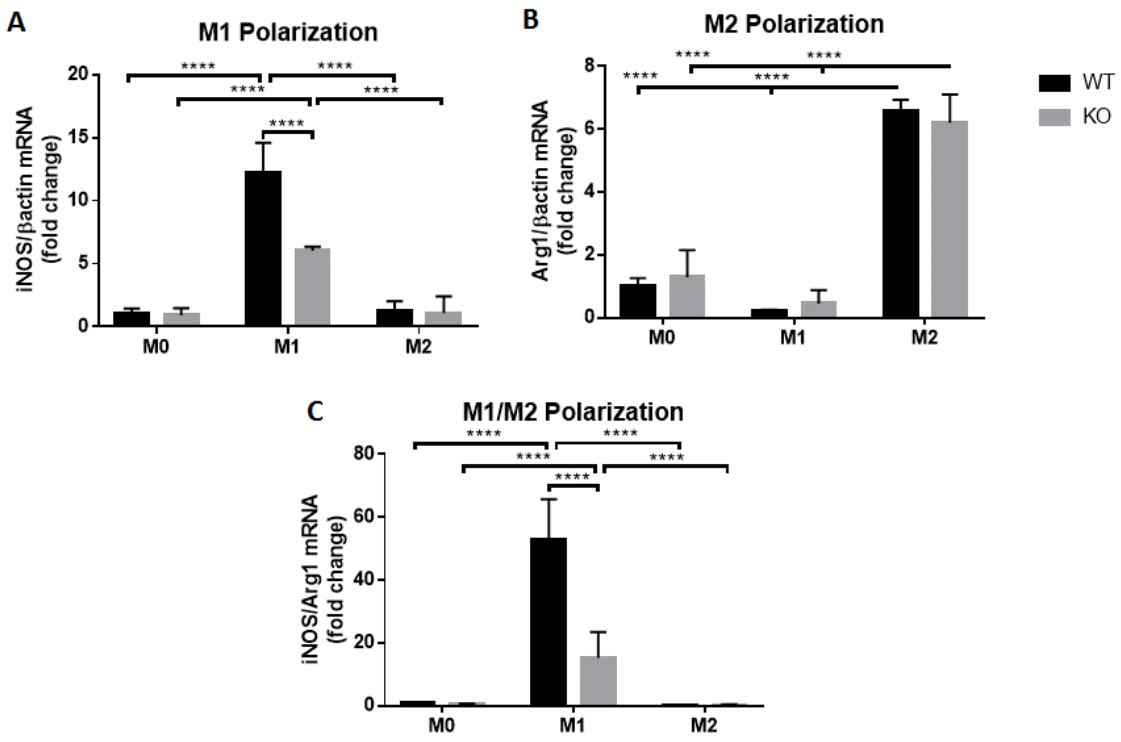
A
M1 Polarization
iNOS/βactin mRNA (fold change)
M0
M1
M2
B
M2 Polarization
Arg1/βactin mRNA (fold change)
WT
KO
C
M1/M2 Polarization
iNOS/Arg1 mRNA (fold change)
****

Effect of GSK3α deficiency on UPR activation in M1 and M2 macrophages

After polarizing the macrophages towards the M1 or M2 phenotype, we elicited ER stress through the treatment of ER stress inducing agents, thapsigargin (Tg, 5 µM or 10 µM) or tunicamycin (Tm, 5 µg/mL or 10 µg/mL), for 24 hours. Exposure to LPS or IL-4 was maintained to preserve the M1 or M2 phenotype, respectively. The induction of ER stress on these cells was determined by assessing the expression levels of the UPR genes encoding GRP78, GRP94, and CHOP **(Figure 4.3)**. As expected, the ER stress inducing agent increased the expression levels of each of these UPR genes, indicating that these treatments did indeed elicit ER stress in these macrophages. However, there were no differences in ER stress levels between the treated GSK3α floxed and the respective GSK3α knockout (KO) macrophages. Therefore, the deficiency of GSK3α does not appear to affect the unfolded protein response to ER stress.

Figure 4.3. GSK3α deficiency in cultured bone marrow derived macrophages did not alter the unfolded protein response. Bone marrow derived macrophages were isolated from Ldlr-deficient mice with floxed GSK3α or deficiency in GSK3α. Macrophages were treated *in vitro* with ER stress inducing agents thapsigargin (Tg, 5 or 10 μM), or tunicamycin (Tm, 5 or 10 μg/mL), or left untreated (UT, DMSO vehicle) for 24 hours after macrophage polarization. Gene expression level of **A.** GRP78, **B.** GRP94, and **C.** CHOP, were quantified. Data are normalized to the βactin reference gene. Results are reported as the fold change relative to the M0 *GSK3α* floxed (WT) untreated (UT) control. n=3-4; mean ± SD; * is relative to the respective UT group, and † is the comparison between M0, M1, and M2 within treatments; *p<0.05, **p<0.01, ***$p < 0.001$, ****$p < 0.0001$; (Three-way ANOVA).

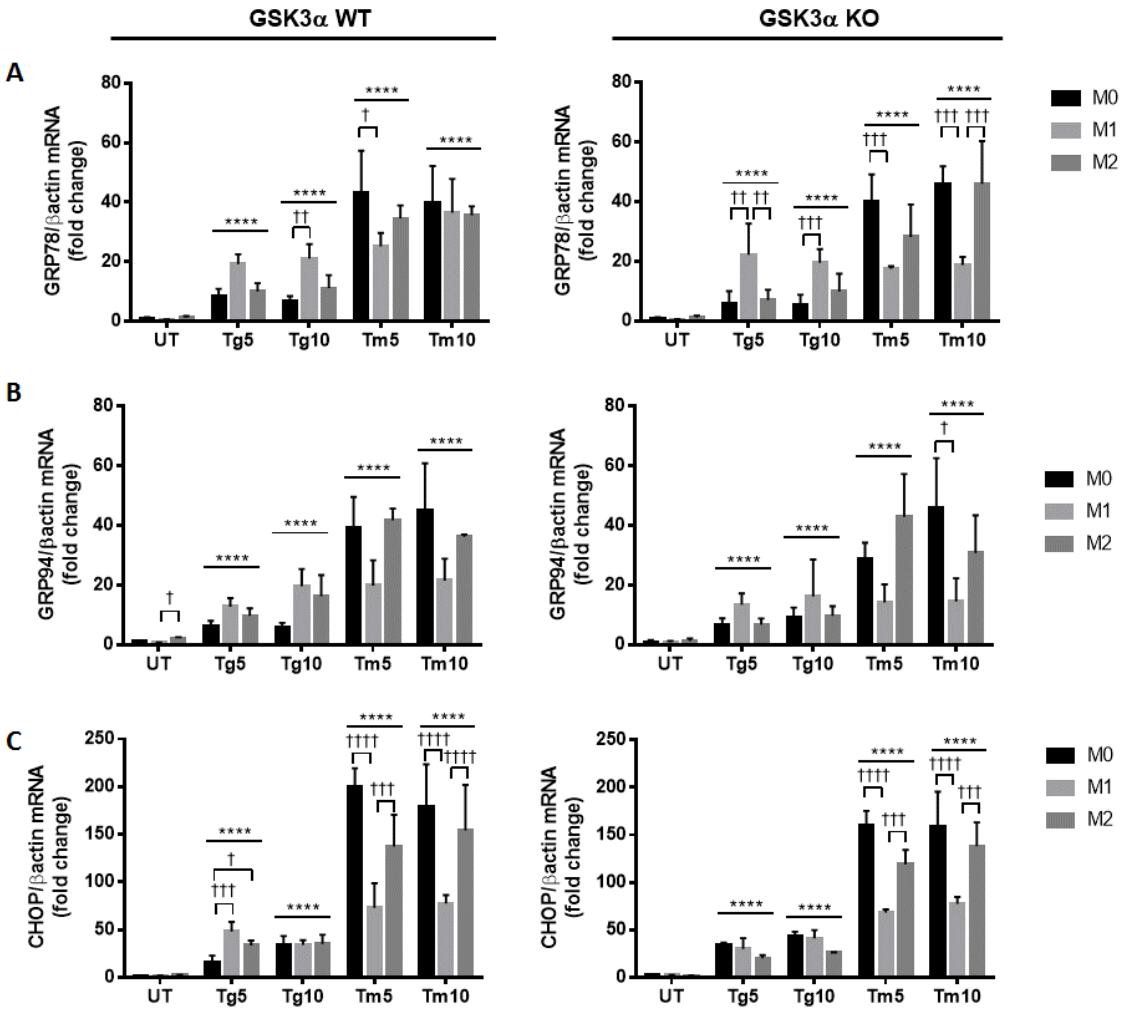
GSK3α WT
GSK3α KO
A
B
C
GRP78/βactin mRNA (fold change)
GRP94/βactin mRNA (fold change)
CHOP/βactin mRNA (fold change)
UT
Tg5
Tg10
Tm5
Tm10
M0
M1
M2

Effects of polarization in ER-stressed induced M0, M1, or M2 GSK3α deficient macrophages

To determine if the ER stress inducing agents affected macrophage polarization, iNOS and Arg1 expression levels were assessed upon Tg or Tm treatment. There was a modest decrease in iNOS expression after 48 hours of LPS induction compared to 24 hours of treatment **(Figure 4.2A, Figure 4.4A)**. However, Tg treatment augmented iNOS expression in M1 polarized macrophages, while Tm treatment did not affect iNOS mRNA levels. GSK3α deficiency did not significantly influence iNOS expression. Arg1 mRNA levels remained elevated after 48 hours of IL-4 induction **(Figure 4.4B)**. Both Tg and Tm treatment elevated Arg1 expression in M0 macrophages. These results suggest that conditions of ER stress promote M0 macrophages to polarize towards an M2 state. Interestingly, treatment of GSK3α deficient M0 macrophages with Tg resulted in elevated Arg1 expression, while Tm treatment reduced Arg1 expression. The differential results of Tg and Tm treatments suggests that these effects are most likely drug-specific, rather than related to the induction of ER stress. To determine the proportions of M1 and M2 phenotypic states, we calculated the iNOS and Arg1 ratios **(Figure 4.4C)**. GSK3α deficient M1 macrophages have a reduced ratio of iNOS/Arg1 mRNA level when treated with Tg compared to the controls.

Figure 4.4. M1 and M2 polarization in ER stressed cultured bone marrow derived macrophages. Bone marrow derived macrophages were cultured from Ldlr-deficient mice with floxed GSK3α or deficiency in GSK3α. Macrophages were treated with 10 ng/ml LPS (M1 polarization) or IL-4 (M2 polarization) for 24 hours. Cells were then treated with ER stress inducing agents thapsigargin (Tg, 5 or 10 μM), or tunicamycin (Tm, 5 or 10 μg/mL), or left untreated (UT, DMSO vehicle) for 24 hours. The expression level of the **A.** M1 polarization marker iNOS, **B.** M2 polarization marker Arg1, and **C.** M1/M2 ratio of iNOS/Arg1 mRNA expression were assessed. Results are reported as the fold change relative to the M0 *GSK3α* floxed (WT) untreated (UT) control. n=3-4; mean ± SD; * is relative to the respective UT group, † is the comparison between M0, M1, and M2 within treatments, and # is the comparison between WT and KO; *p<0.05, **p<0.01, ***$p < 0.001$, ****$p < 0.0001$; (Three-way ANOVA).

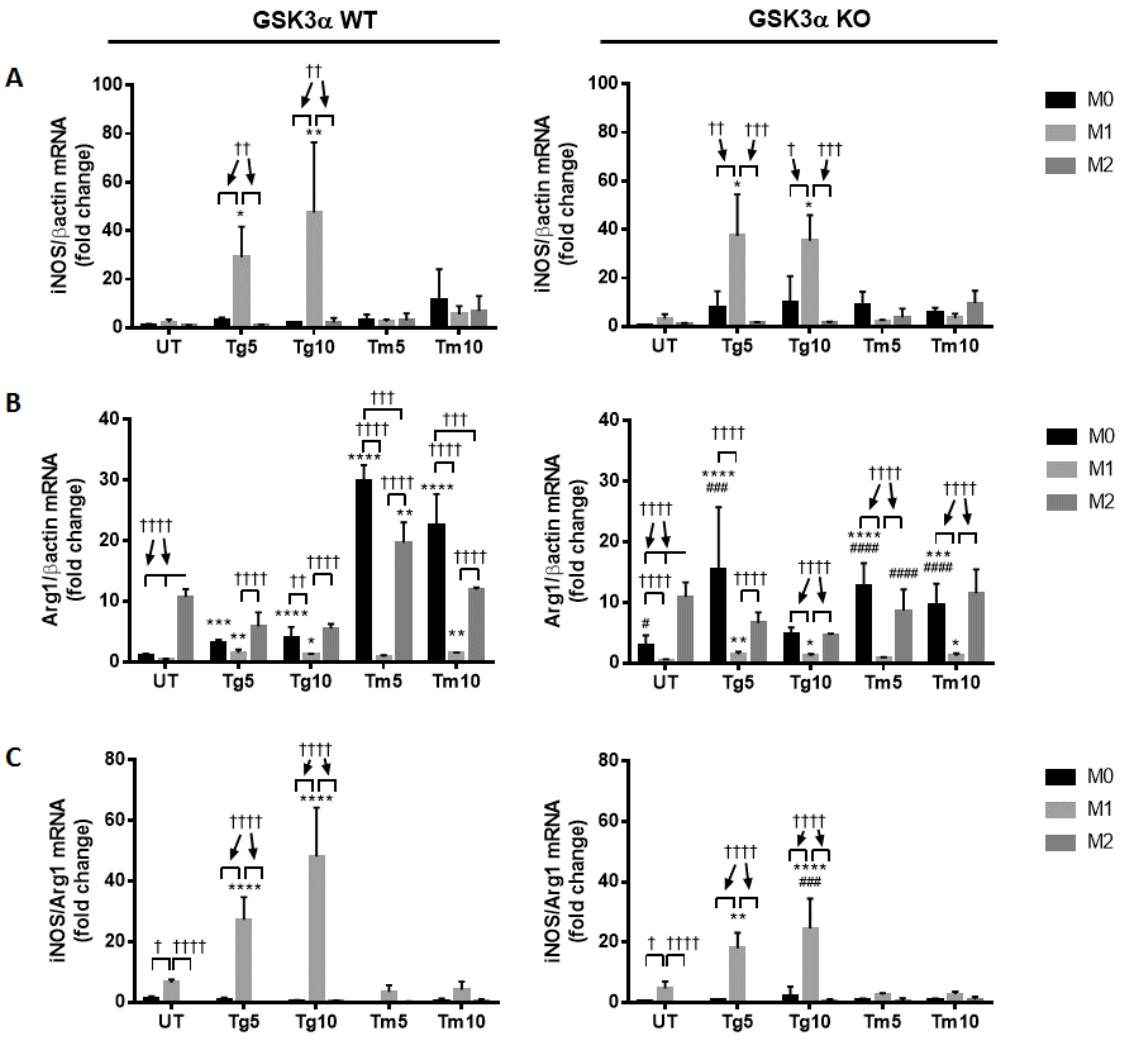
GSK3α WT
GSK3α KO
A
B
C
iNOS/βactin mRNA (fold change)
Arg1/βactin mRNA (fold change)
iNOS/Arg1 mRNA (fold change)
UT
Tg5
Tg10
Tm5
Tm10
M0
M1
M2

Assessing cell viability on GSK3α or GSK3β deficient macrophages

Having successfully polarized the macrophages and demonstrated the ability of Tg and Tm to activate the UPR, we then assessed cell viability to determine if macrophages with GSK3α or GSK3β deficiency are protected against the cytotoxic effects of Tg or Tm. Bone marrow derived macrophages with GSK3α or GSK3β KO were cultured as M0, M1, or M2 macrophages. The cells were then treated with Tg or Tm, and cell viability was assessed using the Alamar Blue assay **(Figure 4.5)**. M1 macrophages have drastically enhanced viability while M2 macrophages have no alterations in cell viability, compared to the M0 macrophages. There were no differences in cell viability between the GSK3α KO or WT macrophages **(Figure 4.5A)**. However, GSK3β deficient M1 and M2 macrophages slightly worsened cell viability **(Figure 4.5B)**. The viability of M0 macrophages were not significantly affected by GSK3β deficiency. Macrophages deficient in GSK3α and GSK3β have significantly improved viability for all M0, M1, and M2 under all treatment conditions **(Figure 4.5C)**.

To further assess for alterations in cell viability, TUNEL staining was performed to determine the proportion of apoptotic macrophages. Staining on the treated cells revealed a dose response relationship between ER stress and the percentage of TUNEL positive apoptotic cells, where only macrophages treated with the higher concentrations of Tg or Tm had significant increases in the proportion of TUNEL positive cells **(Figure 4.6)**. Consistent with the results informed by the Alamar Blue assay, M1 macrophages have relatively low levels of TUNEL positive cells, suggestive of higher cell viability. Further, there were no differences in TUNEL staining between the GSK3α KO or floxed

macrophages, indicating that GSK3α deficiency does not affect ER stress induced apoptosis **(Figure 4.6A)**. The M0 macrophages with GSK3β deficiency have a significantly higher proportion of cells which were stained positive with TUNEL when treated with Tg or Tm at high concentrations **(Figure 4.6B).**

Figure 4.5. Characterization of the toxic effects of thapsigargin (Tg) or tunicamycin (Tm) following 24 hours of treatment in Ldlr-deficient GSK3α or GSK3β KO bone marrow derived macrophages. Alamar Blue cell viability assay was used to measure the amount of reduced Alamar Blue as an indication of cell viability. Cytotoxic effects of Tg or Tm was assessed by determining the cell viability of the **A.** GSK3α KO, **B.** GSK3β KO, or **C.** GSK3α/β KO macrophages. Cell viability was quantified by normalizing the reduced Alamar Blue values to their respective untreated control. For the **A.** GSK3α KO and **B.** GSK3β KO macrophages, n = 4, and for the **B.** GSK3β KO macrophage, n = 8. Data are shown as mean ± SD; * is the comparison between WT and KO; **p<0.01, ***$p < 0.001$, ****$p < 0.0001$; (Three-way ANOVA).

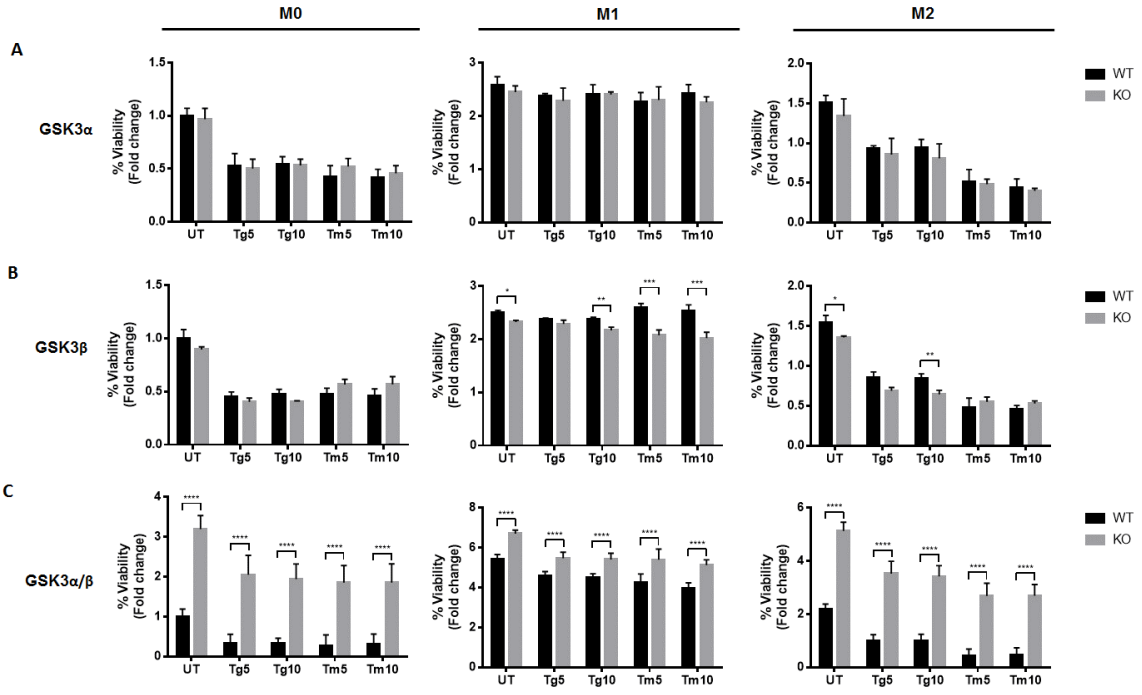
M0
M1
M2
A
GSK3α
B
GSK3β
C
GSK3α/β
% Viability (Fold change)
UT
Tg5
Tg10
Tm5
Tm10
WT
KO

Figure 4.6. TUNEL staining in ER stressed cultured bone marrow derived macrophages. Bone marrow derived macrophages were cultured from Ldlr-deficient mice with floxed GSK3α or deficiency in GSK3α. Macrophages were treated with ER stress inducing agents thapsigargin (Tg, 5 or 10 μM), or tunicamycin (Tm, 5 or 10 μg/mL), or left untreated (UT, DMSO vehicle) for 24 hours after macrophage polarization. Terminal deoxynucleotidyl transferase (TdT) dUTP Nick-End Labeling (TUNEL) staining were performed on the **A.** GSK3α KO or **B.** GSK3β KO macrophages. Data are normalized to the total cell count determined by the DAPI nuclei staining. Results are reported as the fold change relative to the M0 *GSK3α* floxed (WT) untreated (UT) control. For the **A.** GSK3α KO macrophages, n = 11-12, and for the **B.** GSK3β KO macrophage, n = 7-8. Data are sown as the mean ± SEM; * is the comparison between WT and KO; ***$p < 0.001$, ****$p < 0.0001$; (Three-way ANOVA).

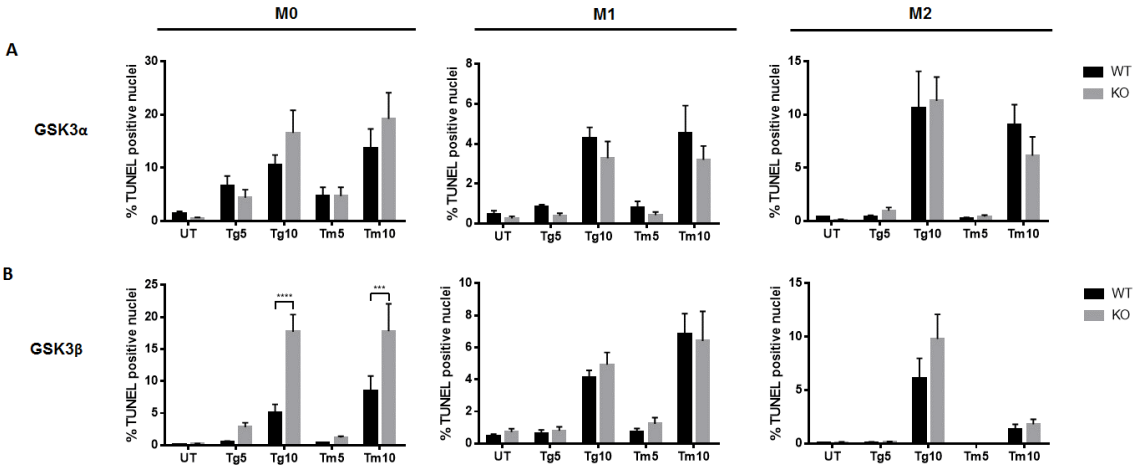
M0
M1
M2
A
GSK3α
B
GSK3β
% TUNEL positive nuclei
UT
Tg5
Tg10
Tm5
Tm10
WT
KO
****
***

Lipid accumulation in bone marrow derived macrophages

We wanted to determine if the loss of GSK3α would affect the accumulation of lipids in foam cells. To examine this, cultured GSK3α deficient macrophages were treated with the ER stress inducing agent, Tg or Tm, to upregulate the expression of genes associated with the accumulation of lipids. The expression levels of transcripts associated with lipid biosynthesis and uptake were determined by RT-PCR. The expression of genes involved in regulating lipid metabolism such as FAS and HMG-CoA reductase, were upregulated upon ER stress **(Figure 4.7A, B)**. The expression of ABCG1, which mediates cellular cholesterol efflux to HDL, was suppressed under ER stress **(Figure 4.7C)**. The absence of GSK3α appear to only alleviate the Tm induced upregulation of HMG-CoA reductase, but do not significantly alter the HMG-CoA reductase expression elicited by Tg. Together, these results suggest that GSK3α do not affect the expression of genes involved in lipid homeostasis.

Next, we wanted to devise an experiment to assess for lipid uptake. We hypothesized that M2 macrophages have elevated cholesterol uptake capacities compared to M1 macrophages. To examine our ability to effectively quantify the uptake of modified LDL in these macrophages, labelled acetylated low density lipoprotein (AcLDL) was added to M1 or M2 polarized WT macrophages after 24 hours of ER stress treatment. After 2 hours of incubation, AcLDL uptake was determined by quantifying staining intensity using flow cytometry **(Figure 4.8)**. Results showed no alteration in lipid uptake between the polarized macrophages, which suggests that these experimental parameters cannot accurately assess lipid uptake.

Figure 4.7. The role of GSK3α in regulating macrophage lipid metabolism. ER stress was induced Ldlr and GSK3α deficient bone marrow derived M0, M1, or M2 macrophages using thapsigargin (Tg, 5 or 10 μM) or tunicamycin (Tm, 5 of 10 μg/mL). Transcript expression of lipid metabolism genes such as **A.** fatty acid synthase (FAS), **B.** 5-hydroxy-3-methylglutaryl-coenzyme A (HMG-CoA) reductase, and **C.** ATP-binding cassette sub-family G member 1 (ABCG1) were determined by RT-PCR. * is relative to the respective UT group, † is the comparison between M0, M1, and M2 within treatments, and # is the comparison between WT and KO; *p<0.05, **p<0.01, ***$p < 0.001$, ****$p < 0.0001$; (Three-way ANOVA).

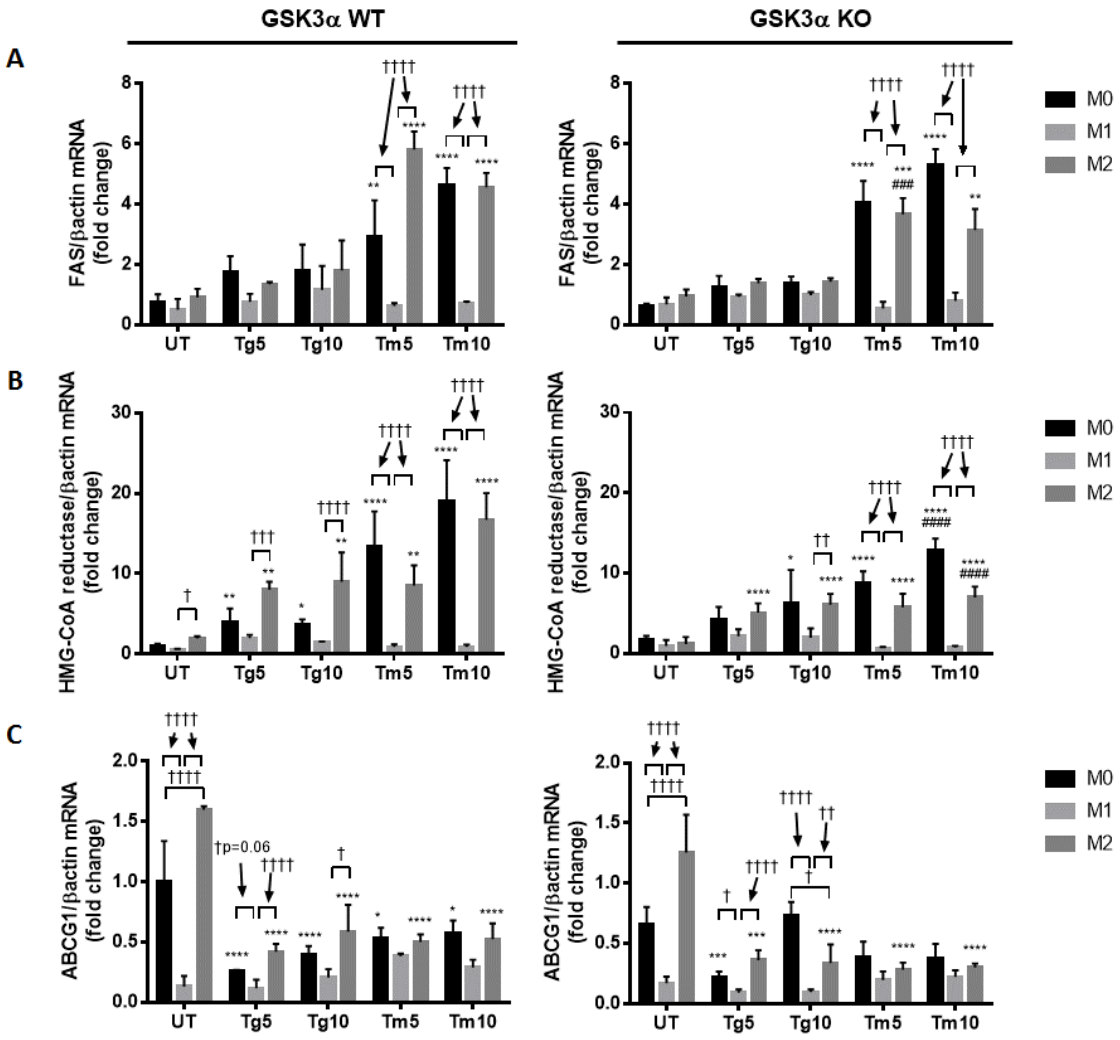
GSK3α WT
GSK3α KO
A
B
C
FAS/βactin mRNA (fold change)
HMG-CoA reductase/βactin mRNA (fold change)
ABCG1/βactin mRNA (fold change)
UT
Tg5
Tg10
Tm5
Tm10
M0
M1
M2
†p=0.06

Figure 4.8. Testing for lipid uptake in bone marrow derived macrophages. Bone marrow derived macrophages were isolated from Ldlr-deficient mice with expressing normal GSK3α/β were polarized to M1 or M2 macrophages for 24 hours in **A.** serum-containing (15% FBS) or **B.** serum-free (0.3% BSA) media. Macrophages were then exposed to 10, 5, or 2.5 μg/mL of labelled AcLDL in serum-free conditions. Lipid uptake was assessed by the mean fluorescence intensity determined by flow cytometry. n = 2; data are shown as mean ± SD.

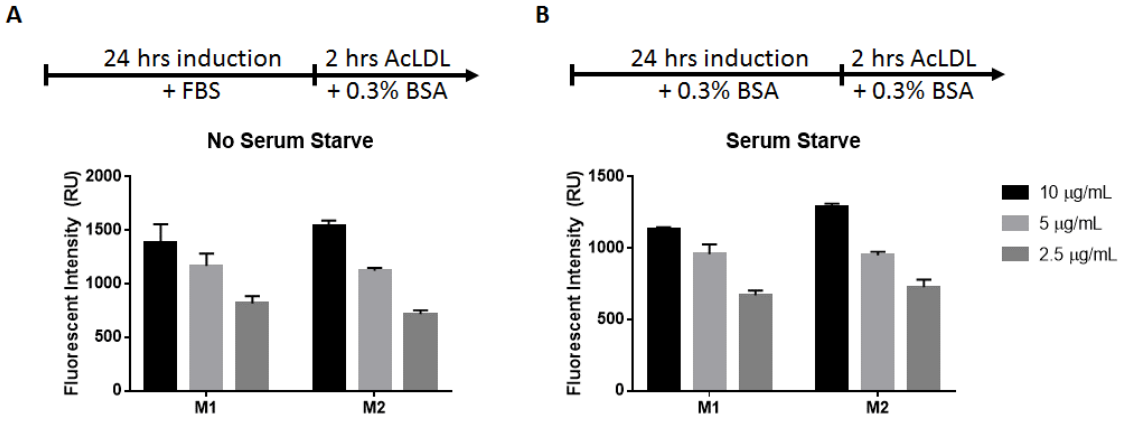
A
24 hrs induction
+ FBS
2 hrs AcLDL
+ 0.3% BSA
No Serum Starve
Fluorescent Intensity (RU)
2000
1500
1000
500
0
M1
M2
B
24 hrs induction
+ 0.3% BSA
2 hrs AcLDL
+ 0.3% BSA
Serum Starve
Fluorescent Intensity (RU)
1500
1000
500
0
M1
M2
10 μg/mL
5 μg/mL
2.5 μg/mL

4.6 DISCUSSION

Evidence suggests a causative role for ER stress in the development and progression of atherosclerosis[16–18]. However, the mechanism of how ER stress induces promotes atherosclerosis is poorly understood. We have previously demonstrated that ER stress signalling activates GSK3α/β through the unfolded protein response (UPR)[12]. The use of pharmacological inhibitors of GSK3α/β attenuates atherogenesis in mice[11,13]. However, it is unclear whether this was a consequence of inhibiting one of the two isoforms or if this effect only occurs upon inhibiting both isoforms. Mice with myeloid specific GSK3α deficiency develop smaller atherosclerotic lesions and have elevated levels of the M2 anti-inflammatory cytokines[15]. Atherosclerosis development and macrophage polarization was not affected in mice with myeloid GSK3β deficiency. While these isoforms can be involved in divergent cellular processes[9], the functional differences of GSK3α and GSK3β in macrophages have yet to be explored.

In this study, we investigated the role of these isoforms by characterizing the phenotypic differences of macrophages with GSK3α or GSK3β deficiency. To initiate signalling through GSK3α/β, macrophages were treated with Tg or Tm to induce ER stress. Consistent with our previous study using these macrophages, we found that the GSK3α deficient macrophages were less M1-like[15]. However, this resistance towards M1 polarization in GSK3α deficient macrophages was greatly diminished or disappeared after 48 hours.

We observed that ER stress induces the expression of Arg1 in macrophages,

indicative of a M2 phenotype. This is consistent with previous studies using ER stress inducing agents on macrophages[10,19]. Interestingly, Tg treatment amplified iNOS expression in M1 macrophages. Furthermore, the absence of GSK3α reduced Arg1 expression in Tm treated macrophages and diminished M1 polarization in Tg treated macrophages. Although we observed differences in polarization states between normal and GSK3α deficient macrophages, we cannot conclude that this is a result of ER stress signaling as different effects were observed between Tg and Tm treatments. This discrepancy may be a result of the distinctly different intracellular effects of Tg and Tm. Tg inhibits the sarcoplasmic/endoplasmic reticulum Ca^{2+}-ATPase and causes a reduction in ER calcium levels, while Tm inhibits N-acetylglucosamine-1-phosphate transferase (GPT) and interferes with the biosynthesis of glycoprotein in the ER[20]. This suggests that the role of GSK3α deficiency in the modulation of macrophage polarization is dependent on the specific mode of action causing ER stress.

Chronic ER stress induces to macrophage death and contribute towards the growing pro-thrombotic necrotic core, increasing the risk of plaque rupture[21,22]. The expression of CHOP and macrophage apoptosis have been correlated with advanced lesions, and the genetic deletion of CHOP in *Apoe*$^{-/-}$ and *Ldlr*$^{-/-}$ mice have reduced lesional macrophage apoptosis and plaque necrosis[23,24]. Since mice with myeloid specific GSK3α or GSK3β deficiency have smaller necrotic core, we hypothesized that the GSK3α or GSK3β deficient macrophage would be resistant to apoptosis and exhibit enhanced viability. We assessed cell viability by performing the Alamar Blue cell viability assay and staining for apoptotic TUNEL positive cells. Macrophages with

GSK3α deficiency did not confer any protection against the cytotoxic effects of Tg or Tm. The contrasting findings between the *in vivo* studies and our *in vitro* experiments may indicate that our cell culture conditions cannot capture the stresses or complexities in atherosclerotic lesions, or the smaller necrotic cores observed in our previous study are caused by other cell types, such as the apoptosis of smooth muscle cells or the clearance of apoptotic bodies by phagocytic cells. Interestingly, results from the Alamar Blue assay suggested that macrophages with GSK3α or GSK3β deficiency were protected against the toxic effects of Tm and demonstrated higher cell viability. This suggests that GSK3α and GSK3β have redundant functions in regulating cell viability.

Both M1 and M2 macrophages have the ability to ingest lipids and become foam cells[25]. Foam cells promote the progression of atherosclerosis and is a pathological hallmark of the disease[21]. Although the formation of foam cells is typically linked to a pro-inflammatory phenotype, the mechanisms which link cholesterol loading to inflammatory reactions in macrophages are not well defined[26]. In human plaques, M2 macrophages were found to be localized in more stable regions of the lesion away from the necrotic core[27]. The M2 foam cells contained smaller lipid droplets compared to M1 foam cells. M2 macrophages from healthy donors showed less foam cell formation compared with resting macrophages[27]. Contrastingly, M2 polarized macrophages from human diabetic macrophages demonstrated increased modified LDL cholesterol uptake through the upregulation of scavenger receptor CD36 and SR-A1[19], while M1 macrophages have reduced CD36 expression[28]. In the lesions of *Apoe*$^{-/-}$ mice fed a high fat diet, M2 macrophages were localized toward the centre of the plaque and had higher

cholesterol deposition while M1 macrophages localized to the periphery of the plaque and accumulated less cholesterol[19]. In addition, the induction of ER stress was reported to be sufficient to generate the M2 phenotype in macrophages through p-JNK-PPARγ signalling. Inhibiting ER stress decreased foam cell formation by reducing cholesterol uptake and increasing cholesterol efflux. Our results were consistent with these findings, where the macrophages treated with the ER stress inducing agents Tg and Tm elevated the expression the M2 polarization marker Arg1. Moreover, the ER stressed and M2 polarized macrophages show increased FAS and HMG-CoA reductase expression (cholesterol and fatty acid synthesis), and decreased ABCG1 expression (cholesterol efflux), suggestive of a greater capability to become foam cells. Together, the suppression of macrophage ER stress, or its distal components, may be a potential therapy for atherosclerosis. We have previously shown that inhibiting GSK3α/β, serine/threonine kinase attenuates ER stress associated foam cell formation. Therefore this may be a target to treat atherosclerosis[10]. Interestingly, the deletion of GSK3α appear to ameliorate the expression of HMG-CoA reductase (cholesterol synthesis), although the results were only significant in M0 and M2 macrophages treated with 10 μg/mL of the ER stress inducer, Tm.

Together, gene analysis assays revealed that GSK3α deficient macrophages are resistant towards a M1 polarization. Therefore, the atheroprotective effect observed in myeloid GSK3α deficient mice[15] may be due to a resistance towards the pro-inflammatory M1 polarization with no impact on the ability of macrophages to undergo apoptosis. Interestingly, GSK3α/β deficiency improved cell viability. Further work needs

to be conducted to determine the effect of GSK3α deficiency on lipid uptake and foam cell formation, as well as the investigation on the effects of GSK3β and GSK3α/β deficiency.

4.7 REFERENCES

1. Hilgendorf, I., Swirski, F. K. & Robbins, C. S. Monocyte fate in atherosclerosis. *Arterioscler. Thromb. Vasc. Biol.* **35,** (2015).

2. Hansson, G. K. & Libby, P. The immune response in atherosclerosis: a double-edged sword. *Nat. Rev. Immunol.* **6,** 508–519 (2006).

3. Murray, P. J. & Wynn, T. A. Protective and pathogenic functions of macrophage subsets. *Nat. Rev. Immunol.* **11,** 723–737 (2011).

4. Chinetti-Gbaguidi, G., Colin, S. & Staels, B. Macrophage subsets in atherosclerosis. *Nat. Rev. Cardiol.* **12,** 10–17 (2014).

5. Colin, S., Chinetti-Gbaguidi, G. & Staels, B. Macrophage phenotypes in atherosclerosis. *Immunol. Rev.* **262,** 153–166 (2014).

6. De Paoli, F. *et al.* Macrophage Phenotypes and Their Modulation in Atherosclerosis. *Circ. J.* **78,** 1775–1781 (2014).

7. Doble, B. W. & Woodgett, J. R. GSK-3: tricks of the trade for a multi-tasking kinase. *J. Cell Sci.* **116,** (2003).

8. Doble, B. W., Patel, S., Wood, G. A., Kockeritz, L. K. & Woodgett, J. R. Functional Redundancy of GSK-3α and GSK-3β in Wnt/β-Catenin Signaling Shown by Using an Allelic Series of Embryonic Stem Cell Lines. *Dev. Cell* **12,** 957–971 (2007).

9. Wang, Q. M., Park, I. K., Fiol, C. J., Roach, P. J. & DePaoli-Roach, A. A. Isoform

differences in substrate recognition by glycogen synthase kinases 3.alpha. and 3.beta. in the phosphorylation of phosphatase inhibitor 2. *Biochemistry* **33,** 143–147 (1994).

10. McAlpine, C. S. & Werstuck, G. H. Protein kinase R-like endoplasmic reticulum kinase and glycogen synthase kinase-3α/β regulate foam cell formation. *J. Lipid Res.* **55,** 2320–2333 (2014).

11. Choi, S.-E. *et al.* Atherosclerosis induced by a high-fat diet is alleviated by lithium chloride via reduction of VCAM expression in ApoE-deficient mice. *Vascul. Pharmacol.* **53,** 264–272 (2010).

12. McAlpine, C. S., Bowes, A. J., Khan, M. I., Shi, Y. & Werstuck, G. H. Endoplasmic Reticulum Stress and Glycogen Synthase Kinase-3β Activation in Apolipoprotein E-Deficient Mouse Models of Accelerated Atherosclerosis. *Arterioscler. Thromb. Vasc. Biol.* **32,** 82–91 (2012).

13. Bowes, A. J., Khan, M. I., Shi, Y., Robertson, L. & Werstuck, G. H. Valproate attenuates accelerated atherosclerosis in hyperglycemic ApoE-deficient mice: evidence in support of a role for endoplasmic reticulum stress and glycogen synthase kinase-3 in lesion development and hepatic steatosis. *Am. J. Pathol.* **174,** 330–342 (2009).

14. Kerkela, R. *et al.* Deletion of GSK-3beta in mice leads to hypertrophic cardiomyopathy secondary to cardiomyoblast hyperproliferation. *J. Clin. Invest.* **118,** 3609–18 (2008).

15. McAlpine, C. S. *et al.* Deletion of myeloid GSK3α attenuates atherosclerosis and promotes an M2 macrophage phenotype. *Arterioscler. Thromb. Vasc. Biol.* **35,** 1113–1122 (2015).

16. Hotamisligil, G. S. Endoplasmic reticulum stress and atherosclerosis. *Nat. Med.* **16,** 396–399 (2010).

17. Minamino, T. & Kitakaze, M. ER stress in cardiovascular disease. *J. Mol. Cell. Cardiol.* **48,** 1105–1110 (2010).

18. Scull, C. M. & Tabas, I. Mechanisms of ER Stress-Induced Apoptosis in Atherosclerosis. *Arterioscler. Thromb. Vasc. Biol.* **31,** (2011).

19. Oh, J. *et al.* Endoplasmic reticulum stress controls M2 macrophage differentiation and foam cell formation. *J. Biol. Chem.* **287,** 11629–41 (2012).

20. Oslowski, C. M. & Urano, F. Measuring ER stress and the unfolded protein response using mammalian tissue culture system. *Methods Enzymol.* **490,** 71–92 (2011).

21. Moore, K. J., Sheedy, F. J. & Fisher, E. A. Macrophages in atherosclerosis: a dynamic balance. *Nat. Rev. Immunol.* **13,** 709–21 (2013).

22. Tabas, I. The Role of Endoplasmic Reticulum Stress in the Progression of Atherosclerosis. *Circ. Res.* **107,** (2010).

23. Thorp, E. *et al.* Reduced Apoptosis and Plaque Necrosis in Advanced Atherosclerotic Lesions of Apoe−/− and Ldlr−/− Mice Lacking CHOP. *Cell*

Metab. **9,** 474–481 (2009).

24. Han, S. *et al.* Macrophage insulin receptor deficiency increases ER stress-induced apoptosis and necrotic core formation in advanced atherosclerotic lesions. *Cell Metab.* **3,** 257–266 (2006).

25. Leitinger, N. & Schulman, I. G. Phenotypic Polarization of Macrophages in Atherosclerosis. *Arterioscler. Thromb. Vasc. Biol.* **33,** (2013).

26. Dushkin, M. I. Macrophage/foam cell is an attribute of inflammation: Mechanisms of formation and functional role. *Biochem.* **77,** 327–338 (2012).

27. Chinetti-Gbaguidi, G. *et al.* Human Atherosclerotic Plaque Alternative Macrophages Display Low Cholesterol Handling but High Phagocytosis Because of Distinct Activities of the PPAR and LXR Pathways. *Circ. Res.* **108,** 985–995 (2011).

28. Nakagawa, T. *et al.* Oxidized LDL increases and interferon-gamma decreases expression of CD36 in human monocyte-derived macrophages. *Arterioscler. Thromb. Vasc. Biol.* **18,** 1350–7 (1998).

CHAPTER 5: GENERAL DISCUSSION

Even with the ongoing research on atherosclerosis, heart disease and stroke continue to be the leading cause of death worldwide[1,71]. Family history and age are non-modifiable risk factors attributed to atherosclerotic CVD. Modifiable risk factors which contributes to the disease include diabetes, high cholesterol, obesity, physical inactivity, and smoking[5]. CVD mortality rates have been declining, which may be caused by a combination of lifestyle changes, more effective treatments, and preventative medicine[1]. Lipid lowering therapy is often prescribed to help patients achieve lower LDL cholesterol levels. Despite the success of statins in lowering lipid levels and reducing cardiovascular risk, patients are still at risk for atherosclerosis and CVD[78]. In this project, we explored an alternative molecular pathway in atherosclerosis that can be targeted therapeutically, and works independently from the lipid lowering strategies **(Chapter 1, Figure 1.3)**.

The ER stress-GSK3α/β signalling pathway have previously been suggested to be involved in atherosclerosis[42,43]. As presented in chapter 3, *Ldlr*$^{-/-}$ mice developed atherosclerosis when fed a high fat diet. Mice were treated with the ER stress alleviating agent 4PBA or the GSK3α/β inhibitor VPA during various stages of atherosclerosis. Plasma cholesterol and triglyceride levels were unaffected by the treatments. The cross sectional areas of the atherosclerotic lesions were quantified at the aortic root, an atherosclerosis-prone region in mice. Inhibiting ER stress or GSK3α/β effectively

impeded plaque development and progression. Our findings were consistent with previous studies that investigated the effects of modulating ER stress or GSK3α/β in *Apoe*$^{-/-}$ mice, which is a different mouse model of atherosclerosis[42,43].

To assess whether targeting this pathway would be an effective strategy to treat atherosclerosis beyond preventative therapy, 4PBA or VPA treatment were administered in mice with advanced lesions. Immunofluorescence and immunohistochemistry staining was performed on the aortic sections to further characterize the plaques. The treatments in established mouse atherosclerosis did not alter plaque size, but lesions had smaller necrotic cores, increased VSMC, and increased collagen content which are features of less vulnerable plaques. This study is the first to investigate the effects of suppressing ER stress or GSK3α/β in mice with established atherosclerosis. Together, these data suggest that inhibiting the ER stress-GSK3α/β pathway may be plausible strategy to treat vulnerable plaques by reducing plaque progression and promoting plaque stability.

4PBA is approved by the Food and Drug Administration (FDA) for managing urea-cycle disorders. It is a chemical chaperone which prevents protein aggregation and assists in the folding of misfolded proteins in the ER lumen; thereby decreasing the amount of misfolded proteins and alleviating ER stress[79]. VPA is currently used in the treatment of bipolar disease and epilepsy[80]. It has also been shown to inhibit GSK3[81]; however, it is unclear as to whether VPA inhibits GSK3α/β directly or indirectly by inhibiting upstream components[82]. It is also not known if the GSK3α/β inhibitory activity of VPA is responsible for its efficacy as an anti-convulsant[83,84]. Although we assume that 4PBA and VPA can effectively modulate ER stress, small molecule drugs could

potentially affect other cellular pathways. For example, both 4PBA and VPA have also been shown to inhibit histone deacetylases (HDACs)[85–87]. However, given that HDAC inhibition exacerbates atherosclerosis, it is unlikely that the observed reduction in atherosclerosis is a result of the inhibition of HDACs[88].

Another evidence supporting that the inhibition of GSK3α/β attenuates the progression of atherosclerosis comes from the use of lithium, which like VPA, is a GSK3α/β inhibitor[89]. The use of lithium in HFD fed *Apoe*$^{-/-}$ mice reduced atherosclerotic lesion size by 8.2% after 6 weeks of treatment and 14% after 14 weeks of treatment. Despite the evidence of a role of GSK3α/β in the progression of atherosclerosis, the isoform specific functions of GSK3α and GSK3β are unclear as small molecules such as lithium and VPA can inhibit both isoforms. *Ldlr*$^{-/-}$*GSK3α*$^{-/-}$ mice have smaller atherosclerotic lesions, suggesting a role for GSK3α in atherosclerosis; however, the role of GSK3β is unclear since the whole body deletion of GSK3β is embryonically lethal[39]. Furthermore, the systemic inhibition of GSK3α/β means that the target responsible for hampering atherosclerosis is unknown. To elucidate the role of GSK3α and GSK3β isoforms in atherosclerosis and determine their tissue specific function, our lab have recently developed *Ldlr*$^{-/-}$ mice with hepatocyte or myeloid cell specific GSK3α or GSK3β deficiency[44]. GSK3α or GSK3β deficiency in hepatic or myeloid cells did not affect plasma lipid levels. Hepatic deletion of GSK3α or GSK3β did not affect atherosclerosis development. Myeloid GSK3α deficiency attenuated atherosclerotic, evident by a reduction in lesion size and necrotic volume, and promoted an anti-inflammatory plasma cytokine profile. GSK3β deficiency in myeloid cells did not affect

lesion size, but the plaques had smaller necrotic cores. This study identified homolog and tissue specific functions of GSK3α or GSK3β in the development of atherosclerosis. However, the molecular mechanisms and pathways that underlie these phenotypic differences and their corresponding contributions to the development of atherosclerosis were unclear.

In chapter 4, we characterized the effects of abolishing GSK3α or GSK3β in macrophages. These experiments were performed on bone marrow derived macrophages obtained from the *Ldlr*$^{-/-}$ mice lacking myeloid GSK3α or GSK3β as mentioned above. Consistent with the observation of a less inflammatory and more anti-inflammatory cytokine profile in the myeloid GSK3α deficient mice, the cultured bone marrow derived macrophages were resistant towards polarization to the pro-inflammatory M1 phenotype. However, GSK3α deficiency did not significantly affect macrophage viability, modify the response to ER stress, or alter the expression of genes involved in lipid metabolism. Contrastingly, the absence of GSK3β slightly amplified ER stress induced apoptosis. Interestingly, the deletion of GSK3α/β improved cell viability. These results suggest that there may be isoform redundant function between GSK3α and GSK3β in regulating cell viability. Additional experiments are required to further delineate the characteristics of these GSK3α or GSK3β deficient macrophages.

We presented evidence suggesting that inhibiting GSK3α/β may be a viable strategy to treat atherosclerosis. GSK3α/β inhibition attenuated the progression of atherosclerosis and stabilizes existing lesions, thus limiting the chance of rupture, which results in secondary cardiovascular events. Given that the pharmacological inhibition of

GSK3α/β with VPA would be a systemic effect, it is difficult to pinpoint the cause to a single cell type. Nevertheless, this may have in part resulted from the attenuated M1 polarization upon the inactivation of GSK3α in macrophages. The imbalance in the M1 and M2 macrophage ratio has been implicated in various diseases or inflammatory conditions, including atherosclerosis. Classically activated M1 macrophages promote inflammation and are polarized by Th1 cytokines such as IFNγ, IL-1β, and LPS[90,91]. Alternatively activated M2 macrophages promote an anti-inflammatory resolution and are polarized by Th2 cytokines such as IL-4 and IL-13. Generally, M1 macrophages are thought to promote atherosclerosis, and M2 macrophages attenuates atherosclerosis. The attenuation of M1 polarization through the myeloid deletion of IκB kinase in *Ldlr*$^{-/-}$ mice attenuated macrophage inflammatory responses and decreased lesion formation[92]. The myeloid-specific deficiency of either peroxisome proliferator activated receptor γ (PPARγ) or Krüppel-like factor 4, regulators of M2 polarization, suppressed M2 macrophage polarization and accelerated lesion formation in both *Apoe*$^{-/-}$[93] and *Ldlr*$^{-/-}$[94] mice. Moreover, macrophages switch from an M1 phenotype to an M2 phenotype during lesion regression[95,96]. This implicates that methods to decrease the ratio of M1/M2 macrophages may be an effective therapy for patients with atherosclerosis.

GSK3α/β have previously been shown to be involved the production of inflammatory cytokines through the activation of the inflammatory transcription factor NF-κB[97]. The inhibition of GSK3α/β reduced the production of pro-inflammatory IL-1β, IL-6, TNF-α, IL-12 and IFN-γ, and augmented the production of the anti-inflammatory cytokine IL-10 in human monocytes stimulated with LPS. The decrease in inflammatory

response was shown to be a result of augmenting the cyclic AMP response element binding protein (CREB) activity and promoting its association with the nuclear co-activator CREB-binding protein, and decreasing CREB-binding protein (CBP) association with NF-κB and suppressing NF-κB activity.

Isoform specific roles of GSK3α and GSK3β have been previously reported in the regulation of mouse T cell polarization[98]. The deficiency of GSK3α reduced the polarization of $CD4^+$ T cells to Th1 cells, but did not affect other T cell polarization subtypes such as Th2, Th17, or Treg. Contrastingly, the reduction ($GSK3\beta^{+/-}$) or absence ($GSK3\beta^{-/-}$) of GSK3β in $CD4^+$ T cells impaired the production of Th17 cells but did not alter differentiation to Th1, Th2, or Treg cells. Interestingly, it appears that GSK3α/β regulates the polarization of macrophages (myeloid lineage) and T cells (lymphoid lineage) in a similar fashion. The results of this study were consistent with our observation where the deletion of GSK3α in bone marrow derived macrophages were resistant towards M1 polarization.

Our results suggest that the ER stress-GSK3α/β signalling pathway play a critical role in the development of atherosclerosis. Inhibiting ER stress and/or GSK3α/β may be an effective strategy to treat patients with atherosclerosis. This pathway presents itself as a novel and exciting target to treat atherosclerosis that works different from the conventional lipid lowering strategies. The difference in the mode of actions suggests the possibility of combining both treatment strategies for a more effective or potent effect. However, further studies are required to investigate this hypothesis and question remains on whether our findings in the mouse model would translate to human patient care. A

better understanding of GSK3α/β signalling will help determine how GSK3α/β promotes atherosclerosis development and progression. Moreover, the identification of homolog differences between GSK3α and GSK3β may help elucidate the potential side effects from inhibiting these isoforms.

CHAPTER 6: FUTURE WORK

6.1 Completion of the study in chapter 4

To complete the study presented in chapter 4, further characterization of the macrophages with GSK3α or GSK3β deficiency will be required. This will involve

a) investigating additional markers of apoptosis (e.g. cleaved caspase-3),
b) determining expression levels of additional markers involved in lipid metabolism (e.g. ABCA1, SREBP1/2, SRA, CD36, and SRB1),
c) optimizing the AcLDL lipid uptake experiments to assess for foam cell formation, and
d) extending the experiments to macrophages with GSK3β deficiency.

Further experimentation may involve determining the molecular mechanism of GSK3α or GSK3β in the regulation of lipid metabolism by gene expression profiling. Analyzing the changes in gene expression may give insight to the molecular pathway by which GSK3α or GSK3β targets to regulate lipid metabolism. Moreover, future analysis could include macrophages with both GSK3α and GSK3β deficiency. This would allow us to examine for any redundant functions of GSK3α and GSK3β.

As a control in the above experiments, GSK3α or GSK3β will be introduced into the corresponding GSK3α or GSK3β deficient macrophages using the adenovirus vector Ad-GSK3α and Ad-GSK3β, respectively, to determine if the observed effects can be alleviated by the adenovirus vector.

In addition to completing this study, there are other experiments that can be conducted to further delineate the specific functions of GSK3α or GSK3β and determine the efficacy of inhibiting one or both of these homologs in the treatment of atherosclerosis.

6.2 Prolonged regression model: Assessing the effects of reducing ER stress or inhibiting GSK3α/β for an extended period of time

In chapter 3, we presented a model to investigate atherosclerotic regression in mice. In this model, the mice were given the treatment of 4PBA or VPA for only 4 weeks. We observed changes in the plaque composition, but did not see any evidence of regression. However, question remains as to what would happen if these mice were treated for a longer period of time. Would we still see differences in plaque content? Would we see smaller plaque sizes (regression)? Would the prolonged duration of treatment be detrimental to the health of these mice?

In order to address these questions, we started a similar regression experiment to the one in chapter 3, but these mice would be place on treatment for 10 weeks instead of 4 weeks. Briefly, 4 week old female *Ldlr*$^{-/-}$ mice were placed on a HFD for 16 weeks to allow for the development of established lesions. Some of these mice were sacrificed at this time for the baseline, while other subsets of mice had their diets switched to a chow diet for control, or chow diet with 4PBA or VPA treatment for 10 weeks. Some of these mice have already been harvested and preliminary data suggests that the mice with VPA treatment have significantly lower levels of fasting blood glucose compared to the

baseline or control groups. 4PBA treatment did not alter fasting blood glucose levels. Treatments did not affect body weight, liver weight, or fat pad (adipose) weight. Experiments are underway to investigate for any differences in plaque size and composition.

6.3 Regression analysis on mice with inducible myeloid GSK3α and/or β deficiency

A limitation of the data presented in chapter 3, we assumed that the results obtained were the result of VPA inhibiting GSK3α/β. However, VPA has previously been reported to also inhibit CYP2C9, epoxide hydrolase, glucuronyl transferase, and histone deacetylases (HDACs)[85,86,99–102]. To overcome this limitation, our regression model could be extended into a system where we could specifically delete the GSK3α and/or GSK3β genes in myeloid cells.

To do this, we are currently working on creating *Ldlr*$^{-/-}$ mice with a myeloid cell-specific tamoxifen inducible Cre recombinase system. These mice contains a Cre recombinase which is flanked on both ends with a mutated G525R murine estrogen receptor (mer) which is under the control of the mouse colony stimulating factor 1 receptor (Csf1r) promotor. This Mer-Cre-Mer double fusion protein does not bind to its natural ligand, estrogen, but will bind to the synthetic estrogen receptor ligand, tamoxifen. These mice will be crossed with *Ldlr*$^{-/-}$ mice containing a loxP-flanked sequence on the ends of *GSK3α* or *GSK3β* (*GSK3α*$^{fl/fl}$ or *GSK3β*$^{fl/fl}$). The resulting *Ldlr*$^{-/-}$*Csf1r-Mer-Cre-MerGSK3α*$^{fl/fl}$ and *Ldlr*$^{-/-}$*Csf1r-Mer-Cre-MerGSK3β*$^{fl/fl}$ mice will be placed on a HFD for lesion development. These mice will then be injected with tamoxifen or saline for control. The Mer-Cre-Mer protein complex undergoes nuclear translocation in the presence of

tamoxifen, allowing the Cre to mediate the site-specific recombination. This results in the excision of the genes between the floxed sites and ultimately ablating the expression of *GSK3α*$^{fl/fl}$ or *GSK3β*$^{fl/fl}$. With the ability to dictate the genetic deletion of *GSK3α* or *GSK3β*, this system will allow us to investigate the role of GSK3α and GSK3β at various times during lesion progression or regression.

REFERENCES FOR GENERAL INTRODUCTION, GENERAL DISCUSSION, AND FUTURE WORK

1. Mozaffarian, D. *et al.* Executive summary: heart disease and stroke statistics—2015 update. *Circulation* **131,** 434–441 (2015).

2. Minister of Industry. *Health Fact Sheets: The 10 leading causes of death, 2013*. (Statistics Canada, 2017). doi:82-625-X

3. Public Health Agency of Canada. *Tracking heart disease and stroke in Canada, 2009*. (Public Health Agency of Canada, 2009). doi:HP32-3/2009E

4. Brogan, I. Canadian Pharmaceutical Trends. Top 10 Dispensed Therapeutic Classes in Canada 2010. (2015). Available at: https://www.imshealth.com/de_DE/about-us/News-and-Events/canada-pharmaceutical-trends-(canada–english). (Accessed: 23rd April 2017)

5. Grundy, S. M., Pasternak, R., Greenland, P., Smith, S. & Fuster, V. Assessment of Cardiovascular Risk by Use of Multiple-Risk-Factor Assessment Equations. *Circulation* **100,** (1999).

6. Zarins, C. K. *et al.* Carotid bifurcation atherosclerosis. Quantitative correlation of plaque localization with flow velocity profiles and wall shear stress. *Circ. Res.* **53,** (1983).

7. Cybulsky, M. I. *et al.* A major role for VCAM-1, but not ICAM-1, in early atherosclerosis. *J. Clin. Invest.* **107,** 1255–62 (2001).

8. Johnson-Tidey, R. R., McGregor, J. L., Taylor, P. R. & Poston, R. N. Increase in the adhesion molecule P-selectin in endothelium overlying atherosclerotic plaques. Coexpression with intercellular adhesion molecule-1. *Am. J. Pathol.* **144,** 952–61 (1994).

9. To, K., Agrotis, A., Besra, G., Bobik, A. & Toh, B.-H. NKT Cell Subsets Mediate Differential Proatherogenic Effects in ApoE−/− Mice. *Arterioscler. Thromb. Vasc. Biol.* **29,** (2009).

10. Lane, A. *et al.* Cytokine production by cholesterol-loaded human peripheral monocyte-macrophages: the effect on fibrinogen mRNA levels in a hepatoma cell-line (HepG2). *Biochim. Biophys. Acta - Mol. Basis Dis.* **1097,** 161–165 (1991).

11. Webster, W. S., Bishop, S. P. & Geer, J. C. Experimental aortic intimal thickening. I. Morphology and source of intimal cells. *Am. J. Pathol.* **76,** 245–64 (1974).

12. Nikkari, S. T. *et al.* Interstitial Collagenase (MMP-1) Expression in Human Carotid Atherosclerosis. *Circulation* **92,** (1995).

13. Romanic, A. M. *et al.* Myocardial protection from ischemia/reperfusion injury by targeted deletion of matrix metalloproteinase-9. *Cardiovasc. Res.* **54,** (2002).

14. Hayashidani, S. *et al.* Targeted deletion of MMP-2 attenuates early LV rupture and late remodeling after experimental myocardial infarction. *Am. J. Physiol. - Hear. Circ. Physiol.* **285,** (2003).

15. Lewis, D. R. *et al.* Sugar-based amphiphilic nanoparticles arrest atherosclerosis in

vivo. *Proc. Natl. Acad. Sci.* **112,** 2693–2698 (2015).

16. Harrison, D., Griendling, K. K., Landmesser, U., Hornig, B. & Drexler, H. Role of oxidative stress in atherosclerosis. *Am. J. Cardiol.* **91,** 7–11 (2003).

17. Singh, U. *et al.* Oxidative stress and atherosclerosis. *Pathophysiol. Off. J. Int. Soc. Pathophysiol.* **13,** 129–42 (2006).

18. Matés, J. M., Segura, J. A., Alonso, F. J. & Márquez, J. Intracellular redox status and oxidative stress: implications for cell proliferation, apoptosis, and carcinogenesis. *Arch. Toxicol.* **82,** 273–299 (2008).

19. Judkins, C. P. *et al.* Direct evidence of a role for Nox2 in superoxide production, reduced nitric oxide bioavailability, and early atherosclerotic plaque formation in ApoE-/- mice. *AJP Hear. Circ. Physiol.* **298,** H24–H32 (2010).

20. Jaquet, V., Scapozza, L., Clark, R. A., Krause, K.-H. & Lambeth, J. D. Small-Molecule NOX Inhibitors: ROS-Generating NADPH Oxidases as Therapeutic Targets. *Antioxid. Redox Signal.* **11,** 2535–2552 (2009).

21. Steinhubl, S. R. Why Have Antioxidants Failed in Clinical Trials? *Am. J. Cardiol.* **101,** S14–S19 (2008).

22. Kim, I., Xu, W. & Reed, J. C. Cell death and endoplasmic reticulum stress: disease relevance and therapeutic opportunities. *Nat. Rev. Drug Discov.* **7,** 1013–1030 (2008).

23. Beriault, D. R., Werstuck, G. H., Beriault, D. R. & Werstuck, G. H. The Role of

Glucosamine-Induced ER Stress in Diabetic Atherogenesis. *Exp. Diabetes Res.* **2012,** 1–11 (2012).

24. Novoa, I., Zeng, H., Harding, H. P. & Ron, D. Feedback Inhibition of the Unfolded Protein Response by GADD34-Mediated Dephosphorylation of eIF2α. *J. Cell Biol.* **153,** (2001).

25. Zinszner, H. *et al.* CHOP is implicated in programmed cell death in response to impaired function of the endoplasmic reticulum. *Genes Dev.* **12,** 982–95 (1998).

26. Misra, U. K., Deedwania, R. & Pizzo, S. V. Activation and cross-talk between Akt, NF-kappaB, and unfolded protein response signaling in 1-LN prostate cancer cells consequent to ligation of cell surface-associated GRP78. *J. Biol. Chem.* **281,** 13694–707 (2006).

27. Hofmann, M. A. *et al.* Hyperhomocysteinemia enhances vascular inflammation and accelerates atherosclerosis in a murine model. *J. Clin. Invest.* **107,** 675–83 (2001).

28. Beriault, D. R., Sharma, S., Shi, Y., Khan, M. I. & Werstuck, G. H. Glucosamine-supplementation promotes endoplasmic reticulum stress, hepatic steatosis and accelerated atherogenesis in apoE−/− mice. *Atherosclerosis* **219,** 134–140 (2011).

29. Khan, M. I., Pichna, B. A., Shi, Y., Bowes, A. J. & Werstuck, G. H. Evidence supporting a role for endoplasmic reticulum stress in the development of atherosclerosis in a hyperglycaemic mouse model. *Antioxid. Redox Signal.* **11,**

2289–2298 (2009).

30. Kunjathoor, V. V, Wilson, D. L. & LeBoeuf, R. C. Increased atherosclerosis in streptozotocin-induced diabetic mice. *J. Clin. Invest.* **97,** 1767–73 (1996).

31. Phiel, C. J., Wilson, C. A., Lee, V. M.-Y. & Klein, P. S. GSK-3α regulates production of Alzheimer's disease amyloid-β peptides. *Nature* **423,** 435–439 (2003).

32. Nikoulina, S. E. *et al.* Potential role of glycogen synthase kinase-3 in skeletal muscle insulin resistance of type 2 diabetes. *Diabetes* **49,** (2000).

33. Klein, P. S. & Melton, D. A. A molecular mechanism for the effect of lithium on development. *Proc. Natl. Acad. Sci. U. S. A.* **93,** 8455–9 (1996).

34. Mukai, F., Ishiguro, K., Sano, Y. & Fujita, S. C. Alternative splicing isoform of tau protein kinase I/glycogen synthase kinase 3β. *J. Neurochem.* **81,** 1073–1083 (2002).

35. Woodgett, J. R. Molecular cloning and expression of glycogen synthase kinase-3/factor A. *EMBO J.* **9,** 2431–8 (1990).

36. Doble, B. W., Patel, S., Wood, G. A., Kockeritz, L. K. & Woodgett, J. R. Functional Redundancy of GSK-3α and GSK-3β in Wnt/β-Catenin Signaling Shown by Using an Allelic Series of Embryonic Stem Cell Lines. *Dev. Cell* **12,** 957–971 (2007).

37. Wang, Q. M., Park, I. K., Fiol, C. J., Roach, P. J. & DePaoli-Roach, A. A. Isoform

differences in substrate recognition by glycogen synthase kinases 3.alpha. and 3.beta. in the phosphorylation of phosphatase inhibitor 2. *Biochemistry* **33,** 143–147 (1994).

38. Song, L., De Sarno, P. & Jope, R. S. Central role of glycogen synthase kinase-3beta in endoplasmic reticulum stress-induced caspase-3 activation. *J. Biol. Chem.* **277,** 44701–8 (2002).

39. Banko, N. S. *et al.* Glycogen synthase kinase 3α deficiency attenuates atherosclerosis and hepatic steatosis in high fat diet–fed low density lipoprotein receptor–deficient mice. *Am. J. Pathol.* **184,** 3394–3404 (2014).

40. McAlpine, C. S. & Werstuck, G. H. Protein kinase R-like endoplasmic reticulum kinase and glycogen synthase kinase-3α/β regulate foam cell formation. *J. Lipid Res.* **55,** 2320–2333 (2014).

41. Martin, M., Rehani, K., Jope, R. S. & Michalek, S. M. Toll-like receptor–mediated cytokine production is differentially regulated by glycogen synthase kinase 3. *Nat. Immunol.* **6,** 777–784 (2005).

42. Erbay, E. *et al.* Reducing endoplasmic reticulum stress through a macrophage lipid chaperone alleviates atherosclerosis. *Nat. Med.* **15,** 1383–1391 (2009).

43. Bowes, A. J., Khan, M. I., Shi, Y., Robertson, L. & Werstuck, G. H. Valproate attenuates accelerated atherosclerosis in hyperglycemic ApoE-deficient mice: evidence in support of a role for endoplasmic reticulum stress and glycogen

synthase kinase-3 in lesion development and hepatic steatosis. *Am. J. Pathol.* **174,** 330–342 (2009).

44. McAlpine, C. S. *et al.* Deletion of myeloid GSK3α attenuates atherosclerosis and promotes an M2 macrophage phenotype. *Arterioscler. Thromb. Vasc. Biol.* **35,** 1113–1122 (2015).

45. Olesen, J. B. *et al.* Valproate attenuates the risk of myocardial infarction in patients with epilepsy: a nationwide cohort study. *Pharmacoepidemiol. Drug Saf.* **20,** 146–153 (2011).

46. Dave, T., Ezhilan, J., Vasnawala, H. & Somani, V. Plaque regression and plaque stabilisation in cardiovascular diseases. *Indian J. Endocrinol. Metab.* **17,** 983–9 (2013).

47. Friedman, M., Byers, S. O. & Rosenman, R. H. Resolution of Aortic Atherosclerotic Infiltration in the Rabbit by Phosphatide Infusion. *Exp. Biol. Med.* **95,** 586–588 (1957).

48. Rayner, K. J. *et al.* Antagonism of miR-33 in mice promotes reverse cholesterol transport and regression of atherosclerosis. *J. Clin. Invest.* **121,** 2921–2931 (2011).

49. Chistiakov, D. A., Myasoedova, V. A., Revin, V. V., Orekhov, A. N. & Bobryshev, Y. V. The phenomenon of atherosclerosis reversal and regression: Lessons from animal models. *Exp. Mol. Pathol.* **102,** 138–145 (2017).

50. Birbrair, A. & Frenette, P. S. Niche heterogeneity in the bone marrow. *Ann. N. Y.*

Acad. Sci. **1370,** 82–96 (2016).

51. Geissmann, F. *et al.* Development of monocytes, macrophages, and dendritic cells. *Science* **327,** 656–61 (2010).

52. Biswas, S. K. & Mantovani, A. Macrophage plasticity and interaction with lymphocyte subsets: cancer as a paradigm. *Nat. Immunol.* **11,** 889–896 (2010).

53. De Paoli, F. *et al.* Macrophage Phenotypes and Their Modulation in Atherosclerosis. *Circ. J.* **78,** 1775–1781 (2014).

54. Jablonski, K. A. *et al.* Novel Markers to Delineate Murine M1 and M2 Macrophages. *PLoS One* **10,** e0145342 (2015).

55. Martinez, F. O., Sica, A., Mantovani, A. & Locati, M. Macrophage activation and polarization. *Front. Biosci.* **13,** 453–61 (2008).

56. Lesnik, P. *et al.* Decreased atherosclerosis in CX3CR1-/- mice reveals a role for fractalkine in atherogenesis. *J. Clin. Invest.* **111,** 333–40 (2003).

57. Khallou-Laschet, J. *et al.* Macrophage Plasticity in Experimental Atherosclerosis. *PLoS One* **5,** e8852 (2010).

58. Stöger, J. L. *et al.* Distribution of macrophage polarization markers in human atherosclerosis. *Atherosclerosis* **225,** 461–468 (2012).

59. Chinetti-Gbaguidi, G. *et al.* Human atherosclerotic plaque alternative macrophages display low cholesterol handling but high phagocytosis because of distinct activities of the PPARγ and LXRα pathways. *Circ. Res.* **108,** 985–95 (2011).

60. Davis, M. J. *et al.* Macrophage M1/M2 polarization dynamically adapts to changes in cytokine microenvironments in Cryptococcus neoformans infection. *MBio* **4,** e00264-13 (2013).

61. Chiu, I. M. *et al.* A Neurodegeneration-Specific Gene-Expression Signature of Acutely Isolated Microglia from an Amyotrophic Lateral Sclerosis Mouse Model. *Cell Rep.* **4,** 385–401 (2013).

62. Murray, P. J. *et al.* Macrophage Activation and Polarization: Nomenclature and Experimental Guidelines. *Immunity* **41,** 14–20 (2014).

63. Xue, J. *et al.* Transcriptome-Based Network Analysis Reveals a Spectrum Model of Human Macrophage Activation. *Immunity* **40,** 274–288 (2014).

64. Hilgendorf, I., Swirski, F. K. & Robbins, C. S. Monocyte fate in atherosclerosis. *Arterioscler. Thromb. Vasc. Biol.* **35,** (2015).

65. Robbins, C. S. *et al.* Local proliferation dominates lesional macrophage accumulation in atherosclerosis. *Nat. Med.* **19,** 1166–72 (2013).

66. Ensan, S. *et al.* Self-renewing resident arterial macrophages arise from embryonic CX3CR1+ precursors and circulating monocytes immediately after birth. *Nat. Immunol.* **17,** 159–168 (2015).

67. Kojima, Y. *et al.* CD47-blocking antibodies restore phagocytosis and prevent atherosclerosis. *Nature* **536,** 86–90 (2016).

68. Randolph, G. J. Emigration of monocyte-derived cells to lymph nodes during

resolution of inflammation and its failure in atherosclerosis. *Curr. Opin. Lipidol.* **19,** 462–468 (2008).

69. Shankman, L. S. *et al.* KLF4-dependent phenotypic modulation of smooth muscle cells has a key role in atherosclerotic plaque pathogenesis. *Nat. Med.* **21,** 628–637 (2015).

70. Iwata, H. & Aikawa, M. in *Muscle Cell and Tissue* (InTech, 2015). doi:10.5772/61089

71. O'Donnell, M. J. *et al.* Global and regional effects of potentially modifiable risk factors associated with acute stroke in 32 countries (INTERSTROKE): a case-control study. *Lancet* **388,** 761–775 (2016).

72. Lewis, S. J. Prevention and Treatment of Atherosclerosis: A Practitioner's Guide for 2008. *Am. J. Med.* **122,** S38–S50 (2009).

73. Kannel, W. B. Blood Pressure as a Cardiovascular Risk Factor. *JAMA* **275,** 1571 (1996).

74. Little, P. J., Chait, A. & Bobik, A. Cellular and cytokine-based inflammatory processes as novel therapeutic targets for the prevention and treatment of atherosclerosis. *Pharmacol. Ther.* **131,** 255–268 (2011).

75. Davidson, M. H. Overview of prevention and treatment of atherosclerosis with lipid-altering therapy for pharmacy directors. *Am. J. Manag. Care* S260-9 (2007).

76. Davignon, J. Beneficial Cardiovascular Pleiotropic Effects of Statins. *Circulation*

109, (2004).

77. Bittencourt, M. S. & Cerci, R. J. Statin effects on atherosclerotic plaques: regression or healing? *BMC Med.* **13,** 260 (2015).

78. Silvestre-Roig, C. *et al.* Atherosclerotic Plaque Destabilization. *Circ. Res.* **114,** (2014).

79. Cao, S. S. & Kaufman, R. J. Unfolded protein response. *Curr. Biol.* **22,** R622–R626 (2012).

80. Penry, J. K. & Dean, J. C. The scope and use of valproate in epilepsy. *J. Clin. Psychiatry* **50 Suppl,** 17–22 (1989).

81. Chen, G., Huang, L.-D., Jiang, Y.-M. & Manji, H. K. The mood-stabilizing agent valproate inhibits the activity of glycogen synthase kinase-3. *J. Neurochem.* **72,** 1327–1330 (2008).

82. De Sarno, P., Li, X. & Jope, R. S. Regulation of Akt and glycogen synthase kinase-3β phosphorylation by sodium valproate and lithium. *Neuropharmacology* **43,** 1158–1164 (2002).

83. Di Daniel, E., Cheng, L., Maycox, P. R. & Mudge, A. W. The common inositol-reversible effect of mood stabilizers on neurons does not involve GSK3 inhibition, myo-inositol-1-phosphate synthase or the sodium-dependent myo-inositol transporters. *Mol. Cell. Neurosci.* **32,** 27–36 (2006).

84. O'Brien, W. T. *et al.* Glycogen synthase kinase-3beta haploinsufficiency mimics

the behavioral and molecular effects of lithium. *J. Neurosci.* **24,** 6791–8 (2004).

85. Phiel, C. J. *et al.* Histone Deacetylase Is a Direct Target of Valproic Acid, a Potent Anticonvulsant, Mood Stabilizer, and Teratogen. *J. Biol. Chem.* **276,** 36734–36741 (2001).

86. Gottlicher, M. *et al.* Valproic acid defines a novel class of HDAC inhibitors inducing differentiation of transformed cells. *EMBO J.* **20,** 6969–6978 (2001).

87. Ma, J. *et al.* Histone Deacetylase Inhibitor Phenylbutyrate Exaggerates Heart Failure in Pressure Overloaded Mice independently of HDAC inhibition. *Sci. Rep.* **6,** 34036 (2016).

88. Choi, J.-H. *et al.* Trichostatin A Exacerbates Atherosclerosis in Low Density Lipoprotein Receptor–Deficient Mice. *Arterioscler. Thromb. Vasc. Biol.* **25,** (2005).

89. Choi, S.-E. *et al.* Atherosclerosis induced by a high-fat diet is alleviated by lithium chloride via reduction of VCAM expression in ApoE-deficient mice. *Vascul. Pharmacol.* **53,** 264–272 (2010).

90. Murray, P. J. & Wynn, T. A. Protective and pathogenic functions of macrophage subsets. *Nat. Rev. Immunol.* **11,** 723–737 (2011).

91. Chinetti-Gbaguidi, G., Colin, S. & Staels, B. Macrophage subsets in atherosclerosis. *Nat. Rev. Cardiol.* **12,** 10–17 (2014).

92. Park, S.-H. *et al.* Myeloid-Specific IκB Kinase β Deficiency Decreases

Atherosclerosis in Low-Density Lipoprotein Receptor–Deficient Mice. *Arterioscler. Thromb. Vasc. Biol.* **32,** (2012).

93. Sharma, N. *et al.* Myeloid Krüppel-like factor 4 deficiency augments atherogenesis in ApoE-/- mice--brief report. *Arterioscler. Thromb. Vasc. Biol.* **32,** 2836–8 (2012).

94. Babaev, V. R. *et al.* Conditional Knockout of Macrophage PPAR Increases Atherosclerosis in C57BL/6 and Low-Density Lipoprotein Receptor-Deficient Mice. *Arterioscler. Thromb. Vasc. Biol.* **25,** 1647–1653 (2005).

95. Feig, J. E. *et al.* Regression of Atherosclerosis Is Characterized by Broad Changes in the Plaque Macrophage Transcriptome. *PLoS One* **7,** e39790 (2012).

96. Peled, M. & Fisher, E. A. Dynamic Aspects of Macrophage Polarization during Atherosclerosis Progression and Regression. *Front. Immunol.* **5,** 579 (2014).

97. Martin, M., Rehani, K., Jope, R. S. & Michalek, S. M. Toll-like receptor-mediated cytokine production is differentially regulated by glycogen synthase kinase 3. *Nat. Immunol.* **6,** 777–84 (2005).

98. Beurel, E. *et al.* Regulation of Th1 Cells and Experimental Autoimmune Encephalomyelitis by Glycogen Synthase Kinase-3. *J. Immunol.* **190,** (2013).

99. Kerr, B. M. *et al.* Inhibition of human liver microsomal epoxide hydrolase by valproate and valpromide: In vitro/in vivo correlation. *Clin. Pharmacol. Ther.* **46,** 82–93 (1989).

100. Yuen, A., Land, G., Weatherley, B. & Peck, A. Sodium valproate acutely inhibits lamotrigine metabolism. *Br. J. Clin. Pharmacol.* **33,** 511–513 (1992).

101. Wen, X., Wang, J. S., Kivistö, K. T., Neuvonen, P. J. & Backman, J. T. In vitro evaluation of valproic acid as an inhibitor of human cytochrome P450 isoforms: preferential inhibition of cytochrome P450 2C9 (CYP2C9). *Br. J. Clin. Pharmacol.* **52,** 547–53 (2001).

102. Gunes, A. *et al.* Inhibitory Effect of Valproic Acid on Cytochrome P450 2C9 Activity in Epilepsy Patients. *Basic Clin. Pharmacol. Toxicol.* **100,** 383–386 (2007).